

Validation of MERIS, MODIS and SeaWiFS Level-2 products with ground based *in-situ* measurements in Atlantic case 1 waters

Diplomathesis

by

Anja Theis



Faculty 1 - Physics and electrical engineering - at the
University of Bremen
prepared at the Alfred Wegener Institute for Polar and Marine Research
in the PHYTOOPTICS Group

Bremen, November 2009

Contents

Abstract	I
Abbreviations	III
1. Introduction	1
1.1. Motivation	3
1.2. Aims and objectives	3
2. Theory and Basics	5
2.1. Physical background: ocean color remote sensing	5
2.1.1. Interactions of electromagnetic radiation with matter	5
2.1.2. Spectral radiance	5
2.1.3. Spectral irradiance	6
2.1.4. Reflectance and remote sensing reflectance	8
2.1.5. Optical properties of water	8
2.1.6. Remote Sensing of open ocean waters	10
2.2. Satellite instruments	12
2.2.1. MERIS	12
2.2.1.1. MERIS data processing	14
2.2.1.2. MERIS flagging	14
2.2.2. MODIS	16
2.2.2.1. MODIS data processing	18
2.2.2.2. MODIS flagging	19
2.2.3. SeaWiFS	19
2.2.3.1. SeaWiFS data processing	20
2.2.3.2. SeaWiFS flagging	22
2.3. Radiometers	22
3. <i>In-situ</i> Data Acquisition	27
3.1. Measurement method	27
3.2. Measurement sites	28
3.3. Measurement quality control	29
4. Analysis	31
4.1. Data processing	31
4.1.1. <i>In-situ</i> data quality control	31

4.1.2.	Satellite data quality control	32
4.1.3.	Water leaving remote sensing reflectance ρ_w calculation and further processing	33
4.2.	Validation process	35
4.3.	Statistical interpretation and valuation process	36
4.4.	Uncertainties	36
5.	Results and Discussion	37
5.1.	Results	37
5.1.1.	Validation of collocated satellite water leaving remote sensing reflectance with <i>in-situ</i> data	37
5.1.1.1.	Superclassifications "all data", "all without cloud flagged data" and "no bad" data	38
5.1.1.2.	Not flagged	43
5.1.1.3.	Cloud flagged	44
5.1.1.4.	Glint flagged	45
5.1.1.5.	Low or negative L_w and pcd_1_13 flagged	49
5.1.1.6.	Mixed flagged	50
5.1.2.	Validation of band ratios used for chl- <i>a</i> retrieval and chl- <i>a</i> products with <i>in-situ</i> measurements	50
5.1.2.1.	Band ratio validation	51
5.1.2.2.	Level-2 product chl- <i>a</i> validation	53
5.2.	Discussion	55
5.2.1.	Validation of the water leaving reflectance	55
5.2.2.	Chl- <i>a</i> product validation	61
6.	Conclusions and Outlook	65
	Bibliography	67
	A. Appendix	71
	Acknowledgements	91
	Erklärung	93

List of Figures

1.1. Different species of phytoplankton	1
1.2. Absorption spectra of different pigments	2
2.1. Radiant flux	6
2.2. Definition of radiance	7
2.3. Illustration of variables in Fresnel equations	9
2.4. MERIS instrument	13
2.5. MERIS Field of view (FOV)	13
2.6. Processing structure for MERIS data	15
2.7. MODIS instrument	16
2.8. Processing structure for MODIS data	18
2.9. SeaWiFS instrument	20
2.10. Processing structure for SeaWiFS data	21
2.11. Beam path of spectrometers used in RAMSES radiometers	23
2.12. RAMSES radiometers	23
3.1. RAMSES instrument set-up	27
3.2. Measurement sites	28
3.3. Mounted RAMSES radiometers	29
3.4. RAMSES position on RV Polarstern	30
5.1. Example of collocated reflectance measurements for MERIS	38
5.2. Comparison of reflectance of collocated measurements for MERIS	38
5.3. Example of collocated reflectance measurements for MODIS	39
5.4. Comparison of reflectance of collocated measurements for MODIS	39
5.5. Reflectance comparison for all data	40
5.6. Reflectance comparison for all but cloud flagged data	41
5.7. Reflectance comparison for “not bad” data	41
5.8. Reflectance comparison for “not bad” data (wavelength separated)	42
5.9. Reflectance comparison for not flagged data	44
5.10. Reflectance comparison for not flagged data (wavelength separated)	45
5.11. Reflectance comparison for “high cloud” flagged data	46
5.12. Same Figure as 5.11 but with a different scale	46
5.13. Reflectance comparison for “medium cloud” flagged data	47
5.14. Reflectance comparison for “low cloud” flagged data	47
5.15. Reflectance comparison for “high glint” flagged data	48

5.16. Reflectance comparison for “medium glint” flagged data	48
5.17. Reflectance comparison for “low or negative Lw” flagged data	49
5.18. Reflectance comparison for “pcd_1_13” flagged data	50
5.19. Chl- <i>a</i> reflectance ratio comparison	52
5.20. Chl- <i>a</i> reflectance ratio comparison for “not bad” flagged data	52
5.21. Chl- <i>a</i> comparison	53
5.22. Chl- <i>a</i> comparison for “not bad” flagged data	54
A.1. Reflectance comparison for all data (wavelength separated)	74
A.2. Reflectance comparison for all without cloud flagged data (wavelength separated)	75
A.3. Reflectance comparison for “not bad” flagged data (wavelength separated)	76
A.4. Reflectance comparison for “high cloud” flagged data (wavelength separated)	77
A.5. Reflectance comparison for “medium cloud” flagged data	78
A.6. Reflectance comparison for “medium cloud” flagged data (wavelength separated)	79
A.7. Reflectance comparison for “low cloud” flagged data	80
A.8. Reflectance comparison for “low cloud” flagged data (wavelength separated)	81
A.9. Reflectance comparison for “high glint” flagged data (wavelength separated)	82
A.10. Reflectance comparison for “medium glint” flagged data (wavelength separated)	83
A.11. Reflectance comparison for “low or negative Lw” flagged data (wavelength separated)	84
A.12. Reflectance comparison for “pcd_1_13” flagged data (wavelength separated)	85
A.13. Reflectance comparison for “high mixed” flagged data	86
A.14. Reflectance comparison for “medium mixed” flagged data	87
A.15. Reflectance comparison for “medium mixed” flagged data (wavelength separated)	88
A.16. Reflectance comparison for “low mixed” flagged data	89

List of Tables

2.1. MERIS bands and applications	14
2.2. MODIS bands and applications	17
2.3. SeaWiFS bands and applications	20
2.4. RAMSES technical details	24
3.1. Overview: Ship cruises	29
4.1. Considered flags	33
4.2. Classification of collocations	34
4.3. Validated wavelength bands	35
5.1. Collocations contributing to the “no bad” classification	40
5.2. Statistics for reflectance comparison for “no bad” classification	43
5.3. Available data for chl- <i>a</i> product and band ratio validation	51
5.4. Statistics for the classifications	56
5.5. Wavelength separated statistics from different studies	59
5.6. Summarized statistics from different studies	61
5.7. Statistics for band ratio comparison	62
5.8. Statistics for chl- <i>a</i> comparison	62
A.1. Collocation assignment to the different classifications	71
A.2. Collocations considered in “no bad” classification	73

Abstract

Ocean color remote sensing measurements play a major role in research focusing on global ecosystem and carbon cycle modeling by providing information on global phytoplankton biomass distribution. As satellites provide continuous monitoring and environmental observations on a global scale, their measurements are used for climate modeling or forecasts. Nevertheless, these data have to be validated in order to evaluate their quality and temporal stability.

Several studies dealing with the validation of the satellite measurements and their products with ground based *in-situ* measurements are available for coastal, respectively case 2 waters.

For this work *in-situ* measurements were performed in open ocean or case 1 waters during ship cruises with RV Polarstern across the Atlantic Ocean. A system of hyperspectral RAMSES radiometers was used to measure radiances above the sea surface and calculate the remote sensing reflectance.

Details of this data acquisition and the results of the validation are depicted in this thesis. The collocated measurements from the three major ocean color satellite instruments MERIS, MODIS and SeaWiFS, operated by ESA and NASA, respectively, are validated with the *in-situ* remote sensing reflectance data. The validation was accomplished for different classifications of satellite data concerning their contamination by flagged pixels. Additionally, chl-*a* concentrations from *in-situ* water samples are used to validate the satellite Level-2 product chl-*a* of all three instruments.

Validation shows the best agreements between satellite derived and *in-situ* reflectance values for clear sky conditions, respectively not flagged satellite images. While MERIS shows a good agreement for this “not flagged” category, MODIS has a larger discrepancy to the ground-based measurements. It also shows often poor performances especially for the low wavelength band (412 nm). This indicates, that the atmospheric correction requires improvement. Otherwise flagged collocations (for example “cloud flagged”) are proven to be not suitable in terms of validation.

As there are no collocations for SeaWiFS in the “not flagged” classification and as the number of collocations generally for the individual classifications is rather small, further data sampling is necessary in order to prove these results.

This is further true for the chl-*a* validation. A slight correlation between the satellite Level-2 product chl-*a* concentration and the *in-situ* measured concentration is detected but with respect to the small number of matchable data, the validity of the comparison as to be enhanced with further accumulation.

Abbreviations and acronyms

AWI	Alfred Wegener Insitute for Polar and Marine Research
AQUA	Second major EOS satellite
Chl- <i>a</i>	Chlorophyll a
CO ₂	Carbon Dioxide
CCD	Charge coupled device
DOM	Dissolved organic matter
ESA	European Space Agency
EOS	Earth Observing System (US, with international components)
ENVISAT	Environmental Satellite (ESA)
FOV	field-of-view
GKSS	GKSS Research Center
IFM-GEOMAR	Leibniz Institute of Marine Sciences
IUP	Institute of Environmental Physics (University of Bremen)
IR	Infrared
MERIS	Medium Resolution Spectrometer on ENVISAT
MODIS-A	Moderate Resolution Spectrometer on AQUA
MODIS-T	Moderate Resolution Spectrometer on TERRA
MMS	Monolithic Miniature-Spectrometer (Carl Zeiss AG)
NASA	United States National Aeronautics and Space Administration
OSC	Orbital Science Corporation

ROI	Region of interest
SeaWiFS SeaStar	Sea-viewing Wide Field-of-view Sensor on Orb-view-II satellite (OSC), also called Orb-view-II
TERRA TOA	First major EOS satellite (not an abbreviation) Top of atmosphere
USB	Universal Serial Bus
UTC	Coordinated Universal Time
UV	Ultraviolet

1. Introduction

Marine Phytoplankton - algae - are plants with a large variety of species, living in the ocean. Phytoplankton contribute only to about one to two percent to the world's biomass but provide 30 to 60 % of the global primary production¹. Because they require sunlight, water and nutrients for growth, phytoplankton remain at or near the sea surface.

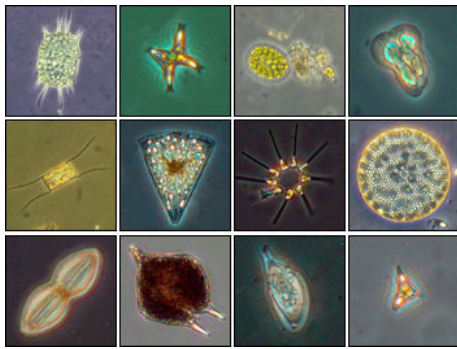


Figure 1.1.: *Different species of phytoplankton*
(Source: http://cmore.soest.hawaii.edu/cruises/operex/images/Phytoplankton-Variations_full.jpg)

Phytoplankton build the foundation of the marine food web² and play an important role in the global carbon cycle (see Bracher et al. (2009)). During photosynthesis oxygen is produced and inorganic carbon is fixed and exported to the deep sea with the dead phytoplankton cells sinking to the bottom of the ocean. The largest source of carbon is the atmosphere where it acts in form of carbon dioxide as greenhouse gas. This dissolves into the ocean and is available to the algae there. Altogether about 90%² of the world's total carbon content has settled to the bottom of the ocean, primarily in the form of dead biomass. Thereby, the ocean is the largest sink for one of the most prominent greenhouse gases.

Phytoplankton depend upon certain conditions for growth, like incident sun radiation, water temperature and nutrients such as iron and carbon. Due to the strong decrease of solar radiation with water depth most phytoplankton grow in the very upper layers of the ocean. Cold surface waters lead to an unstable water column that wells up water from lower depth that is rich in nutrients. Thus the water temperature influences the phytoplankton growth.

The fixation of carbon and thereby its export, strongly relies on the size and composition of the cells. Different species of phytoplankton can fix different amounts of carbon and thus reduce atmospheric carbon dioxide. This is one reason why phytoplankton are of primary interest to oceanography, earth and climate science. Physical or chemical variance in any of phytoplankton influencing parameters like nutrient concentration, temperature or sunlight will affect the phytoplankton concentration on a short timescale².

¹Carr et al. (2006)

²David Herring on <http://earthobservatory.nasa.gov/Features/Phytoplankton/>

Optical properties of water are affected by its constituents and determine the spectral composition of the backscattered light. Ocean color satellite sensors are constructed to record this light in different wavelength bands. Mostly, phytoplankton is the dominant light absorbing part of water constituents and thus, information about phytoplankton can be retrieved from satellite ocean color measurements.

Oxygen is produced by photosynthesis in plants that absorb light primarily using the pigment chlorophyll-*a* (chl-*a*). Besides chl-*a*, plants also use other pigments, for example carotenoids, phycobillins, chlorophyll-*b* and chlorophyll-*c*. Every pigment shows a specific absorption spectrum¹. Examples are depicted in Figure 1.2. A particular species of phytoplankton has its very specific composition of pigments and has consequently its own characteristic absorption spectrum.

Chl-*a* absorbs light primarily at about 430 nm (blue) and 680 nm (red). The green wavelength range is rarely absorbed. By determining the ratio of backscattered light in the blue to the green wavelength range, chl-*a* concentrations can be derived.

Such ocean color measurements from satellite instruments like the Medium Resolution Imaging Spectrometer (MERIS), the Moderate Resolution Imaging Spectrometer (MODIS) or the Sea Viewing Wide Field of View Sensor (SeaWiFS) operated by European Space Agency (ESA) and National Aeronautics and Space Administration (NASA), respectively, are nowadays one of the essential sources of climatological and environmental modeling. They provide continuous data sets to monitor and observe biogeochemical properties in the upper layer of the ocean on a global scale. The measured spectral radiances at the top of atmosphere are atmospherically corrected and the so called remote sensing reflectance (radiation emerging from the ocean surface) are determined. By means of particular algorithms biogeochemical properties, like chl-*a* concentration, can be derived from this.

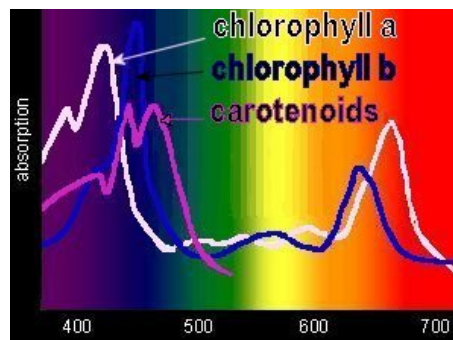


Figure 1.2.: Absorption spectra of different pigments (Source: <http://photos1.blogger.com/blogger/4178/911/1600/chlorophyll-carotenoid-abs.jpg>)

The accuracy of satellite products is generally accepted by the international missions for values of $\pm 5\%$ for water leaving radiances and $\pm 35\%$ for chl-*a* in the open ocean³.

As satellites use the measured remote sensing reflectance to compute products like chl-*a* it is useful to validate and reduce errors in remote sensing reflectance determination. In this study, therefore *in situ* remote sensing reflectances were determined across the Atlantic Ocean, a case-1 water, with a set of hyperspectral radiometers (RAMSES) and

¹Bracher (2008)

³McClain (2009)

additionally, chl-*a* measurements were obtained to validate the satellite products.

1.1. Motivation

The Helmholtz-University Young Investigators Group PHYTOOPTICS under the lead of Dr. A. Bracher, a cooperation between Alfred-Wegener-Institute (AWI) and Institute of Environmental Physics at the University of Bremen (IUP) was incorporated with the aim to improve global estimates of marine primary production to promote a better knowledge of the sinks and sources of carbon dioxide (CO₂) in the ocean and a better understanding of changes in the world's climate.

In order to improve global primary production estimates, new biooptical information from the European satellite SCIAMACHY is retrieved and data of the common ocean color sensors the Medium Resolution Imaging Spectrometer (MERIS), the Sea Viewing Wide Field of View Sensor (SeaWiFS) and the Moderate Resolution Spectrometer (MODIS) are used.

In order to validate these satellite data with ground-truth data and to give an impression on the uncertainty of satellite derived biogeochemical properties like chl-*a* concentration this study was conducted.

1.2. Aims and objectives

The aim of this work is to validate MERIS, MODIS and SeaWiFS remote sensing reflectances and their Level-2 product chl-*a* with ground based *in-situ* measurements.

There are several studies about validation of satellite products for case 2 waters (e.g. Park et al. (2006)). Due to large organizational efforts and often high financial costs *in-situ* data for open ocean or case 1 waters are scarce. An example of a case 1 validation study has been performed within the BOUSSOLE project (Antoine et al. (2008)). Another study is presented in Bailey and Werdell (2006).

During different ship cruises with RV Polarstern a set of three hyperspectral RAMSES radiometers is used to obtain *in-situ* radiance and irradiance data at the sea surface across the Atlantic Ocean. From that, the remote sensing reflectance is calculated.

This ground-truth data is compared to collocated remote sensing reflectance measurements from all three satellite instruments, MERIS, MODIS and SeaWiFS. As a second part, the collocated Level-2 product chl-*a* is validated with *in-situ* measured chl-*a* that is assessed at water samples using High Pressure Liquid Chromatography (HPLC). Additionally, the reflectance ratios used for satellite chl-*a* determination are compared to the respective ground based RAMSES reflectance ratio.

Statistical analysis of all comparisons quantify the magnitude of the agreements and allow to interpret the validation. Results may help to evaluate the atmospheric correction applied to MERIS, MODIS and SeaWiFS data and assess the quality of the satellite derived measurements.

The second chapter gives a short introduction to the relevant aspects of satellite- and ocean remote sensing, and a description of the radiometers used for *in-situ* data sampling. Data acquisition with measurement method, sites and quality control are explained in chapter three. A detailed description of all steps of the analysis is given in chapter four. All results of the validation are depicted in chapter five divided in three sections: validation of the remote sensing reflectances, validation of the Level-2 product chl-*a* and interpretation and discussion for both. The last chapter concludes the results of this work and gives an outlook on future aspects.

2. Theory and Basics

To give an overview of the basic physical principles underlying the topic of this work the first section of this chapter describes the background and physical concepts of ocean color remote sensing. The satellite instruments MERIS, MODIS and SeaWiFS, which remote sensing reflectance and chl-*a* data are validated in this work are introduced in the second part. The last section deals with the RAMSES radiometers used for *in-situ* data sampling.

2.1. Physical background: ocean color remote sensing

Most of the information given in this sub chapter is taken from Seelye (2004), Cracknell and Hayes (2007), Elachi (1987) and Kirk (1983), where further information is available. Concepts and formulas to depict the physical background of the methods and analysis that are applied later are introduced.

2.1.1. Interactions of electromagnetic radiation with matter

Light propagating through the atmosphere and the ocean interacts with the respective surrounding matter. The possible reactions are:

- absorption α
- reflection ρ
- transmission τ
- emission ϵ

The processes are drawn in Figure 2.1: An initial beam of light Ψ_i propagating through a medium ΔV can be splitted in an absorbed Ψ_α , a reflected Ψ_ρ and a transmitted part Ψ_τ . The absorbed fraction can be emitted Ψ_ϵ from the medium and is then seen as a scattered part Ψ_s of the initial beam. It is always true that $\alpha + \rho + \tau = 1$.

2.1.2. Spectral radiance

To describe radiometric processes it is important to know the concept of the spectral radiant flux $\Psi(\lambda)$, that is defined as the change in radiant energy ∂Q per unit time ∂t and wavelength $\partial \lambda$.

$$\Psi(\lambda) = \frac{\partial Q}{\partial t \partial \lambda} \quad (2.1)$$

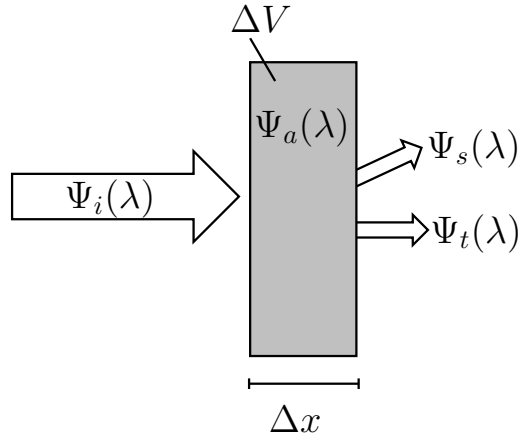


Figure 2.1.: The incoming radiant flux $\Psi_i(\lambda)$ can be split in an absorbed $\Psi_a(\lambda)$, a transmitted $\Psi_t(\lambda)$ and a scattered part $\Psi_s(\lambda)$ when it passes a medium with thickness Δx and Volume ΔV .

The unit of spectral radiant flux is Watt per nanometer

$$\frac{W}{nm}$$

The radiant flux coming from a certain direction ξ with the solid angle $d\Omega$ through an area dA is named radiance. Figure 2.2 illustrates the definition of radiance. With the solid angle defined as

$$d\Omega = \sin \theta \, d\theta \, d\varphi \quad (2.2)$$

the radiance is

$$L(x, t, \xi) := \frac{\partial^2 \psi}{\partial A \partial \Omega} = \frac{\partial^3 Q}{\partial t \partial A \partial \Omega} \quad (2.3)$$

Area dA and solid angle $d\Omega$ are assumed to be infinitesimal. In case dA is tilted against the direction of incoming radiant flux the radiance has to be determined using the effective area $dS = dA \cdot \cos \theta$ where θ is the tilting angle.

Spectral radiance is more useful with respect to wavelength dependency:

$$L(x, t, \xi, \lambda) := \frac{\partial^3 Q}{\partial t \partial A \partial \Omega \partial \lambda} \quad (2.4)$$

Its dimension is

$$\frac{J}{s \, m^2 \, sr \, nm} = \frac{W}{m^2 \, sr \, nm}$$

2.1.3. Spectral irradiance

By introducing the spectral irradiance it is possible to quantify the radiant flux (see Section 2.1.2). By definition the spectral irradiance is the integral of the normal component

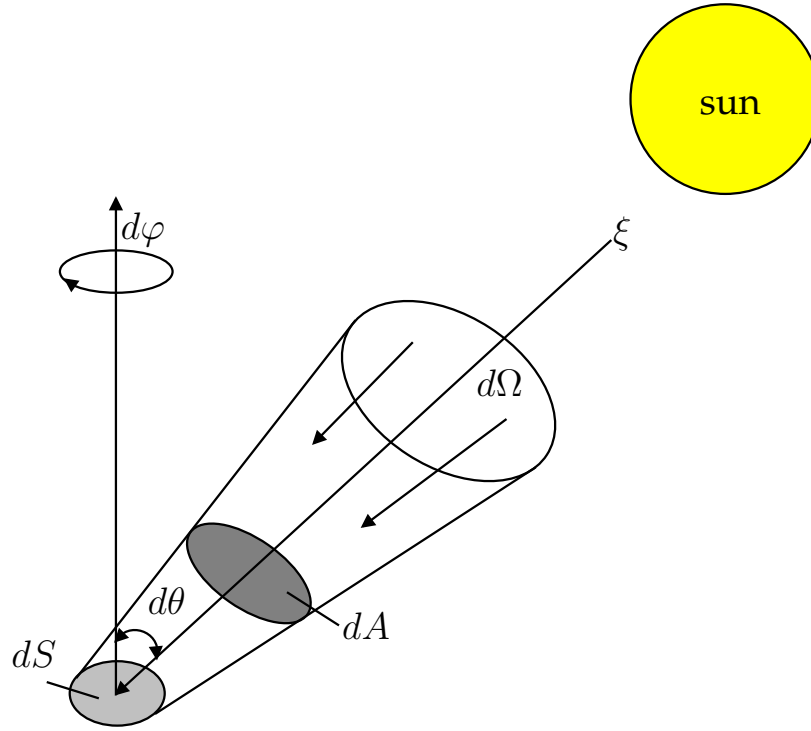


Figure 2.2.: Definition of radiance. Radiant flux from direction ξ with the solid angle $d\Omega = \sin \theta d\theta d\varphi$ through an area dA is named radiance. The effective area dS is necessary in case dA is tilted against the direction of the incoming radiant flux

of the spectral radiance over one hemisphere:

$$E_d(x, t, \lambda) := \int_{\varphi=0}^{2\pi} \int_{\theta=0}^{\pi/2} L(x, t, \theta, \varphi, \lambda) \cdot \cos \theta d\Omega \quad (2.5)$$

Equation 2.5 gives the downwelling spectral irradiance. Upwelling spectral irradiance is consequently defined as:

$$E_u(x, t, \lambda) := \int_{\varphi=0}^{2\pi} \int_{\theta=\pi/2}^{\pi} L(x, t, \theta, \varphi, \lambda) \cdot \cos \theta d\Omega \quad (2.6)$$

The dimension of spectral irradiance is

$$\frac{W}{m^2 nm}$$

Total irradiance is determined by integrating spectral irradiance over all wavelengths:

$$E_t(x, t) := \int_{\lambda=0}^{\text{inf}} E(x, t) d\lambda \quad (2.7)$$

Integration of total irradiance over the Area dA leads to the definition of the total flux Φ with its dimension W :

$$\Phi(t) := \int E_t(x, t) dA \quad (2.8)$$

2.1.4. Reflectance and remote sensing reflectance

Reflectance in general is the ratio of upwelling to downwelling irradiance. In case of ocean color remote sensing it is useful to determine reflectance with respect to wavelength λ and depth d in the water:

$$R(\lambda, d) := \frac{E_u(\lambda, d)}{E_d(\lambda, d)} \quad (2.9)$$

Because of the satellite instruments' small field-of-view (FOV) it is useful and common to deal with remote sensing reflectance, R_{RS} , that is defined as the ratio of upwelling radiance, L_u , to downwelling irradiance, E_d :

$$R_{RS}(\xi, \lambda, \theta, \varphi, d) := \frac{L_u(\xi, \lambda, d)}{E_d(\xi, \lambda, d)} \quad (2.10)$$

Its dimension is sr^{-1} .

If the upwelling radiance is measured from a ship, the measured radiance has to be corrected for the sky radiance, L_s , which is measured by directly viewing into the sky. The so-called water-leaving radiance is defined as:

$$L_w(\lambda) = L_u(\lambda) + \rho_{as}(\lambda) L_s(\lambda) \quad (2.11)$$

where ρ_{as} is the Fresnel reflectance of the water surface that is further explained in Section 2.1.5.

2.1.5. Optical properties of water

The optical properties of water are usually divided in two different types.

Inherent optical properties are those that depend only on the medium. They are described with the physical properties of water and its constituents and are independent of the light field. An example is the attenuation coefficient $a(\lambda)$ that describes the attenuation of an initial beam of light with intensity I_0 by absorption when propagating through a medium with thickness Δx (compare 2.1).

$$I(\lambda, x) = I_0 e^{-a(\lambda) \cdot x} \quad (2.12)$$

This is called the law of Lambert-Beer.

Apparent optical properties are those that depend on both, light field and inherent optical properties. Examples are reflection and remote sensing reflection that are described in section 2.1.4.

Particular information on optical properties of water are given in Kirk (1983). Regarding the light moving from the air into the water one has to take Fresnel's equations into account. Fresnel's equations describe the general behavior of light when moving between two media of different refractive indices:

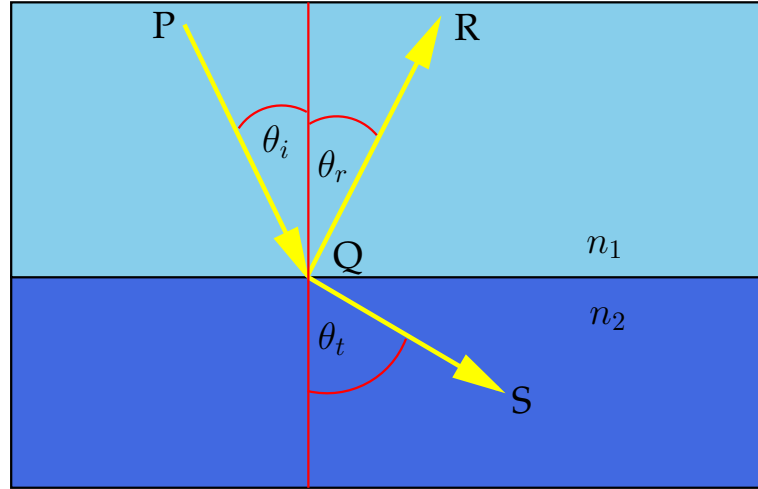


Figure 2.3: Illustration of variables used in Fresnel equations: Two media with different refractive indices n_1 and n_2 cause reflection and / or refraction to an incident beam of light. θ_i , θ_r , and θ_t describe the incident, the reflected and the transmitted angle, respectively.

When light moves from a medium with refractive index n_1 into a medium with refractive index n_2 it may be reflected and / or refracted. Figure 2.3 illustrates the way of an incident beam of light PQ, that hits the interface between both media in Q with the angle θ_i . The beam can be partially reflected (as ray QR) with angle θ_r and partially refracted (as ray QS) with the angle θ_t . The relationships between the refractive indices of both media and the mentioned angles are given in Snell's law:

$$\frac{\sin \theta_i}{\sin \theta_t} = \frac{n_2}{n_1} \Leftrightarrow n_1 \sin \theta_i = n_2 \sin \theta_t \quad (2.13)$$

The fraction of the incident beam that is reflected is the reflectance defined by Fresnel equation in case the light is polarized perpendicular to the plane of Figure 2.3 (s-polarized):

$$R_s = \left[\frac{\sin(\theta_t - \theta_i)}{\sin(\theta_t + \theta_i)} \right]^2 \quad (2.14)$$

and in case the light is polarized in the plane of the figure (p-polarized)

$$R_p = \left[\frac{\tan(\theta_t - \theta_i)}{\tan(\theta_t + \theta_i)} \right]^2 \quad (2.15)$$

If the incident light is unpolarized with an equal mixture of p- and s-polarizations, the reflection coefficient is

$$R = \frac{R_s + R_p}{2} \quad (2.16)$$

Transmission is always $T = 1 - R$.

In case of air and water the refractive indices are different from each other and additionally, the refractive index of water varies with

- temperature
- salinity
- surface roughness / wind speed
- wavelength.

Often the refractive index of water is treated as a constant or as a function of wind speed within the visible spectral range (see for example Lee and Carder (2004) or Park et al. (2006)).

As the refractive index varies with wavelength this assumption may cause significant errors in computing the spectral water leaving reflectance. Further information on this is given in Doerffer (2008). In this study an algorithm developed by Roland Doerffer from GKSS to compute the fresnel reflection coefficient as a function of wavelength, salinity and temperature was adjusted to imply a wind speed dependency. This algorithm, used within this study, is described in chapter 4.

2.1.6. Remote Sensing of open ocean waters

- Case-1 and case-2 waters

Oceanic waters can be divided in two different categories following Morel and Prieur (1977). "Blue"¹ or Case-1 waters are featured through a strict coherence between phytoplankton concentration and other suspended matter. Absorption by chlorophyll is the dominant part determining the total absorption of light in the water, beside the absorption by the water itself. Total absorption α_{total} is determined as the sum of absorption of pure sea water α_w , pigments α_p , suspended matter α_s and yellow substance α_y .

$$\alpha_{total} = \alpha_w + \alpha_p + \alpha_s + \alpha_y \quad (2.17)$$

As the absorption of light by the water itself becomes larger with wavelength and is nearly one in wavelength rangel greater than around 900 nm ocean color remote sensing confines to the generous visible part of the electromagnetic spectrum.

In "green"² or Case-2 waters especially dissolved and suspended matter increase scattering and absorption. Those are not correlated with phytoplankton concentration because of terrigenous contributions. Particularly coastal and inland waters like rivers are part of this category.

- Case-1 empirical algorithm for chl-*a* concentration retrieval
Phytoplankton or chl-*a* concentration in case-1 waters determine the attenuation of

¹Morel and Prieur (1977), page 712

²Morel and Prieur (1977), page 715

incident light in the water. The absorption of water is constant but as the attenuation by yellow substance of light in the water is correlated with chl-*a* concentration. Some empirical algorithms are used to determine chl-*a* concentrations from remotely sensed data using the band ratio of two wavelengths λ_1 and λ_2 . The first wavelength is chosen out of a large interval with broad absorption of phytoplankton (400 nm - 500 nm) and the second wavelength is chosen out of an interval with low pigment absorption (500 nm - 600 nm). The ratio of the remote sensing reflectance of both wavelengths can be assumed to be proportional to the ratio of backscattering b_b to absorption α of the respective wavelengths. Since backscattering is constant for the two wavelengths, the following approximation holds true:

$$\frac{R_{RS}(\lambda_1)}{R_{RS}(\lambda_2)} \propto \frac{b_b(\lambda_1)}{\alpha(\lambda_1)} \cdot \frac{\alpha(\lambda_2)}{b_b(\lambda_2)} \propto \frac{\alpha(\lambda_2)}{\alpha(\lambda_1)} \quad (2.18)$$

As absorption at wavelength λ_1 is caused by phytoplankton and yellow substance and a definite relationship between both is assumed, the total absorption at λ_1 can be taken as proportional to chl-*a* concentration.

$$\frac{R_{RS}(\lambda_1)}{R_{RS}(\lambda_2)} \propto \frac{1}{\alpha(\lambda_1)} \propto \frac{1}{\text{chl-}a \text{ concentration}} \quad (2.19)$$

Based on this empirical algorithm satellite products provide chl-*a* concentrations.

- Sun glint

The direct reflection of sunlight into the satellite sensor is called sun glint. The sun glint is mostly overwhelming the desired observations. Some satellite sensors have mechanisms to suppress effects from sun glint and all strongly influenced pixels of the satellite image are usually flagged. Details are given in the respective subsections of section 2.2

- Atmospheric correction

Satellite instruments measure the properties of the radiation that arrives at the instrument. As the radiation has traveled through the atmosphere before arriving the satellite instrument it has experienced the possible interactions described in 2.1.1. The radiation coming from the target area at the earth's surface is influenced by various processes occurring on its way through the atmosphere.

In order to get information about the target area, the measured radiation has to be atmospherically corrected. An attempt to describe the processes that influence the initial radiation leaving the target area is the set up of the radiative transfer equation.

The radiative transfer theory is essentially for studying the radiation traveling in a certain direction ϕ to the vertical axis and setting up a differential equation for a small horizontal element with thickness dz . To determine the intensity of the radiation leaving the element dz in the direction ϕ , it is necessary to consider

- the radiation entering the element dz from the incident direction,

- the attenuation affecting the radiation within the element dz and
- additional radiation generated within the element dz or scattered into the direction ϕ within the element dz .

The resulting differential equation is the radiative transfer equation. As the atmosphere is a highly dynamic physical system and the atmospheric parameters used in the radiative transfer equation usually vary with the three space variables and the time it is a great challenge to account for correctly atmospheric contributions. Often it is assumed that the atmospheric parameters are a function of height z , but not of the coordinates x and y in a horizontal plane.

Based on geographical location and time of the year models of a “model atmosphere” are constructed to further simplify the radiative transfer equation.

As this assumption is not very realistic because atmospheric conditions differ from the model it is common to use atmospheric parameters that apply at the measurement time.

Still, the radiative transfer equation is a unconstrained inversion problem due to the many unknowns from the atmospheric parameters and only a small number of measurements. The solution of the radiative transfer equation therefor will take some mathematical and physical assumptions.

2.2. Satellite instruments

The validated satellite instruments MERIS, MODIS and SeaWiFS are introduced in this chapter.

2.2.1. MERIS

The information given in the subsection about the Medium Resolution Imaging Spectrometer (MERIS) are mostly taken from the MERIS section on ESA homepage³ and from the ESA MERIS-FAQ from 14. April 2006⁴.

Additional facts and more detailed information can be found in the MERIS handbook⁵ and the MERIS detailed instrument description⁶ provided by ESA.

The instrument MERIS on board the European Space Agency (ESA) Environmental Satellite (ENVISAT) (see Figure 2.4) is an imaging multi-spectral radiometer in the visible and near infrared spectral range. ENVISAT operates, since it was launched in 2002, in a sun-synchronous polar orbit of about 800 km altitude with an inclination of 98° and an equator crossing time of 10 a.m. in a descending mode.

³<http://envisat.esa.int/instruments/meris/>

⁴http://earth.esa.int/pub/ESA_DOC/ENVISAT/MERIS/VT-P017-DOC-005-E-01-00_meris.faq.1_0.pdf

⁵<http://envisat.esa.int/handbooks/meris/CNTR.htm>

⁶http://envisat.esa.int/pub/ESA_DOC/ENVISAT/MERIS/meris.DetailedInstrumentDescription.1_0.pdf

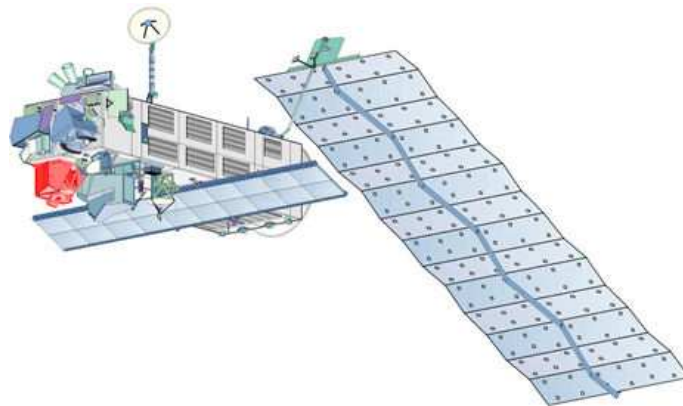


Figure 2.4.: MERIS instrument (highlighted in red color) on ENVISAT (Source: ESA)

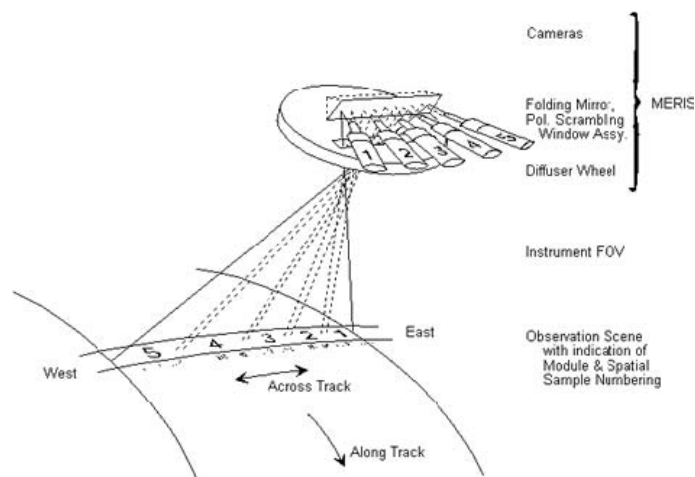


Figure 2.5.: MERIS FOV (Source: ESA)

MERIS consists of five identical cameras, measuring the reflected light coming from the earth's surface in 15 spectral bands (see table 2.1) in a so called *pushbroom* mode. Each of the cameras contains one CCD array for each one of the 15 bands. One image line is measured perpendicular to the flight direction and resolved spectrally on a the two-dimensional CCD detector.

MERIS has been designed for oceanic, coastal, terrestrial and atmospheric measurements, to observe ocean color and biology, vegetation, clouds and precipitation, respectively. With ENVISAT's height of 800 km and MERIS's FOV of 68.5° around nadir, one pixel has a swath width of 1150 km. Figure 2.5 sketches the instruments FOV. A global coverage of two to three days is realized.

All measured data are provided as a *reduced resolution* by ESA and a *full resolution* is processed on demand. The spatial resolution of one pixel is $1.04 \text{ km} \times 1.2 \text{ km}$ in reduced and $260 \text{ m} \times 300 \text{ m}$ in full resolved resolution.

Table 2.1.: *MERIS bands and applications*

Band index	Band center in nm	Band width in nm	Applications
1	412.5	10	Yellow substance and detrital pigments
2	442.5	10	Chlorophyll absorption maximum
3	490	10	Chlorophyll and other pigments
4	510	10	Suspended sediment, red tides
5	560	10	Chlorophyll absorption minimum
6	620	10	Suspended sediment
7	665	10	Chlorophyll absorption & fluo. reference
8	681.25	7.5	Chlorophyll fluorescence peak
9	708.75	10	Fluo. reference, atmosphere corrections
10	753.75	7.5	Vegetation, cloud
11	760.625	3.75	O^2 R-branch absorption band
12	778.75	15	Atmosphere corrections
13	865	20	Vegetation, water vapor reference
14	885	10	Atmosphere corrections
15	900	10	Water vapor, land

2.2.1.1. MERIS data processing

The data processing structure for MERIS data is sketched in Figure 2.6.

Level-0 product is the lowest level product ESA provides for ENVISAT MERIS data. It is roughly the raw data sensed MERIS.

The next step in processing is to geolocate data and it bring to engineering units. This and some additional selected calibrations are applied to Level-1B data.

The Level-1B product is transformed into Level-2 product through higher-level processing to convert engineering units into geophysical quantities and to form a more directly interpretable and useful measurement data set.

2.2.1.2. MERIS flagging

- Glint estimation

The sun glint reflectance is calculated using the Cox and Munk model (1954) as a function of geometry, wind speed modulus and direction. An estimate of glint reflectance is produced and compared to a low glint threshold. If the glint reflectance is below this low glint threshold then no glint correction for this pixel is applied. If the glint reflectance is above the threshold then the glint reflectance is compared to a medium glint threshold. If the glint reflectance is below the medium glint threshold then a medium glint flag is raised and the pixel is corrected for glint reflectance. In case the glint reflectance is above the medium glint threshold then no correction

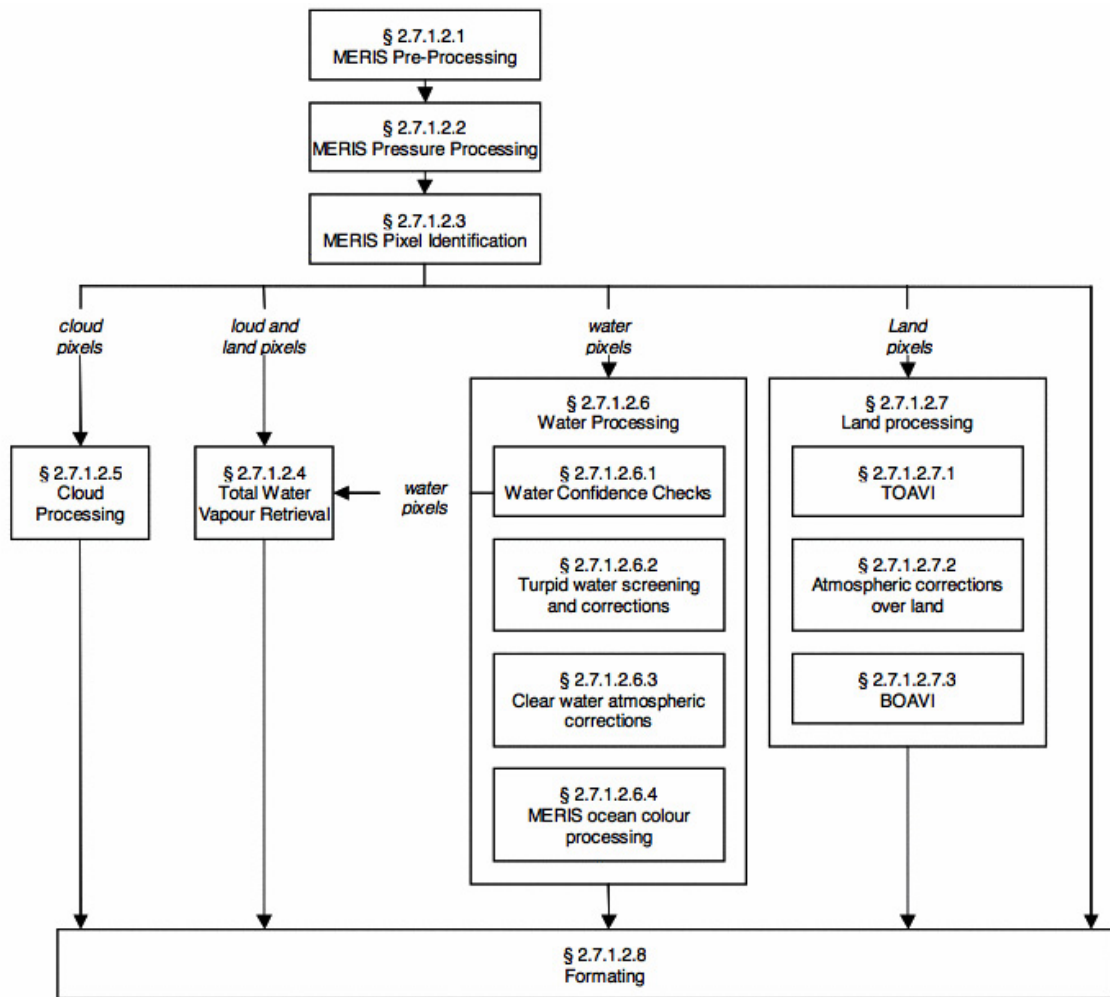


Figure 2.6.: Processing structure for MERIS data (Source: ESA)

is applied and the pixel is flagged as uncorrected sun glint.

- Clouds

For cloud marking in satellite images over ocean, discrimination between cloud and ice or sunglint can be performed from apparent pressure and geometrical considerations. Therefore thresholds have been defined as a function of geometrical conditions.

Flags for the possible occurrence of cirrus clouds or finite clouds are proposed as a warning for the quality of the atmospheric corrections. Over ocean, a first flag can be set from correlations between apparent pressure in O_2 channels and reflectances at a wavelength of 865 nm with a threshold in pressure corresponding to a too high contribution of the cirrus reflectance. Another possibility to detect cloud heterogeneities is to have a test on the spatial homogeneity of barometric pressure from the Oxygen channels.

If a pixel over ocean is not classified as bright, the atmospheric correction scheme will apply even if unwished contributors are present: sub-pixel cloud cover, cirrus clouds, cloud shade. The purpose here is to flag these situations as a warning on suitability of the atmospheric correction.

- pcd_1_13

pcd is the abbreviations for product confidence data. The pcd_1_13 flag signifies that at least one of the thirteen water leaving reflectances is negative.

2.2.2. MODIS

The information about the Moderate Resolution Imaging Spectrometer (MODIS) given in this section are mainly taken from Seelye (2004). Further information and technical details are available on the MODIS website⁷.

The satellite instrument MODIS (see Figure 2.7) is installed on both, TERRA and AQUA that were launched in 1999 and 2002, respectively, and are part of the Earth observing system EOS. Both satellites were constructed to improve understanding of global dynamics and processes occurring on land, the oceans and in the lower atmosphere. In this work only data from MODIS on Aqua are used. In the following MODIS refers to MODIS on AQUA.

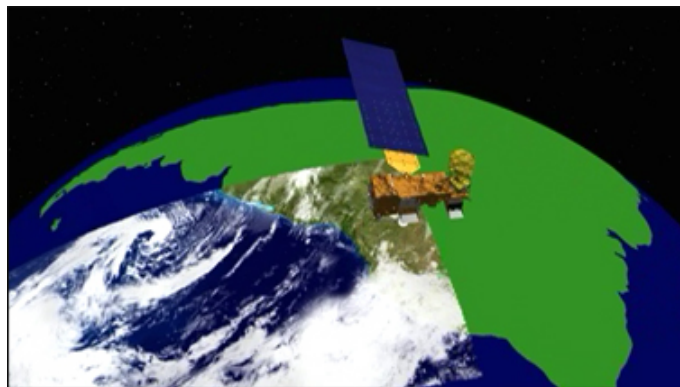


Figure 2.7.: MODIS instrument (Source: NASA)

AQUA has a sun-synchronous near polar orbit in 705 km altitude. The equator crossing time is at 1:30 p.m. in ascending mode. A global coverage within one to two days is achieved.

⁷<http://modis.gsfc.nasa.gov/>

Table 2.2.: MODIS bands and applications

Band index	Band center in nm	Band width in nm	Applications
1 - 2	-	-	Land / cloud / aerosols boundaries
3 - 7	-	-	Land / cloud / aerosols properties
8	412.5	15	Phycoerythrin / total pigment concentration
9	443	10	Detached coccolith / phycoerythrin / total pigment / chl- <i>a</i> / diffuse attenuation coefficient
10	488	10	Phycoerythrin / total pigment / chl- <i>a</i> / diffuse attenuation coefficient
11	531	10	Total pigment / chl- <i>a</i> / diffuse attenuation coefficient
12	551	10	Detached coccolith / phycoerythrin / total pigment / chl- <i>a</i> / diffuse attenuation coefficient
13	667	10	Phycoerythrin / chlorophyll fluorescence efficiency
14	678	10	Chlorophyll fluorescence efficiency
15	748	10	Chlorophyll fluorescence efficiency
16	869.5	10	Aerosols
17 - 19	-	-	Atmospheric water vapor
20 - 23	-	-	Surface / cloud temperature
24 - 25	-	-	Atmospheric temperature
26 - 28	-	-	Cirrus clouds, water vapor
29	-	-	Cloud properties
30	-	-	Ozone
31 - 32	-	-	Surface / cloud temperature
33 - 36	-	-	Cloud top altitude

The instrument MODIS is a cross-track scanner and has a scan-angle of $\pm 55^\circ$ and a swath width of 2330 km in across track and 10 km in along track direction. It has 36 channels from 400 nm to 14.4 μm . As in this work analysis of wavelength greater than 900 nm is irrelevant because no light penetrates into the ocean in this wavelength range, table 2.2 concentrates on MODIS' relevant bands for ocean color and its widths and applications. The interesting bands for ocean color have a spatial resolution of 1 km \times 1 km.

2.2.2.1. MODIS data processing

The processing flow for MODIS data sketched in Figure 2.8 describes two distinct branches: a near real time stream (NRT) and a refined stream. The process begins in either case with Level-0 data. Processing from Level-0 to Level-1A is performed using the standard code developed by the MODIS Science Data Support Team (SDST), known as MOD_PR01 (modis_l1agen in SeaDAS).

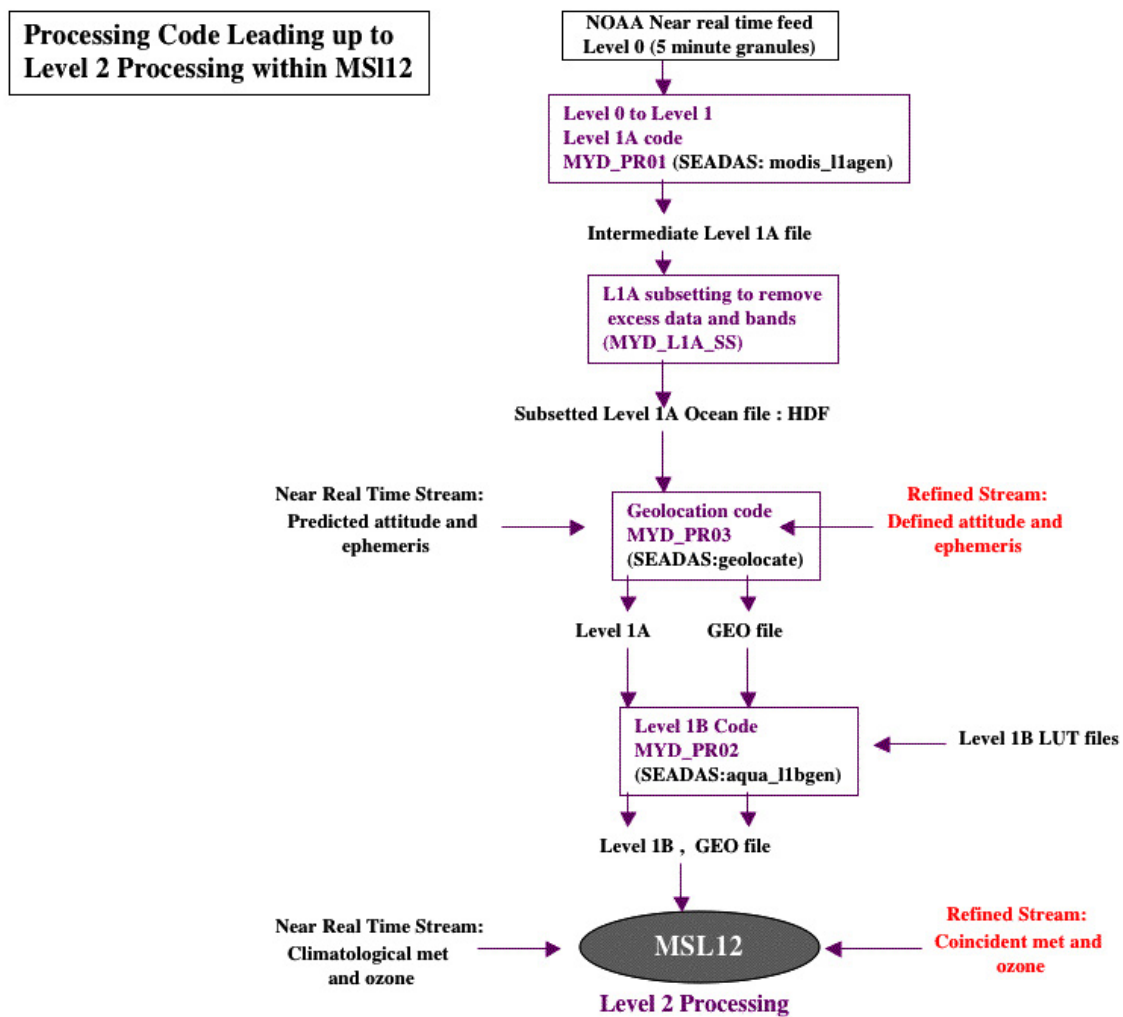


Figure 2.8.: Processing structure for MODIS data (Source: NASA)

The following step in the processing is to generate a geolocation file (GEO). This is performed using standard SDST code known as MOD_PR03 (geolocate in SeaDAS). Subsequently the Level-1A file and the GEO file are fed into the standard MYD_PR02 code developed and maintained by the MODIS Calibration Support Team (MCST) to produce the corresponding Level-1B file. The MYD_PR02 Level-1B code makes use of an instru-

ment calibration look-up table (LUT) that is derived from offline analysis of the MODIS solar diffuser measurements, lunar observations, and onboard lamps. LUTs are updated every few months, to improve tracking of the instrument calibration changes.

Level-2 processing is performed using the Multi-Sensor Level-1 to Level-2 (MSL12) code, which is developed and maintained by the Ocean Biology Processing Group. The Level-2 processing makes use of meteorological and ozone information from ancillary sources. In the NRT stream, climatological meteorological and ozone data are used.

2.2.2.2. MODIS flagging

- Clouds
The “CLDICE”-flag signifies probable cloud or ice contamination of the pixel. It is determined using a threshold at a wavelength of 865nm for cloud or atmospheric ice albedo.
- Bad water leaving reflectance
“LOWLW”-flag is set if the water-leaving radiance is very low. This is especially the case for cloud shadow.
If any band shows a negative water leaving radiance the flag “NEGLW” is set.
- Glint
High sun glint is indicated by the “HIGLINT”-flag. In case the glint reflection exceeds a value of 0.005 “HIGLINT”-flag is set.
Is the pixel contaminated with only moderate glint the “MODGLINT”-flag is set.

2.2.3. SeaWiFS

The source for information given in this section is Seelye (2004). Additional details can be found on the SeaWiFS website ⁸.

On board the SeaStar or OrbView-2 Spacecraft, that was developed by the Orbital Sciences Corporation (OSC) and launched in 1997, is the Sea viewing Wide Field of View Sensor (SeaWiFS). SeaStar operates in a sun-synchronous orbit at 705 km altitude and crosses equator at noon in a descending mode. The SeaWiFS sensor is sketched in Figure 2.9.

The SeaWiFS project has been originated with the main objective to acquire data that are interesting for the understanding of the role of oceans, including the exchange of critical elements and gases between the ocean and the atmosphere, and how these exchanges affect phytoplankton production.

The instrument is an across-track scanner with a scan-angle range of $\pm 58.3^\circ$ and thus a swath width of 2801 km in local area coverage mode (LAC). In global area coverage

⁸<http://oceancolor.gsfc.nasa.gov/SeaWiFS/>

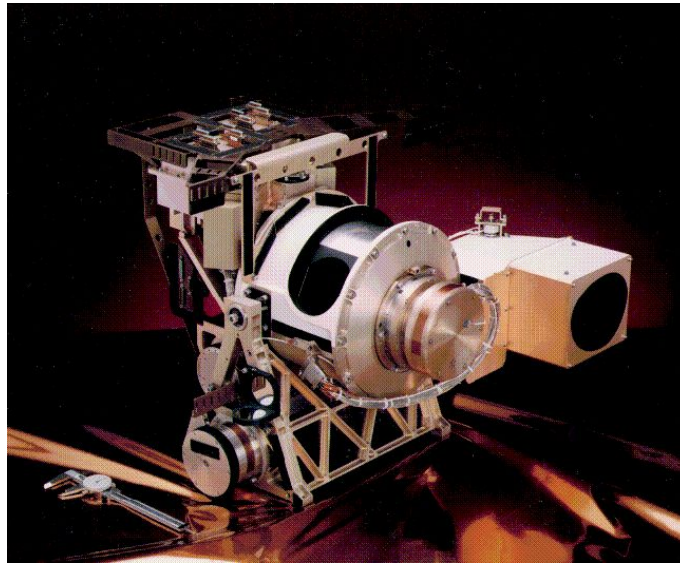


Figure 2.9.: SeaWiFS instrument on spacecraft SeaStar (Source: NASA)

Table 2.3.: SeaWiFS bands and applications

Band index	Band center in nm	Band width in nm	Applications
1	412	20	Dissolved organic matter (incl. yellow substance)
2	443	20	Chlorophyll absorption
3	490	20	Pigment absorption (case 2), K(490)
4	510	20	Chlorophyll absorption
5	555	20	Pigments, optical properties, sediments
6	670	20	Atmospheric correction and sediments (CZCS heritage)
7	765	40	Atmospheric correction, aerosol radiance
8	865	40	Atmospheric correction, aerosol radiance

mode (GAC) Seawifs has a scan-angle range of $\pm 45^\circ$ and reaches a swath width of 1502 km. Its spatial resolution is $1.1 \text{ km} \times 1.1 \text{ km}$ for LAC and $4.5 \text{ km} \times 4.5 \text{ km}$ for GAC. LAC data are broadcast continuously and recorded selectively, while GAC are recorded continuously on board the spacecraft.

SeaWiFS has eight spectral bands that are listed with their applications in Table 2.3.

2.2.3.1. SeaWiFS data processing

The data processing for SeaWiFS data is similar to the processing for MODIS data. Figure 2.10 gives an overview of the processing of SeaWiFS data which begins with Level-0.

The first step is to process SeaWiFS Level-0 to Level-1 data. This is performed by append-

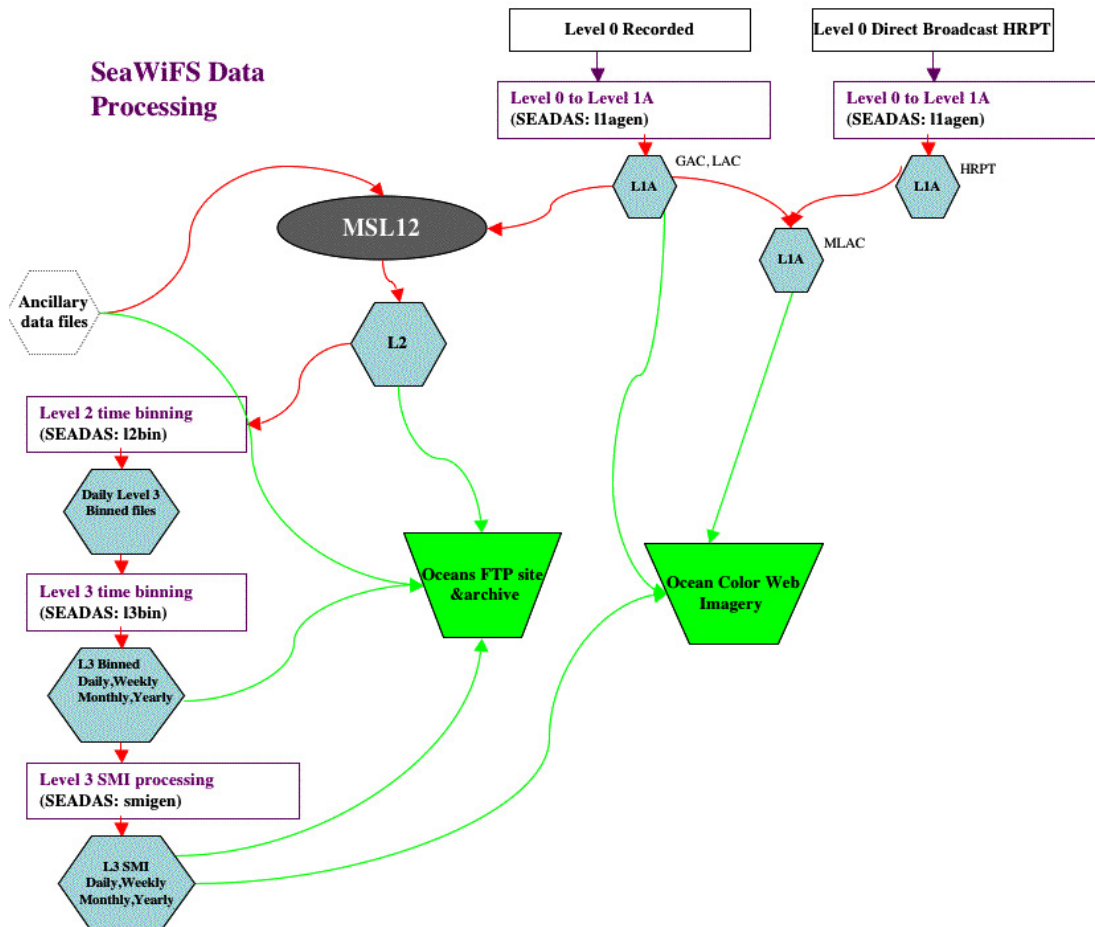


Figure 2.10.: Processing structure for SeaWiFS from Level-0 through Level-3

ing calibration data, navigation data, instrument telemetry information, and selected spacecraft telemetry information. The resulting Level-1A contains raw radiance values for each of the eight SeaWiFS bands.

Four types of Level 1 SeaWiFS data are processed by OBPG: GAC, LAC, HRPT, and MLAC.

- GAC data are subsampled and recorded onboard the spacecraft and subsequently downloaded twice a day at Wallops and NASA/Goddard. These data have an effective resolution of about 4.5 km along the center of the swath.
- LAC data are recorded at full 1.1 km resolution for selected parts of the world and downloaded with the GAC data.
- High Resolution Picture Transmission (HRPT) direct broadcast data have the same basic format and resolution as the LAC data, but they are collected by ground stations within range of the OrbView-2 spacecraft transmitter.
- Merged LAC (MLAC) data contains all available SeaWiFS HRPT and LAC data for

a given orbit. This is done by consolidating all SeaWiFS 1-km-resolution data which have been collected by various HRPT stations, as well as the LAC data recorded onboard the spacecraft into Level-1A files on a per orbit basis. For MLAC data, each product contains the best available full-resolution data for a single orbit, without duplication.

The second step in processing is to perform Level-2 scenes from the corresponding Level-1A scenes using the same Multi-Sensor Level-1 to Level-2 (MSL12) code as used for MODIS Level-2 processing.

Before computing Level-2 data, pixels are eliminated if they contain clouds, sun glint, or other abnormalities. For pixels that pass these screens, an atmospheric correction is applied to subtract the atmospheric scattering components from the total radiance to obtain the water-leaving radiances for bands 1-5.

Ancillary meteorological data and Ozone data are used for atmospheric correction in Level 2 processing. Other Level-2 processing steps include data navigation, computational steps to derive the geophysical products, and tests for anomalous conditions in the data.

2.2.3.2. SeaWiFS flagging

The flagging for SeaWiFS data is essentially the same as for MODIS data. See Section 2.2.2.2.

2.3. Radiometers

For *in-situ* data acquisition a set of RAMSES hyperspectral radiometers were used.

The RAMSES sensors were constructed for *in-situ* solar radiation measurement by TriOS GmbH (Germany) and consist of a Monolithic Miniature-Spectrometer (MMS) from Carl Zeiss AG (Germany).

The content of this chapter is based on the information from the manufacturers TriOS GmbH⁹ and Carl Zeiss AG¹⁰ about the products.

The principle MMS beam path is sketched in Figure 2.11. Light is detected by a bundle of 30 single optical fibres with a total diameter of 0.5 mm. The fibres are arranged in a linear order on the entrance side of the spectrometer. The light is going through a holographic grid and finally detected by a 256 channel photodiode.

The MMS and all required electronics like a low power microcontroller were combined by TriOS GmbH. A command controller enables the user to set sensor configuration, baud-rate, power management and more. The provided software MSDA_XE allows to

⁹www.trios.de

¹⁰www.zeiss.de

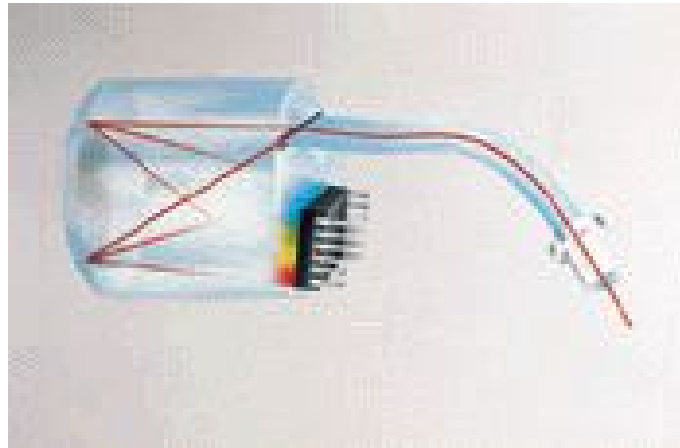


Figure 2.11.: Principle of beam path of Monolithic Miniature-Spectrometers used in RAMSES radiometers (Source: Carl Zeiss AG)



Figure 2.12.: RAMSES ACC-2 VIS radiometer (left side) and RAMSES ARC VIS radiometer (right side)

set measurement details, define integration times and automate measurements.

Two types of RAMSES sensors were used within data production for this thesis: RAMSES ARC VIS and RAMSES ACC-2 VIS (see Figure 2.12) measuring hyperspectral radiance and irradiance, respectively.

Both, ARC VIS and ACC-2 VIS provide measurements in the visible spectrum. They cover a wavelength range from 320 nm to 950 nm with a sampling every 3.3 nm. The spectral accuracy is 0.3 nm and the spectral resolution following the Rayleigh criterion is 10 nm. The Rayleigh criterion defines that two points are resolved if the distance of both main maxima is not smaller than the distance from one maximum to the successive minimum.

In both sensors there is an automatic dark current measurement: 20 - 30 of the 256 photo-diodes that are darkened with a black sheet in front of them measure the dark current with

each single measurement. In VIS sensors the infrared (IR) part of the spectrum (> 950 nm) is used for black current measurements. 190 channels remain usable for sampling.

The accuracy is according to manufacturer's data better than 6 % for the ARC VIS and better than 6 - 10 % for the ACC-2 VIS sensor. It is dependent on the spectral range. The integration time is definable by the user in a range from 4 ms to 8 s and can be set automatically in a range from 4 ms to 4 s.

The radiance measuring ARC VIS sensor has a FOV of 7°. A cosine collector is fixed in front of the irradiance sensor ACC-2 VIS to collect the light.

Both sensors can be connected to the IPS104 interface, that can be linked to the computer via USB or Serial Bus. MSDA_XE software automatically detects the IPS interface and all connected sensors and permits user defined settings for sampling.

Table 2.4.: RAMSES ARC VIS and RAMSES ACC-2 VIS technical details

Specification	RAMSES ARC VIS	RAMSES ACC-2 VIS
optical		
wavelength range*:	320 - 950 nm	
detector type*:	256 channel silicon photodiode array	
spectral sampling*:	3.3 nm/pixel	
spectral accuracy:	0.3 nm	
usable channels:	190	
detection		
field of view:	7° in air (can be optimized)	-
collector type:	-	cosine response
accuracy (depending on spectral range):	better than 6%	better than 6-10%
electrical		
integration time:	4 ms - 8 s (user selectable or auto [4 ms - 4096 ms])	
telemetry data interface:	RS232 or Serial Bus	
physical		
size:	Ø4.7 cm × 29.7 cm	Ø4.7 cm × 26 cm
weight in air:	1.0 kg (stainless steel / POM housing)	
depth range:	300 m	
operating temperature:	-10° C to +50° C	
* specifications from Carl ZEISS AG		

The sensors weigh approximately 1 kg, have a diameter of 4.7 cm and are 26 cm to 30 cm

long. They are suitable for operations down to 300 m depth and to temperatures from -10°C to $+50^{\circ}\text{C}$. Table 2.4 resumes all details and technical specifications of both, RAMSES ARC VIS and RAMSES ACC-2 VIS.

All sensors are calibrated in the factory previous to delivery. The user is issued with calibration certificates and corresponding calibration file for each single sensor. MSDA_XE is able to read in the calibration files for the used sensors and automatically save raw and calibrated data files within the measurement.

The produced data files in .dat format are the basis for further analysis.

3. *In-situ* Data Acquisition

3.1. Measurement method

The *in-situ* data were collected with three hyperspectral RAMSES radiometers. The instruments are described in section 2.3.

In order to determine the water leaving remote sensing reflectance R_{RS} above the sea surface as introduced in chapter 2, Equation 2.10, it is necessary to measure the downwelling irradiance E_d , upwelling radiance L_u and sky radiance L_s .

The experimental setup shown in Figure 3.1, comprises the irradiance sensor ACC-2 VIS measuring E_d vertical into the sky, and the two ARC-VIS radiance sensors in the same azimuthal plane measuring L_u and L_s in angles of $\theta = 40^\circ$ nadir and zenith, respectively. The radiance sensors are ideally oriented in an azimuthal angle of 135° relative to the sun.

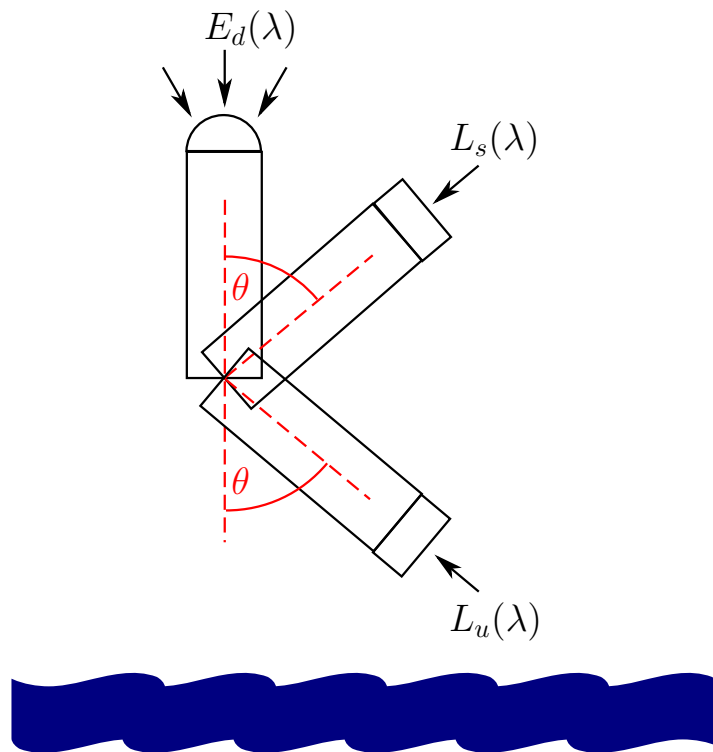


Figure 3.1.: Instrument set-up of three RAMSES hyperspectral radiometers that measure downwelling irradiance, E_d , downwelling sky radiance, L_s and upwelling radiance, L_u .

Sampling intervals are set to 10 s. All three variables E_d , L_u and L_s are measured simultaneously. To ensure a constant azimuth angle of 135° relative to the sun the steel frame is adjusted through a rotary joint.

Continuously during the cruise, the ships' sensors log the current position, weather conditions, water conditions like salinity and temperature and information about the ships' 3-dimensional orientation (heading, pitch and roll). These data are used to control *in-situ* data quality (for example: weather, pitch and roll) and to collocate *in-situ* data with satellite data (by position). A detailed description is given in chapter 4.

3.2. Measurement sites

Measurements analyzed in this thesis were carried out during three ship cruises with the German research vessel *RV Polarstern*.

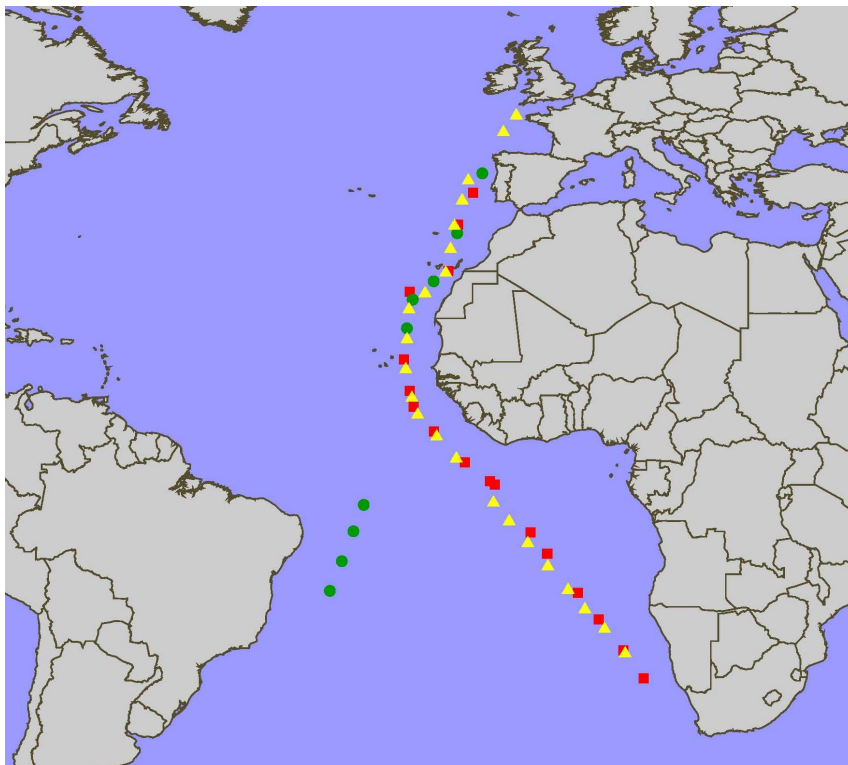


Figure 3.2.: Map with measurement sites during different cruises: red squares for ANT 24-1, green dots for ANT 24-4 and yellow triangles for ANT 25-1

The first cruise was ANT24-1 from Bremerhaven (Germany) to Cape Town (South Africa) in November 2007. In April to May 2008 the second cruise went from Punta Arenas (Chile) to Bremerhaven. The third cruise went from Bremerhaven to Cape Town in November 2008. Details on the cruises are given in Table 3.1.

Table 3.1.: *Overview: Ship cruises*

#	Cruise name	Ship	From	To	Start	End
1	ANT24-1	Polarstern	Bremerhaven	Cape Town	2007/10/26	2007/11/26
2	ANT24-4	Polarstern	Punta Arenas	Bremerhaven	2008/04/18	2008/05/20
3	ANT25-1	Polarstern	Bremerhaven	Cape Town	2008/11/03	2008/12/03

After installing the instruments on board, measurements usually started a few days after departure. The locations of measurement are plotted in Figure 3.2.

3.3. Measurement quality control

To minimize impacts from ship's shadow and reflection, the sensors were mounted in a steel frame as close to the bow of the ship as possible. The adjustment of the sensors in the steel frame is shown in Figure 3.3. It is not possible to install the instruments directly at the bow of *RV Polarstern*, so that measurements were taken from the side of the ship. Figure 3.4 shows the position of the sensors on *RV Polarstern*. The instruments' height

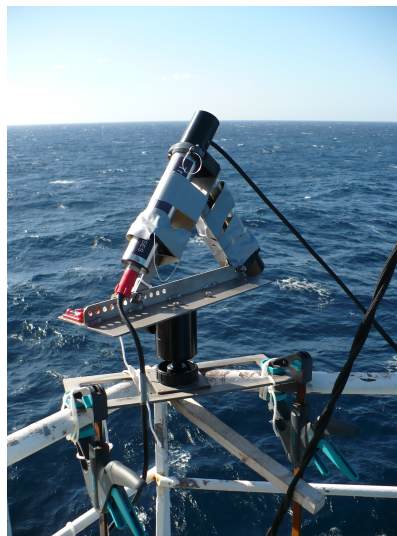


Figure 3.3.: *Steel frame with two RAMSES ARC VIS radiometers mounted on RV Polarstern*

above the water surface should ideally be small but due to technical limitations measurements were carried out at heights of approximately 15 m above sea level.

To prevent the interference of whitecaps, measurements were accomplished while the ship was stationary. This was done only for the two last cruises. During the first cruise, measurements were taken while ship was in motion with velocities of around 10 knots. Additionally, the limiting maximal wind speed was set to 10 m/s to minimize effects due to roughness of the ocean's surface.



Figure 3.4.: Sensor position on RV Polarstern (marked with red circle)

Sampling usually was done around noon to ensure comparability with satellite data, as the equator crossing time is around noon for all three satellite sensors.

One of the basic quality requirements for *in-situ* data acquisition is a nearly clear sky. As samples drastically decrease in number with this requirement strictly applied, the demand was loosened to “no heavy clouds”. To increase data quality, the sky requirement can be raised again in data processing.

The experimental quality requirements for *in-situ* data sampling summarized:

- mount sensors close to the bow
- minimize height above surface if possible (here: approximately 15 m)
- no heavy clouds
- sampling around noon
- windspeed <10 m/s to avoid rough sea
- ship stationary to avoid whitecaps (not valid to the measurements from first cruise ANT 24-1!)

Some additionally quality test were performed during data processing as described in the following chapter.

4. Analysis

Data analysis can be divided in three sections: Initially, in the course of data processing, a quality control has to be done with both, *in-situ* and satellite data. In a second step collocations are determined between *in-situ* and remotely sensed data. Finally the validation itself is accomplished and interpreted with the help of statistical indicators.

4.1. Data processing

This section describes the process that is applied to both, *in-situ* and satellite data. An initial quality control is applied to the *in-situ* data after measurements have been accomplished and the provided Level-2 satellite data.

Subsequently the remote sensing reflectance is computed.

4.1.1. *In-situ* data quality control

The quality requirements for data sampling are described in detail in chapter 3.

Quality tests are obtained from Wernand (2002): To ensure a minimum amount of incoming solar light E_d , measurements with a value smaller than $20 \frac{mW}{m^2 nm}$ at a wavelength of $\lambda = 480 nm$ are neglected.

- By the band ratio of $E_d(\lambda = 470 nm)$ and $E_d(\lambda = 680 nm)$ the shape of the incoming solar radiation is checked. Usually,

$$\frac{E_d(\lambda = 470 nm)}{E_d(\lambda = 680 nm)} > 1$$

for normal daylight spectra.

- The precipitation test:

$$\frac{E_d(\lambda = 940 nm)}{E_d(\lambda = 370 nm)} < 0.2$$

was applied in the early stages of data analysis. But, as it flagged all data sets even if they were sampled under ideal sunny clear sky conditions, this test was not applied to the data of this thesis. Reasons for the precipitation test to fail at the *in-situ* data within this study may be due to the developed tests in Wernand (2002) were taken

at the coast near Den Helder (Netherlands) and verified with ship cruises across the North Sea. Optical conditions are certainly different for open ocean waters (compare chapter 2) and may lead to a failure of this test applied to data collected across the Atlantic Ocean.

- From the ship's position data and the particular date of measurement, solar elevation is calculated for each single measurement to exclude data with a solar zenith angle smaller than 6° .
- The ships' pitch and roll must be less than 5° at the point of measurement to reduce the variability of the viewing angles.
- Data sets passing all of the above described tests are used for further analysis.
- After the water leaving remote sensing reflectance ρ_w is calculated for each set of *in-situ* data (described in section 4.1.3), that passed the previous tests, the downwelling irradiance E_d is checked for variations to make sure no small clouds contaminate the sample. This is realized by discarding all E_d measurements that differ for more than 10 % from the successive or the previous measurement. The resulting batches of fairly "constant" E_d are saved and averaged. Through a temporal alignment the corresponding ρ_w batches are saved as well and can be used to validate the satellite remote sensing data (see section 4.2).
- Before the validation process is started all *in-situ* R_{RS} are checked manually for obviously wrong measurements, for example negative R_{RS} . Reasons for such measurements can be that L_u measurements are affected by whitecaps, waves or direct reflections into the sensor due to ships movement.

4.1.2. Satellite data quality control

Satellite data quality is mainly checked by flagging mechanisms. These are developed and applied to the lower level satellite data by ESA and NASA. Therefore, the used Level-2 data are already flagged. Detailed flagging procedure information is given in section 2.2.

Downloaded satellite Level-2 data are initially reduced to the relevant areas by searching for collocations with *in-situ* data as described later.

The flags considered and annotated with the respective exported ROI are summarized with their descriptions in Table 4.1.

Table 4.1.: *Flags of satellite data considered in this study and their description*

MODIS / SeaWiFS		MERIS	
flag	meaning	flag	meaning
CLDICE	Cloud and / or ice	CLOUD	Cloud product available
HIGLINT	Severe sun glint	high_glint	High (uncorrected) glint
NEGLW	Negative water-leaving radiance in any band		
LOWLW	Low water-leaving radiance at 555 nm		
MODGLINT	Moderate sun glint	medium_glint	corrected for glint
		pcd_1_13	uncertain normalized surface reflectance

As described in section 2.2 MODIS and SeaWiFS CLDICE flag causes the respective pixels' reflectance to be set to zero. These zeros have to be eliminated before averaging over all exported pixel data.

After ρ_{meris} , ρ_{modis} and $\rho_{seawifs}$ are extracted for each collocation, the results are divided into different categories depending on their ROIs' contamination with flags. The different classifications are given in Table 4.2 with their respective description.

The categories *clouds* and *mixed* are divided into subcategories due to their percentage of pixel contamination. Classification *mixed* is applied to all collocation pixels that are not dominated by one single flag but several. Another section is *glint*, divided into a *high* and a moderate or medium *mod* part. The categories *pcd_1_13* and *neg/low L_w* are special for MERIS and for MODIS and SeaWiFS collocations, respectively. The last category is defined as *no_flags* where no flags at all are set within the ROI.

A kind of superordinate classification is defined for collocations that did not belong to the "bad" classifications "clouds_high", "clouds_med" and "clouds_low", "glint_high", "pcd_1_13", "neg or low L_w " and "mixed_high". The collocations in this "no bad" classification containing all collocations from the classifications "no flags", "med glint", "low mixed" and "med mixed".

Statistical interpretations are applied following these classifications. Details are given in section 4.3.

4.1.3. Water leaving remote sensing reflectance ρ_w calculation and further processing

The next step in analysis is calculation of *in-situ* remote sensing reflectance from the measured quantities E_d , L_u and L_s . Using equations 2.10 and 2.11 the water leaving remote sensing reflectance is computed with:

Table 4.2.: Classification of collocations according to their ROIs' contamination with flags

Classification	meaning
clouds_high	> 66 % of ROIs' pixel with CLOUD or CLDICE flag
clouds_med	33 % - 66 % of ROIs' pixel with CLOUD or CLDICE flag
clouds_low	< 33 % of ROIs' pixel with CLOUD or CLDICE flag
glint_high	HIGLINT or high_glint flags dominate ROIs' flagging
glint_mod	MODGLINT or medium_glint flags dominate ROIs' flagging
pcd_1_13	pcd_1_13 flag dominates ROIs' flagging
neg/low L_w	NEGLW or LOWLW flag dominates ROIs' flagging
mixed_high	no single flag dominating but > 66 % of ROIs' pixel contaminated with any flag
mixed_med	no single flag dominating but 33 % - 66 % of ROIs' pixel contaminated with any flag
mixed_low	no single flag dominating but < 33 % of ROIs' pixel contaminated with any flag
no_flags	none of the ROIs' pixels are flagged

$$R_{RS} = \frac{L_u - \rho_{as} L_s}{E_d} \quad (4.1)$$

To be consistent with the MERIS definition of the reflectance product R_{RS} is further multiplied by π :

$$\rho_w = \pi R_{RS} \quad (4.2)$$

All input variables E_d , L_u and L_s that are measured in approximately 3.3 nm intervals are interpolated to 1 nm intervals and ρ_{as} is computed for every single wavelength in the range of 350 nm to 950 nm.

The Fresnel reflection coefficient ρ_{as} is determined using an algorithm developed by Roland Doerffer (see Doerffer (2008)). The algorithm calculates the Fresnel reflection coefficient, ρ_{as} , as a function of wavelength, actual salinity and water temperature that are recorded by the ships' sensors. Further the effect on specular reflectance is considered in the algorithm and the effect of wind is considered by adding two summands to the algorithm calculated $\rho_{as}(\text{algorithm})$ (see Park et al. (2006)):

$$\rho_{as} = \rho_{as}(\text{algorithm}) + 0.00039 \cdot w + 0.000034 \cdot w^2 \quad (4.3)$$

with the wind velocity w in $\frac{m}{s}$.

The ρ_{as} is calculated for a wavelength range from 350 nm to 950 nm in 2.5 nm intervals. To be consistent with the *in-situ* water leaving remote sensing reflectance ρ_w the Fresnel

reflectance is interpolated to 1 nm intervals.

For each batch of “constant” E_d (see section 4.1.2) ρ_w was averaged. This was done for all batches and all collocations.

4.2. Validation process

First part of the validation is to determine the respective match-up data. Satellite data were considered within a time margin of one day previous to one day after the *in-situ* data sampling time and within a location of 3×3 pixels around the pixel in which the *in-situ* measurement was taken.

In case of the first cruise where *in-situ* data were obtained during the ship was in motion, the average latitude and longitude were determined through a temporal alignment with the position data provided by the ship. This average position for the *in-situ* was the basis for the determination of the relevant satellite image pixels. Thresholds were calculated for all satellite instruments to define a local area in the satellite image around the *in-situ* position that are of the same dimension as the 3×3 pixels extraction done for the other cruises.

The MERIS water leaving remote sensing reflectance ρ_{meris} is extracted from the product. For MODIS and SeaWiFS the provided water leaving radiance product is transformed into ρ_{modis} and $\rho_{seawifs}$, respectively, using equations 2.11, 2.10 and 4.2, to allow a homogeneous validation process.

Additionally the chl-*a* Level-2 products from all three satellite instruments are validated with *in-situ* chl-*a* measurements obtained from water samples taken during the cruises. The *in-situ* chl-*a* data were provided with High Performance Liquid Chromatography (HPLC) by Bettina Schmitt and Erika Allhusen (PHYTOOPTICS).

As the chl-*a* concentration retrieval is based on algorithms using a reflectance ratio (see chapter 2) the validation is done for the ratios as well. The wavelength $\lambda_1 = 443 \text{ nm}$ (for SeaWiFS, MODIS and *in-situ*) $\lambda_1 = 442.5 \text{ nm}$ (for MERIS) and $\lambda_2 = 560 \text{ nm}$ (for MERIS), $\lambda_2 = 551 \text{ nm}$ (for MODIS) $\lambda_2 = 555 \text{ nm}$ (for SeaWiFS and *in-situ*) are chosen.

The used satellite bands and wavelengths are summarized in Table 4.3. For each sensor the respective *in-situ* wavelength range was considered within validation.

Table 4.3.: Validated wavelength bands for MERIS, MODIS and SeaWiFS

	approximated center wavelength of band in nm												
MERIS:	412.5	442.5	490	510	560	620	665	680	708	753	778	864	885
MODIS:	412.5	443	488	531	551		667						
SeaWiFS:	412	443	490	510	555		670						

Validation is established for each collocation and each batch. Conclusive plots and scatterplots are produced and necessary statistical parameters are calculated as described in section 4.3.

4.3. Statistical interpretation and valuation process

The validated data are plotted in comparison to the *in-situ* data for each batch of each collocation. Additionally scatterplots are created for every batch of every collocation. A linear regression is applied to the validating data in the scatterplots with MATLAB command "polyfit" that does a linear fit to the *in-situ* and the remotely sensed data and produces slope m and intercept n . The correlation coefficient r^2 is calculated by MATLAB command "corrcoeff" and given in every plot. The parameters are given in the title of the respective plot and scatterplot.

Statistical interpretation is done with the flags-categorized results (see section 4.1.2).

4.4. Uncertainties

The assumed uncertainties for derived *in-situ* reflectances for ρ_w following Antoine et al. (2008) are around $\Delta\rho_w = 6\%$.

As the height of the radiometers above the water is quite large and the wind is only taken into account as a quadratic function through ρ_{as} , the uncertainty might be larger than 6%. Uncertainties from unstable viewing angles due to ship movements and waves can be neglected since the ships' pitch and roll data are checked during analysis.

The temporal distance of \pm one day from the *in-situ* measurement point of time to satellite data time is large and may result in differences in the comparisons to satellite data. Nevertheless, it is a reasonable interval on the evidence of open ocean waters.

The differences between the temporally short and spatially large satellite measurements and the temporally long and spatially small *in-situ* remote sensing reflectance measurements are estimated to compensate each other because in either case a large number of different conditions (waves, local windspeed,...) are measured and averaged. As the samples for *in-situ* chl-*a* determination were taken during very short temporal intervals, the discrepancy between *in-situ* chl-*a* and satellite measurements may be larger than the discrepancy between *in-situ* remote sensing reflectance and satellite measurements.

5. Results and Discussion

The validation of collocated satellite remote sensing reflectance with *in-situ* data will be described in detail for the different classifications. As a second part of the analysis the satellite chl-*a* products and the underlying band ratios will be validated with the corresponding RAMSES remote sensing reflectance ratios and *in-situ* measured chl-*a* concentrations. All results will be interpreted and discussed in the last section of this chapter.

5.1. Results

5.1.1. Validation of collocated satellite water leaving remote sensing reflectance with *in-situ* data

Comparisons between satellite water leaving remote sensing reflectance ρ_{meris} , ρ_{modis} and $\rho_{seawifs}$ and *in-situ* ρ_w were accomplished for every batch of constant E_d and every collocation for all three satellite instruments. Additionally, scatterplots were produced for every batch and every collocation to quantify the agreements. As not all figures can be given here, only a few examples are depicted.

Two comparisons for not flagged collocations are shown in Figures 5.1 and 5.3. The remote sensing reflectance is proportional to the inverse wavelength so that the high reflectances correspond to low wavelengths in the plots. The corresponding scatterplots shown in Figures 5.2 and 5.4 show the respective linear regression and the correlation coefficient.

MERIS shows a good agreement in the first example with a correlation coefficient of $r^2 = 0.99$. Other batches of this collocation show similar results.

Although the conditions are the same as in the previous example (no flags), MODIS measurements do not agree as well with the *in-situ* measurements (Figures 5.3 and 5.4). There are large discrepancies between remotely sensed data and *in-situ* data in the lower wavelength bands, especially in the first wavelength band at 412 nm. This variability was found for all three satellite instruments, with highest differences for MODIS and SeaWiFS data.

In terms of a better overview it is not reasonable to show and discuss the Scatterplots $\rho_{satellite}$ versus *in-situ* ρ_w for every batch of constant E_d or for every day. Therefore, the results are presented for the single classifications (see Section 4.1.2).

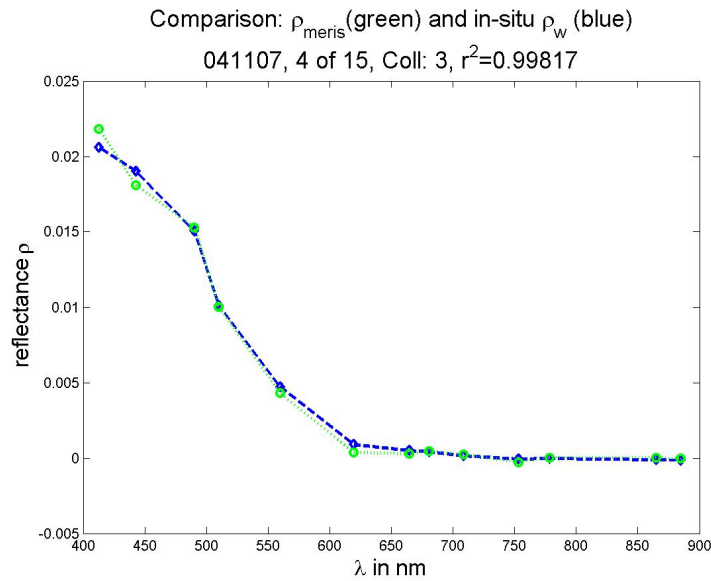


Figure 5.1.: Remote sensing reflectance of collocated measurements of MERIS, ρ_{meris} , and in-situ, ρ_w , for the 4th of November 2007

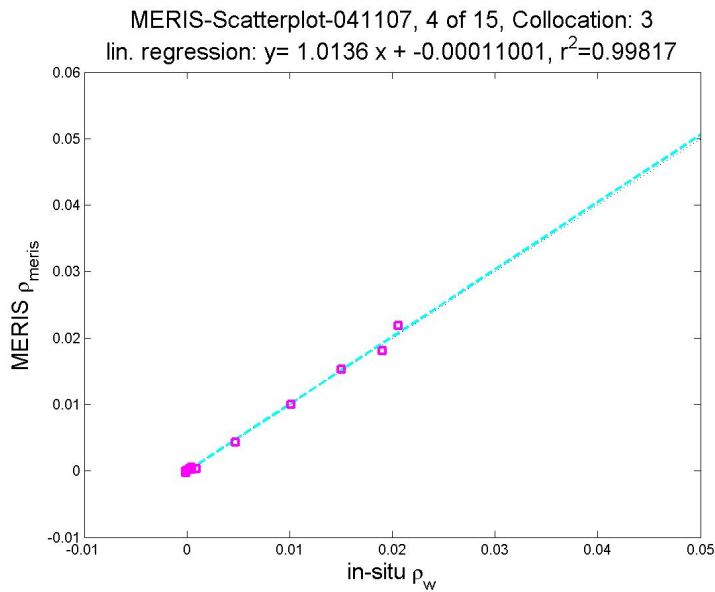


Figure 5.2.: Comparison of reflectance of collocated measurements of MERIS, ρ_{meris} , and in-situ, ρ_w , for the 4th of November 2007. The dashed black line is the angular bisector (1:1-line).

5.1.1.1. Superclassifications “all data”, “all without cloud flagged data” and “no bad” data

The scatterplots in Figures 5.5, 5.6 and 5.7 show comparisons of remote sensing reflectance ρ of all three satellite instruments (SeaWiFS blue, MODIS red and MERIS green) for all wavelength bands to collocated in-situ ρ_w measurements for all data (Figure 5.5),

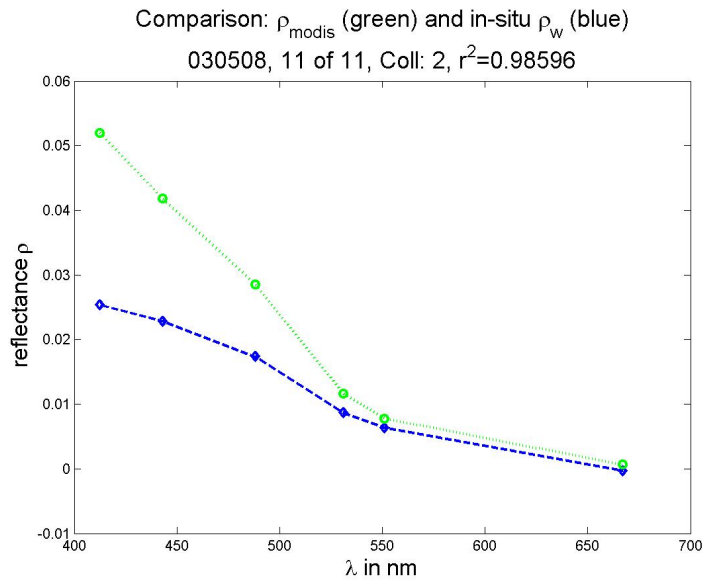


Figure 5.3.: Remote sensing reflectance of collocated measurements of MODIS, ρ_{modis} , and in-situ, ρ_w , for the 3rd of May 2008

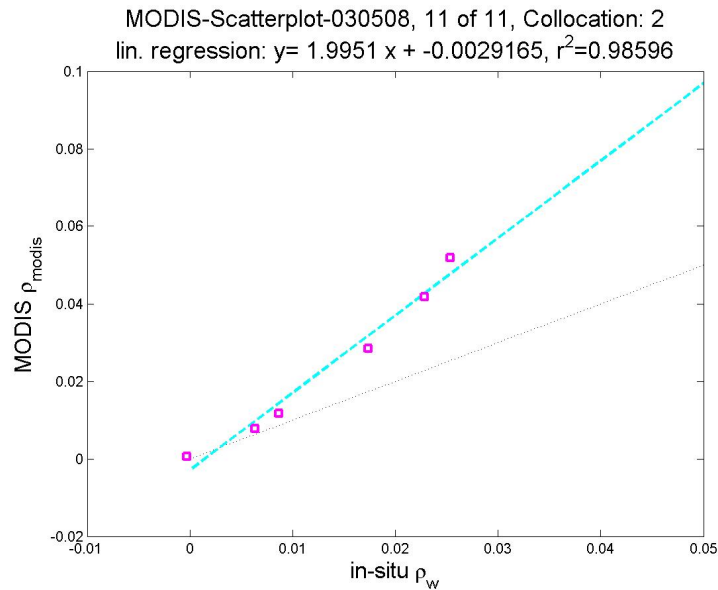


Figure 5.4.: Comparison of reflectance of collocated measurements of MODIS, ρ_{modis} , and in-situ, ρ_w , for the 3rd of May 2008. The dashed black line is the angular bisector (1:1-line).

all data but cloud flagged (Figure 5.6) and “no bad” data (Figure 5.7) as defined before. The variable “N” in the Figure headlines denote the amount of analyzed batches from all collocations.

The collocations in the superordinate “no bad” classification are listed in Table A.2, whereas Table 5.1 gives the different numbers of collocations for the different classifications in the “no bad” class.

Only a few collocations for each satellite instrument contribute to the “no bad” class. SeaWiFS has only three collocations in this category and none of them are not flagged. MERIS contributes with slightly more collocations and MODIS shows the largest number of collocations in the “no bad” classification with 15 all together.

As it will be discussed in Section 5.1.1.3 Figure 5.5 for all data illustrates the large dis-

Table 5.1.: List of contributed flagged collocations to the “no bad” classification containing only “no flags”, “medium glint”, “low mixed” and “medium mixed” classified collocations

Classification	Number of collocations		
	SeaWiFS	MODIS	MERIS
medium glint	2	4	2
medium mixed	1	4	3
low mixed	-	1	-
not flagged	-	6	4

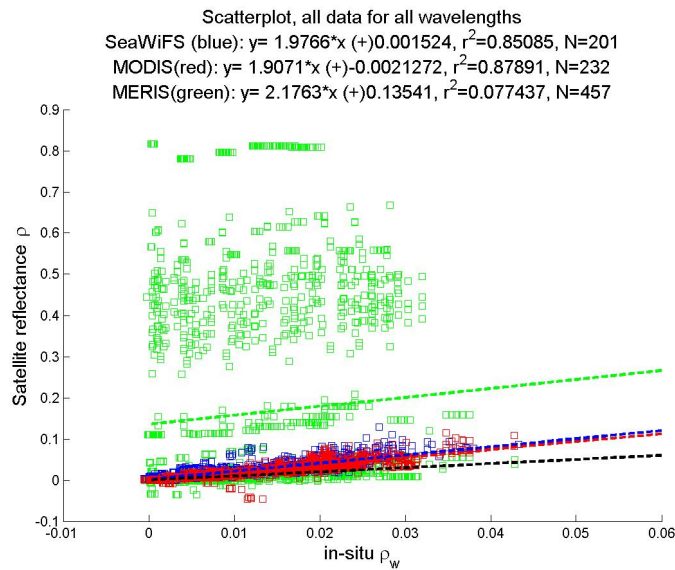


Figure 5.5.: Comparison of reflectance ρ of satellite instruments MERIS, MODIS and SeaWiFS for all data and all wavelength bands to collocated *in-situ* remote sensing reflectance measurements, ρ_w . The dashed black line is the angular bisector (1:1-line).

agreements of MERIS data and slightly better agreements of MODIS and SeaWiFS data with RAMSES *in-situ* measurements. This is due to the fact that the Level-2 algorithms of MODIS and SeaWiFS clear all reflectance measurements of a pixel if it is “cloud”-flagged. That effect is visible in Figure 5.6 where all data except cloud classified are plotted. The correlation coefficient for the MERIS measurements is much higher than in the previous plot, although the agreement of all satellite data with the RAMSES data is still poor.

The best correlation to *in-situ* data can be seen for SeaWiFS, when each wavelength is analyzed separately for all but cloud flagged data (see Figure A.2). MODIS low wavelengths

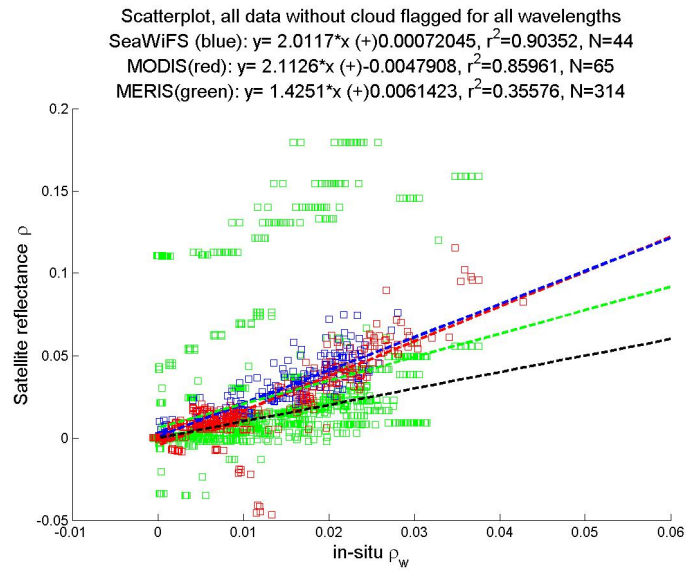


Figure 5.6.: Comparison of reflectance ρ of satellite instruments MERIS, MODIS and SeaWiFS for all - except cloud flagged - data and all wavelength bands to collocated *in-situ* remote sensing reflectance measurements, ρ_w . The dashed black line is the angular bisector (1:1-line).

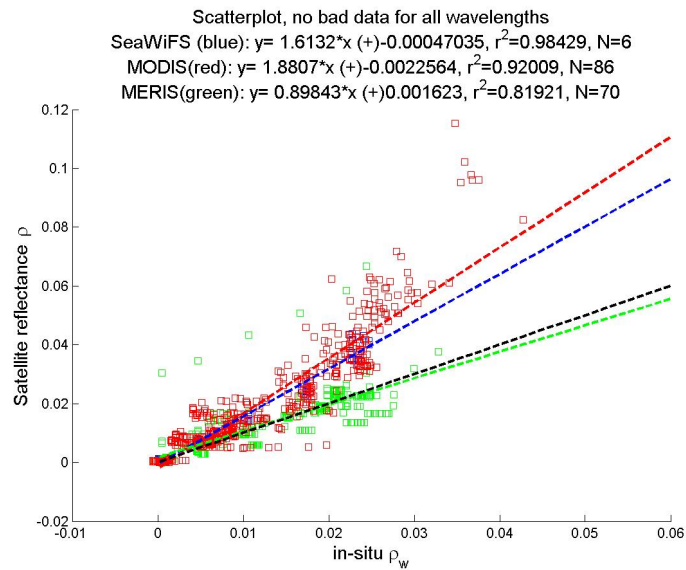


Figure 5.7.: Comparison of reflectance ρ of satellite instruments MERIS, MODIS and SeaWiFS for “not bad”-flagged data as defined in Table A.2 and all wavelength bands to collocated *in-situ* remote sensing reflectance measurements, ρ_w . The dashed black line is the angular bisector (1:1-line).

indicate poorer agreements to *in-situ* data than the higher bands. The large disagreements between *in-situ* and MERIS measurements could be seen in every wavelength band.

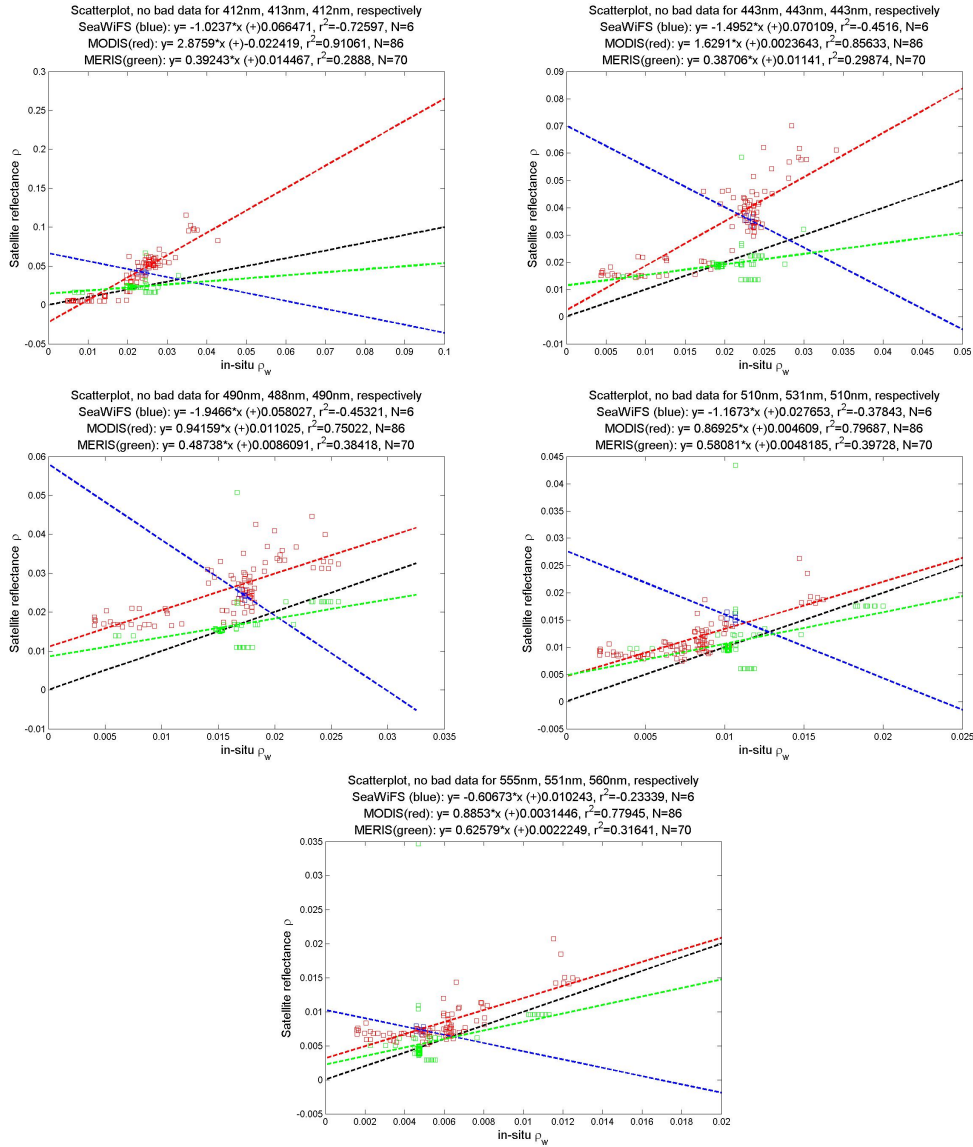


Figure 5.8.: Comparisons of reflectance ρ of satellite instruments MERIS and MODIS for “not bad”-flagged data as defined in Table A.2 to collocated *in-situ* remote sensing reflectance measurements, ρ_w , for different wavelength bands. The dashed black line is the angular bisector (1:1-line).

Neglecting all “bad” flagged collocations as described above and summarized in Table A.2 and 5.1 leads to Figure 5.7. The regression lines shows better values and correlation coefficients are increased to satisfying values, particularly for MERIS.

The wavelength separated plotting of “not bad” flagged data shown in Figure 5.8 and the summarized statistical values in Table 5.2 indicate a bad correlation for SeaWiFS measurements. Since the number of collocated SeaWiFS measurements is small ($N_{seawifs} = 3$) and the values are very close together the regression line for each single wavelength plot

Table 5.2.: Resulting statistical values slope m , intercept n and correlation coefficient r^2 from the comparison of “no bad” satellite data with *in-situ* reflectance for the wavelength bands

wavelength band in nm	SeaWiFS			MODIS			MERIS		
	m	n	r^2	m	n	r^2	m	n	r^2
412 / 412.5	-1.02	0.07	-0.72	2.87	-0.02	0.91	0.39	0.01	0.28
442.5 / 443	-1.49	0.07	-0.45	1.62	<0.01	0.85	0.38	0.01	0.29
488 / 490	-1.94	0.05	-0.45	0.94	0.01	0.75	0.48	<0.01	0.38
510 / 531	-1.16	0.02	-0.37	0.86	<0.01	0.79	0.58	<0.01	0.39
551 / 555 / 560	-0.6	0.01	-0.23	0.88	<0.01	0.77	0.62	<0.01	0.31

is not significant. All SeaWiFS values lie within the range of MERIS and MODIS values. The comparisons to the later two show fairly good regression lines. MODIS higher wavelength bands reveal better agreements than lower bands for *in-situ* measurements. The same holds for MERIS although its accordance with *in-situ* measurements is poorer than MODIS’.

5.1.1.2. Not flagged

The classification “not flagged” gives the best results for validation between satellite data and the *in-situ* measured reflectance, as the satellite data are not contaminated by any significant flag. Unfortunately, no SeaWiFS collocations are available for this category. MERIS and MODIS contribute four and six collocations, respectively with 20 batches and 31 batches, respectively. Figure 5.9 shows a good correlation of MERIS data with *in-situ* data for all wavelength bands pooled together (correlation coefficient $r^2 = 0.92$ and slope $m = 0.95$).

MODIS (red) provides an even better correlation ($r^2 = 0.95$) but its values are generally larger than the *in-situ* values ($m = 1.56$).

In Figure 5.10 the same data has been divided into the different wavelength bands. MODIS remote sensing reflectance mostly shows a positive intercept and always a positive slope of the regression line. Most of the values are too high regarding the corresponding *in-situ* ρ_w . The best match is obtained at 531 nm, 412 nm again shows the poorest agreement.

MERIS, on the other hand, generally shows regression lines with a slope smaller than one. At all wavelength bands MERIS data show better results than MODIS data as the regression line for all single wavelength band traverses the 1:1-line near the centroid of the data points.

For the MERIS-*in-situ* comparison, the larger the wavelength, the worse the slope of the regression line and the correlation coefficient become. The best result is obtained for the 443 nm wavelength band.

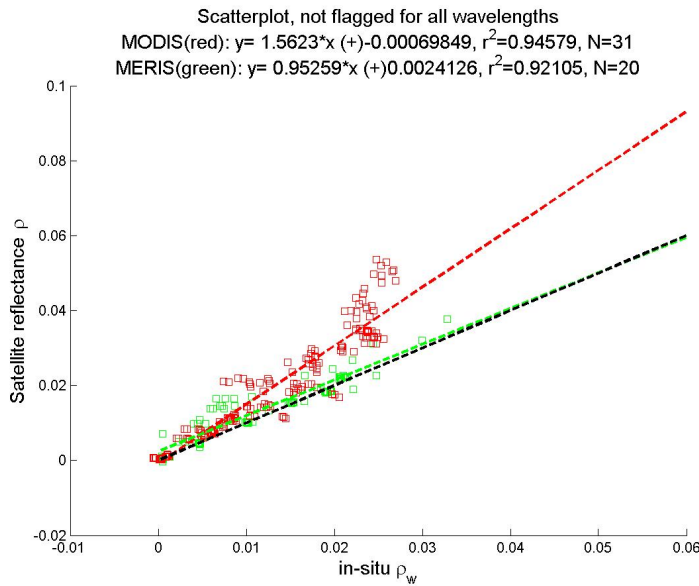


Figure 5.9.: Comparison of reflectance ρ of satellite instruments MERIS, MODIS and SeaWiFS for “not flagged” classification and all wavelength bands to collocated *in-situ* remote sensing reflectance measurements, ρ_w . The dashed black line is the angular bisector (1:1-line).

5.1.1.3. Cloud flagged

Classification of cloud flagged data is divided in high, medium (med) and low cloud flagged collocations (see Chapter 4).

MERIS “high cloud” classified remote sensing reflectances shows no correlation at all with the *in-situ* measurements, while MODIS and SeaWiFS data correlate better (Figure 5.11). SeaWiFS and MODIS flagging algorithm sets all cloud flagged pixels to zero. These pixel are deleted in the analysis process and as a result the not-cloud-flagged pixels of the collocation are considered in the validation process. MERIS however, keeps the values of the cloud flagged pixels, but due to high reflection from clouds into the satellite sensor these measurements are useless for information about water leaving reflectance or water constituents.

Figure 5.12 shows the comparison of MODIS and SeaWiFS to *in-situ* data in a different scale. MODIS and SeaWiFS reflectances are twice as high as the collocated *in-situ* data. The regression lines have slopes of $m = 2.45$ and $m = 1.82$ for SeaWiFS and MODIS, respectively. This might be due to the vicinity of cloud flagged pixels. Although all cloud flagged pixels are neglected for both satellite instruments during the Level-2 algorithm, the remaining pixels can be contaminated by possible cloud shadows. Furthermore, other flags can occur on the remaining pixels as well.

Similar results for all wavelengths were found for moderate and low cloud flagged data due to the same reasons (see Figures 5.13 and 5.14 or Figure A.5). The effect is slightly smaller as there are less cloud flagged pixels in the ROI for MODIS and SeaWiFS than in the “high cloud” flagged category. MERIS medium cloud flagged regression line shows a

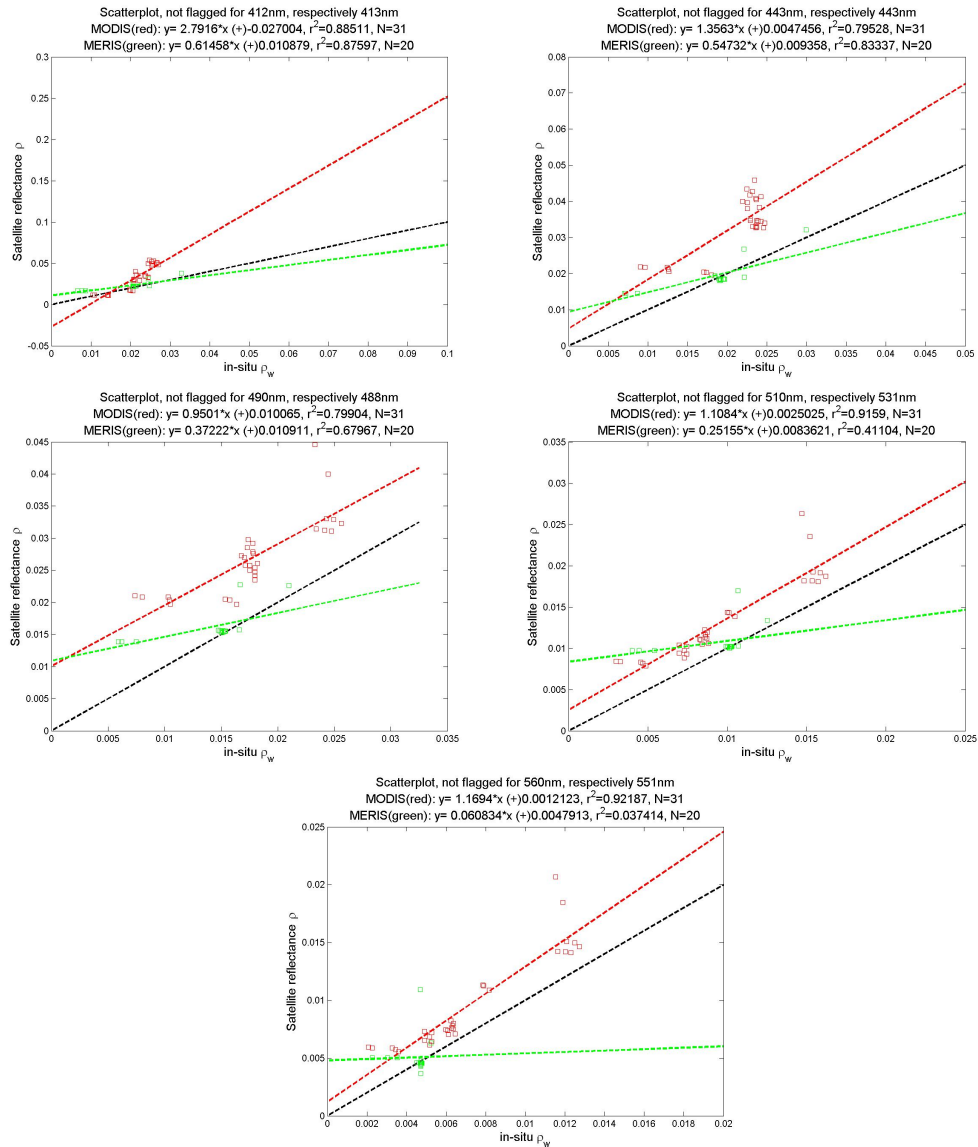


Figure 5.10.: Comparisons of reflectance ρ of satellite instruments MERIS and MODIS for “not flagged” classification to collocated *in-situ* remote sensing reflectance measurements, ρ_w for different wavelength bands. The dashed black line is the angular bisector (1:1-line).

large intercept and the correlation coefficient is small. Unfortunately, there are no MERIS low clouds flagged data.

5.1.1.4. Glint flagged

High glint flagged collocations are available for MERIS and MODIS only (see Figure 5.15). MODIS has only one collocation (with five batches of constant E_d) flagged with high glint. The satellite data are generally two to three times higher than the *in-situ* data. MERIS often shows negative ρ_{meris} for large wavelengths, but a better match with the

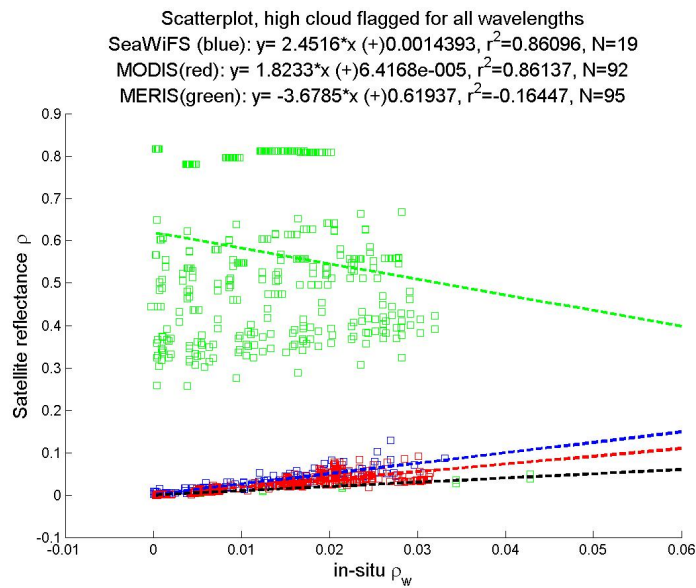


Figure 5.11.: Comparison of reflectance ρ of satellite instruments MERIS, MODIS and SeaWiFS for “high cloud” classification and all wavelength bands to collocated *in-situ* remote sensing reflectance measurements, ρ_w . The dashed black line is the angular bisector (1:1-line).

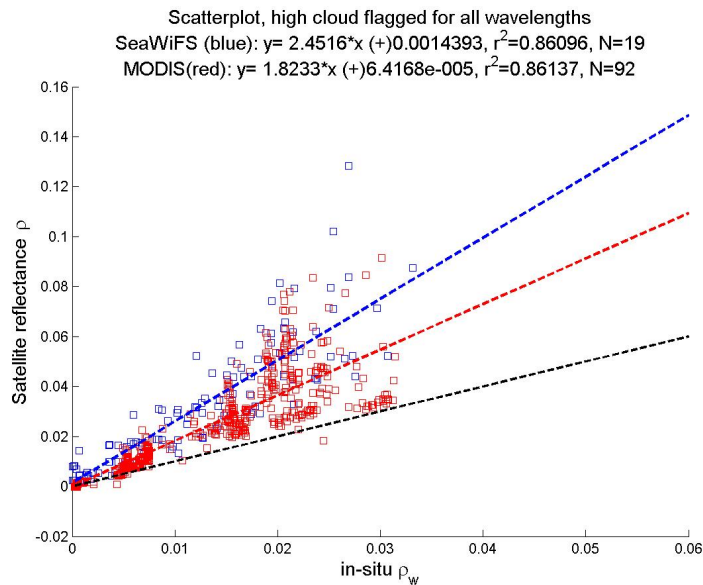


Figure 5.12.: Same Figure as 5.11 but with a different scale for the y-axis and data of the MERIS-*in-situ* comparison are excluded.

in-situ reflectance for smaller wavelengths (see Figure A.9 in Appendix). Nevertheless, the 412 nm band shows poor agreements. Overall there is a weak correlation (linear regression: $y = 1.45x + 0.01$) but with many outliers.

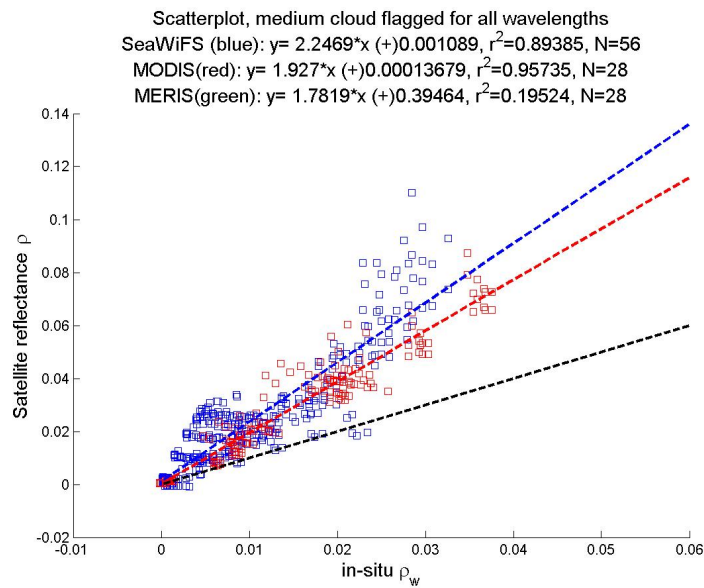


Figure 5.13.: Comparison of reflectance ρ of satellite instruments MODIS and SeaWiFS for “medium cloud” classification and all wavelength bands to collocated *in-situ* remote sensing reflectance measurements, ρ_w . The dashed black line is the angular bisector (1:1-line).

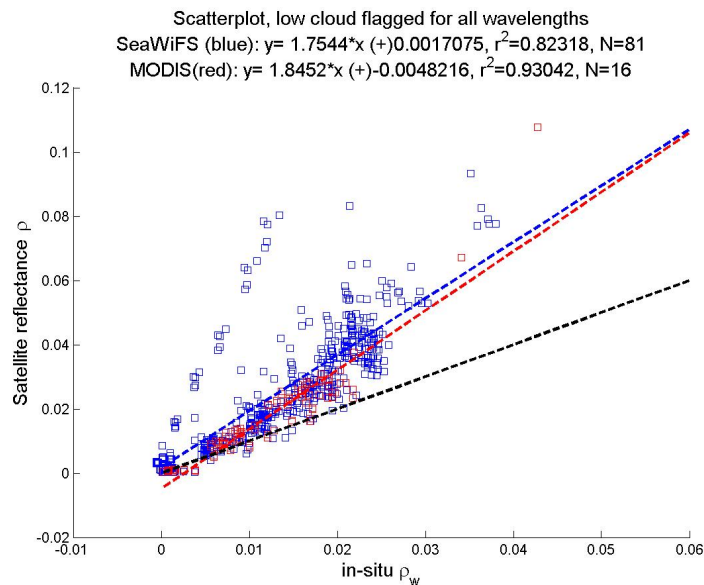


Figure 5.14.: Comparison of reflectance ρ of satellite instruments MODIS and SeaWiFS for “low cloud” classification and all wavelength bands to collocated *in-situ* remote sensing reflectance measurements, ρ_w . The dashed black line is the angular bisector (1:1-line).

Moderate or medium glint flagged satellite data are available for all three sensors (see Figure 5.16). All MERIS Level-2 products are corrected for medium or moderate glint. Thus, the conformity with the *in-situ* data is a sign for the quality of the medium glint correction procedure. MERIS shows an overall good agreement ($r^2 = 0.78$ and $m = 1.11$).

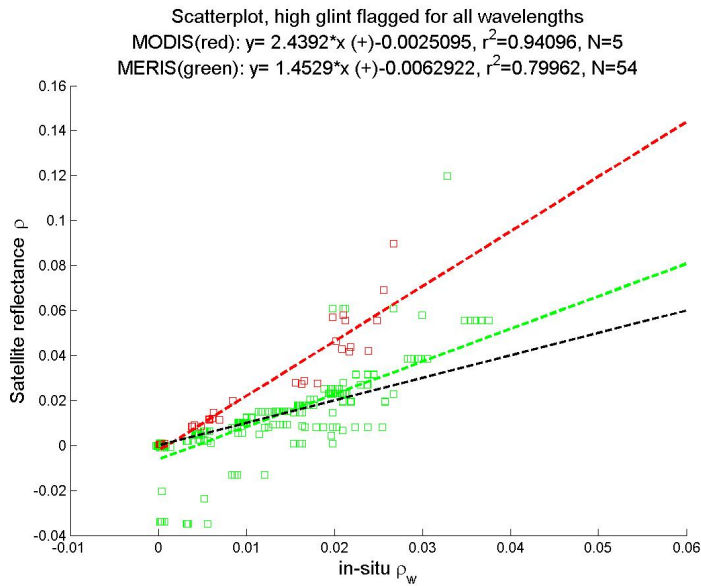


Figure 5.15.: Comparison of reflectance ρ of satellite instruments MERIS, MODIS and SeaWiFS for “high glint” classification and all wavelength bands to collocated *in-situ* remote sensing reflectance measurements, ρ_w . The dashed black line is the angular bisector (1:1-line).

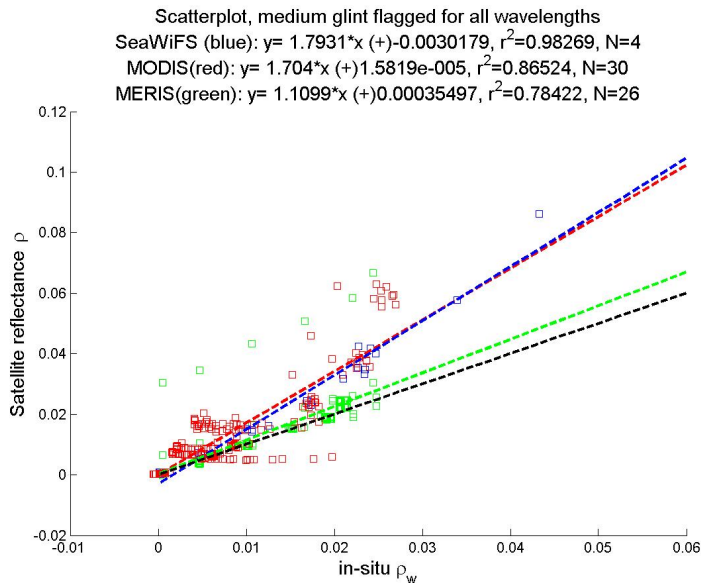


Figure 5.16.: Comparison of reflectance ρ of satellite instruments MERIS, MODIS and SeaWiFS for “medium glint” classification and all wavelength bands to collocated *in-situ* remote sensing reflectance measurements, ρ_w . The dashed black line is the angular bisector (1:1-line).

There are one or two collocations that do not fit the others and are the cause of the low correlation coefficient.

MODIS has higher values than the *in-situ* measurements $m = 1.70$ but a better correla-

tion coefficient ($r^2 = 0.87$) than MERIS. These results confirm that MODIS - in contrast to MERIS - applied no correction for moderate or medium glint.

There are only a few *in-situ*-SeaWiFS collocations ($N = 4$) and the results are comparable to MODIS data.

5.1.1.5. Low or negative L_w and pcd_1_13 flagged

Comparisons of *in-situ* data with satellite data with dominating low or negative water leaving radiance L_w and MERIS “pcd_1_13” flagged satellite pixels are shown in Figures 5.17 and 5.18, respectively.

The classification “low or negative L_w ” contains collocations for MODIS only. Statistics

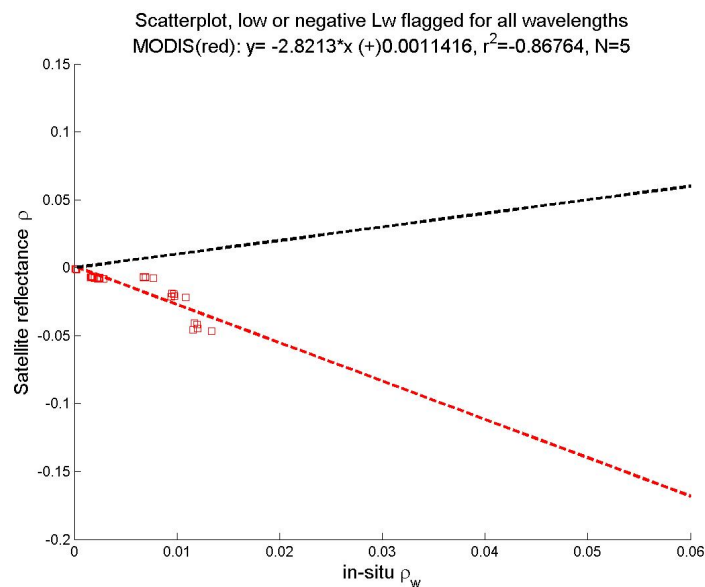


Figure 5.17.: Comparison of reflectance ρ of satellite instrument MODIS (no data for MERIS and SeaWiFS) for “low or negative L_w ” classification and all wavelength bands to collocated *in-situ* remote sensing reflectance measurements, ρ_w

show that such flagged data are not useful in terms of validation and do not reveal suitable information on ocean color.

Comparisons of MERIS pcd_1_13 flagged satellite data with *in-situ* data show a poor correlation ($r^2 = 0.33$). As the flag pcd_1_13 indicates, many data points are negative but due to some extremely high reflectances in all wavelength bands (see Figure A.12 in appendix) the regression line shows seemingly good results. Nevertheless, the pcd_1_13 classified collocations do not agree well with the *in-situ* measurements and should be excluded from further usage.

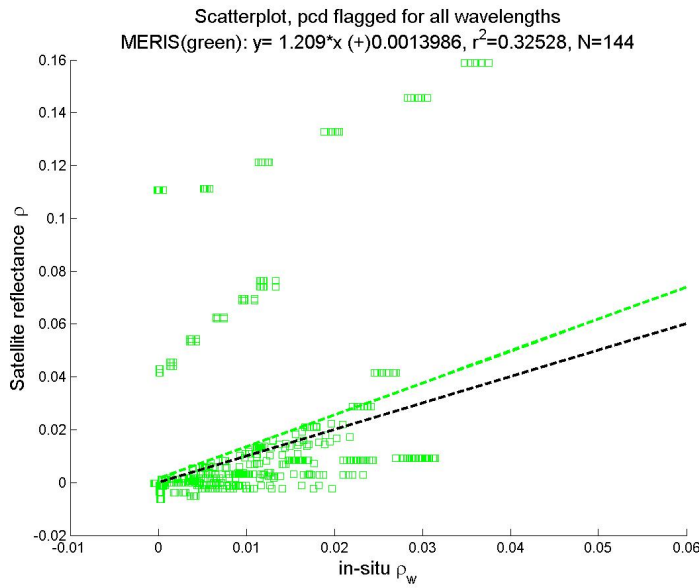


Figure 5.18.: Comparison of reflectance ρ of satellite instrument MERIS (no data for MODIS and SeaWiFS) for "pcd_1_13" classification and all wavelength bands to collocated *in-situ* remote sensing reflectance measurements, ρ_w

5.1.1.6. Mixed flagged

In all three levels of mixed flagged collocations, except the medium mixed flagged collocations from MERIS, the satellite data are much higher than the corresponding *in-situ* measurements (Figures A.13, A.14 and A.16 in Appendix).

The amount of collocations for SeaWiFS in medium mixed classification is only $N_{seawifs} = 3$ (Figure A.15 in Appendix), therefore the significance of the results is small. MERIS medium mixed flagged collocations tend to give too small values. This might be due to a large number of pcd_1_13 flagged pixels in the medium mixed classification. MODIS shows, as expected, too high intensities in remote sensing reflectance for both, medium and low mixed classification.

5.1.2. Validation of band ratios used for chl-*a* retrieval and chl-*a* products with *in-situ* measurements

The results of two different analyses are shown in this section. The first is the validation of the satellites' wavelength band ratios used in the Level-2 chl-*a* algorithms with the corresponding RAMSES ratios. Furthermore, the chl-*a* products for all three satellite instruments are compared to *in-situ* chl-*a* measurements. Both evaluations are accomplished for all available and "no bad" data. Table 5.3 summarizes all chl-*a* *in-situ* data available for comparisons to satellite data.

Table 5.3.: List of available data (x) for chl-a product and band ratio validation for all data and “no bad” data

	all data					“no bad” data				
	<i>in-situ</i> chl-a	SeaWiFS	MODIS	MERIS	RAMSES	<i>in-situ</i> chl-a	SeaWiFS	MODIS	MERIS	RAMSES
01/11/07	x	x		x		x	x	x	x	
02/11/07	x	x	x	x	x	x		x		x
04/11/07	x	x	x	x	x	x			x	x
05/11/07	x	x	x	x		x	x	x	x	
07/11/07	x	x	x	x		x	x	x	x	
08/11/07	x	x	x			x	x	x	x	
09/11/07	x	x	x	x		x	x	x	x	
10/11/07	x	x	x	x		x	x	x	x	
12/11/07	x	x	x	x		x	x	x	x	
13/11/07	x	x	x	x	x	x				x
15/11/07	x		x		x	x			x	x
16/11/07	x	x	x		x	x				x
18/11/07	x	x	x	x		x	x	x	x	
19/11/07	x	x	x			x	x	x	x	
20/11/07		x		x	x				x	x
22/11/07		x	x	x	x			x		x
01/05/08	x	x	x	x	x	x	x	x		x
02/05/08		x	x	x	x			x		x
03/05/08	x			x	x	x		x	x	x
09/05/08	x	x	x	x		x	x	x	x	
10/05/08	x	x	x	x	x	x	x			x
11/05/08	x	x	x	x	x	x				x
13/05/08	x	x		x	x	x			x	x
15/05/08	x	x		x	x	x		x	x	x
05/11/08	x	x	x			x	x	x	x	
08/11/08	x	x	x	x		x	x	x	x	
09/11/08	x	x	x	x		x	x	x	x	
10/11/08	x	x	x	x		x	x	x	x	
11/11/08		x		x	x					x
12/11/08				x	x				x	x
13/11/08			x	x	x			x	x	x
14/11/08		x		x	x			x	x	x
15/11/08				x	x					x
16/11/08	x	x	x	x		x	x	x	x	
17/11/08				x	x					x
18/11/08				x	x					x
19/11/08	x	x	x	x		x	x	x	x	
20/11/08			x	x	x					x
22/11/08				x	x					x
23/11/08				x	x					x
24/11/08				x	x					x
25/11/08				x	x					x
26/11/08				x	x			x	x	x
27/11/08	x	x	x	x		x	x	x	x	
28/11/08				x	x			x	x	x
29/11/08		x		x	x					x

5.1.2.1. Band ratio validation

Figure 5.19 shows MERIS, MODIS and SeaWiFS water leaving remote sensing chl-a reflectance ratios plotted against the particular *in-situ* measured water leaving remote sensing reflectance ratio. The MERIS ratio $\rho_{meris}(443\text{ nm})/\rho_{meris}(560\text{ nm})$ has a poor correlation coefficient ($r^2 = 0.26$) and a regression line with $n = 0.38$ and $m = 0.61$, whereas MODIS shows a sufficient agreement with the RAMSES ratio and a better correlation coefficient ($r^2 = 0.93$ and $m = 1.37$). The best match to *in-situ* reflectance ratios is realized with SeaWiFS. The regression line shows a slope of $m = 0.89$ although the correlation coefficient is slightly small ($r^2 = 0.64$).

Considering the “not bad”-flagged satellite data only, the results are shown in Figure 5.20. Unfortunately, there are only two collocations with SeaWiFS measurements, which precluded statistical analysis. Considering the data points only, they do not differ much

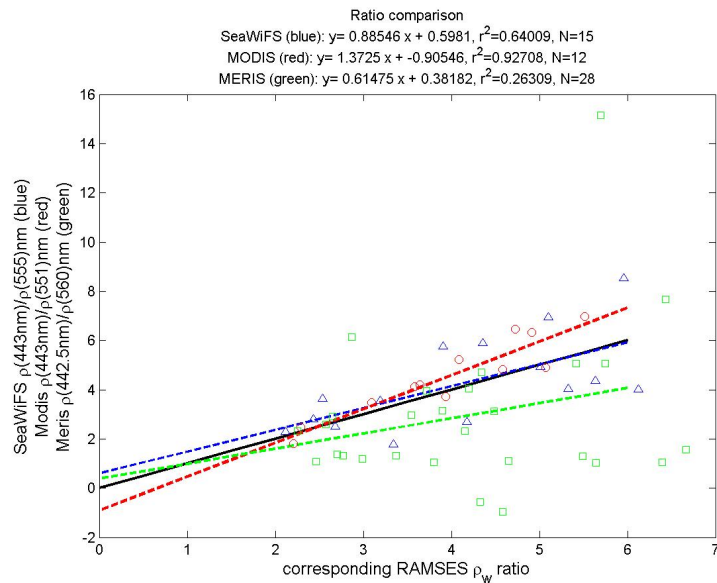


Figure 5.19.: Comparison of collocated satellite reflectance ratio used in the satellite chl-*a* algorithms with *in-situ* reflectance ratio of wavelength bands used in case-1 algorithms of the respective satellite instrument. The black line is the angular bisector (1:1-line).

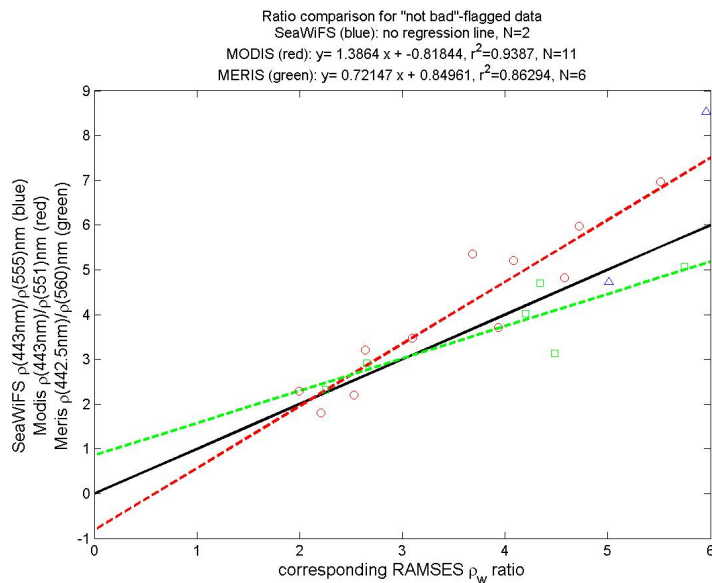


Figure 5.20.: Comparison of collocated satellite reflectance ratio used in the satellite chl-*a* algorithms of "not bad" flagged data with *in-situ* reflectance ratio of wavelength bands used in case-1 algorithms of the respective satellite instrument. The black line is the angular bisector (1:1-line).

from the other satellites' values.

Both, MERIS and MODIS show fairly sufficient agreements with the RAMSES ratio ($r^2 = 0.86$ and $m = 0.72$, $r^2 = 0.94$ and $m = 1.39$, respectively). MERIS and MODIS re-

gression lines are comparable concerning the variation from the ideal case ($m = 1, n = 0$); MERIS ratio tended to be smaller whereas MODIS ratio was generally larger than the corresponding RAMSES *in-situ* ratio.

Although the results are fairly satisfactory, one has to keep in mind that the amount of data points N is not large for all three satellites. Further data collection and analysis are necessary to improve the significance of these results.

5.1.2.2. Level-2 product chl-a validation

Figure 5.21 shows the comparison of the satellites' Level-2 product chl-a with the *in-situ* measured chl-a concentrations.

As in the ratio comparison before, the poorest results are produced by MERIS. In this

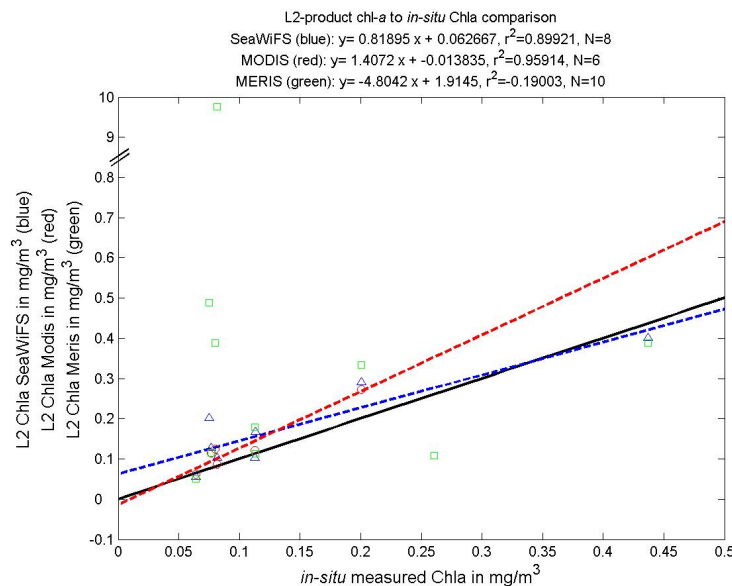


Figure 5.21.: Comparison of level-2 chl-a products with *in-situ* measured chl-a concentrations. Note the non-linear y-axis scale due to one MERIS-outlier at 9.76 mg/m^3 . MERIS regression line is not drawn in consequence of this. The black line is the angular bisector (1:1-line)

case the correlation coefficient is even smaller ($r^2 = 0.19$) due to one obvious outlier.

The results for MODIS and SeaWiFS are also similar to the results from the ratio comparison. MODIS chl-a product regression line shows a slightly higher slope ($m = 1.40$), whereas SeaWiFS's slope is a bit too small ($m = 0.81$). SeaWiFS correlates better with the *in-situ* data. Both correlation coefficients are rather good with $r^2 = 0.96$ and $r^2 = 0.90$ for MODIS and SeaWiFS, respectively.

The "not bad"-flagged satellite chl-a data versus *in-situ* chl-a concentration comparison is given in Figure 5.22. Unfortunately, there are not many collocated data points for chl-a comparisons available (see Figure headlines). Again, only two data points ($N = 2$) for SeaWiFS are available. A regression line was not plotted. MERIS and MODIS regression

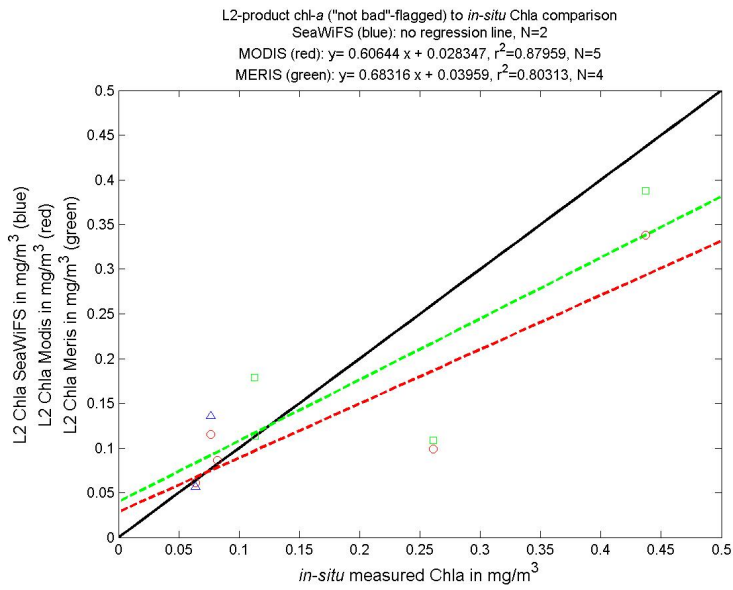


Figure 5.22.: Comparison of “not bad”-flagged level-2 chl-a products with *in-situ* measured chl-a concentrations. The black line is the angular bisector (1:1-line)

lines have slopes of $m = 0.68$ and $m = 0.61$, respectively. Thus, MERIS fits the *in-situ* data slightly better. The correlation coefficients are good with $r^2 = 0.80$ and $r^2 = 0.88$ for MERIS and MODIS, respectively.

5.2. Discussion

5.2.1. Validation of the water leaving reflectance

Analysis of the distinguished classifications as presented above depicts that not all satellite data are suitable for providing ocean color information. The resulting statistical properties for all classifications are listed in Table 5.4 and discussed hereafter.

Since there are very few studies published, the results of the present study are compared to Antoine et al. (2008), Park et al. (2006) and Bailey and Werdell (2006) only. Results for flagged data can not be compared to other studies, as comparable studies discard flagged data a priori (compare: Antoine et al. (2008) or Bailey and Werdell (2006)). Nevertheless, it is possible to reveal information on possible quality of flagged data regarding comparison to *in-situ* data.

- Cloud flagged data

MERIS cloud flagged measurements are extremely high due to reflection of radiation by clouds into the satellite instrument and no correlation can be distinguished. As the Level-2 algorithm for MODIS and SeaWiFS deletes all cloud flagged measurements the data from remaining pixels may be contaminated with other flags. Thus, the result of the validation for MODIS and SeaWiFS remaining data in the “cloud flagged” classification is similar to the outcome of the “mixed flagged” category: Most satellite values are higher than the corresponding *in-situ* values. This is due to the fact that most of the considered flags indicate situations, that increase the reflectance, such as effects from clouds or sun glint.

The comparison of MODIS and SeaWiFS reflectance with *in-situ* data delivers better results the less cloud flagged pixels are within the ROI. Thus, the best result is given for the category “low cloud” (less than 33% of the ROI’s pixels cloud-contaminated).

The wavelength dependent analysis indicates poor correlation coefficients for MODIS and SeaWiFS. A reason for this high variability of reflectance values is the reduced number of pixels contributing to the “high cloud” classification. As the cloud flagged pixels are neglected by the Level-2 algorithm the size of the data set is substantially reduced and thus, the variance of the data is expected to be higher than for a larger data set. The fact, that the number of neglected pixels in the “medium cloud” flagged category is less than in the “high cloud” flagged class explains the increased correlation coefficients in the “medium cloud” classification. In summary, the MERIS cloud flagged water leaving reflectance data cannot be used. MODIS and SeaWiFS show better results, but the reflectance measurements are mostly too high in relation to the *in-situ* data and should be excluded from further usage.

Table 5.4.: Resulting statistical values slope m , intercept n , correlation coefficient r^2 and number of collocations N from the collocated reflectance comparison

Classification	Satellite instrument	m	n	r^2	N
all data	SeaWiFS	1.98	<0.01	0.85	201
	MODIS	1.91	<0.01	0.88	232
	MERIS	2.18	0.14	0.08	457
all without clouds	SeaWiFS	2.01	<0.01	0.9	44
	MODIS	2.11	<0.01	0.86	65
	MERIS	1.43	0.01	0.36	314
no bad data	SeaWiFS	1.61	<0.01	0.98	6
	MODIS	1.88	<0.01	0.92	86
	MERIS	0.9	<0.01	0.82	70
not flagged	SeaWiFS	-	-	-	-
	MODIS	1.56	<0.01	0.95	31
	MERIS	0.95	<0.01	0.92	20
high clouds	SeaWiFS	2.45	<0.01	0.86	19
	MODIS	1.82	<0.01	0.86	92
	MERIS	-3.68	0.62	-0.16	95
medium clouds	SeaWiFS	2.25	<0.01	0.89	56
	MODIS	1.93	<0.01	0.96	28
	MERIS	-	-	-	-
low clouds	SeaWiFS	1.75	<0.01	0.82	81
	MODIS	1.85	<0.01	0.93	16
	MERIS	-	-	-	-
high glint	SeaWiFS	-	-	-	-
	MODIS	2.44	>-0.01	0.94	5
	MERIS	1.45	>-0.01	0.8	54
medium glint	SeaWiFS	1.78	>-0.01	0.98	4
	MODIS	1.7	>-0.01	0.87	30
	MERIS	1.11	>-0.01	0.78	26
low or negative	SeaWiFS	-	-	-	-
	MODIS	-2.82	<0.01	-0.87	5
	MERIS	-	-	-	-
pcd_1_13	SeaWiFS	-	-	-	-
	MODIS	-	-	-	-
	MERIS	1.21	<0.01	0.33	144
high mixed	SeaWiFS	2.11	<0.01	0.91	38
	MODIS	-	-	-	-
	MERIS	1.99	0.04	0.25	66
medium mixed	SeaWiFS	1.64	<0.01	0.99	3
	MODIS	2.33	<0.01	0.94	11
	MERIS	0.81	<0.01	0.92	24
low mixed	SeaWiFS	-	-	-	-
	MODIS	2.15	<0.01	0.98	14
	MERIS	-	-	-	-

- Mixed flagged data

For the “high mixed” classification no MODIS data are available. Both, MERIS and SeaWiFS have too high reflectance measurements. Most of the flags considered

indicate situations that increase measured reflectance values. Thus, the measurements in all “mixed flagged” classifications are much higher than the *in-situ* data. “Medium mixed” collocations show similar results for SeaWiFS and MODIS. MERIS underestimates reflectances in this category due to a large amount of “pcd_1_13” flagged pixels, i.e. negative data. The “low mixed” class only contains 14 batches of one MODIS collocation. Results show again too high reflectances for the same reasons as mentioned before.

- Low or negative and pcd_1_13 flagged data

The “low or negative” flag indicates smaller satellite reflectance values compared to *in-situ* data. The only collocation in this classification is from MODIS and shows negative values for all wavelength bands and thus, can be neglected for further usage.

The “pcd_1_13” flag signals negative reflectance in at least one band for MERIS measurements. The results shown and described above reveal this exactly. In most wavelength bands there are several negative values and some very high reflectances. These high values may of course belong to differently flagged pixels. Nevertheless, most values are still below the corresponding ρ_w and no agreement to *in-situ* data can be perceived.

- Glint flagged data

Due to the higher reflection into the satellite sensor by sun glint the satellite values in the “high glint” category are two to three times larger than the corresponding *in-situ* data. Although the overall agreement is fairly good, MERIS shows many outliers that may be caused by high sun glint reflection or otherwise contaminated pixels. One example could be cloud shadow effects from neighboring pixels that might result in low or negative reflectances.

SeaWiFS does not contribute any collocations to the “high glint” classification.

MODIS contributes to this “high glint” class with only one collocation and thus the evidence of the result has no statistical relevance. The measurements on this collocation however, are also much higher than the corresponding *in-situ* measurements.

“Medium” or “moderate glint” flagged results are similar. Mostly, the satellite data is too high and varies in a large range, especially for MODIS and SeaWiFS.

MERIS Level-2 algorithm corrects the reflectance values for medium glint and thus the result is a measure for the quality of this correction. Indeed, MERIS shows a good agreement with the *in-situ* data except for one collocation where the values are too high. Neglecting this collocation, the regression and the correlation to the *in-situ* data would be best for every single wavelength band. It can be concluded that MERIS correction algorithm is very good but the threshold might be insuffi-

cient due to the outlier-collocation. To validate this presumption more *in-situ* data have to be acquired.

- All and all without cloud flagged data
Considering all data, the satellite remote sensing reflectance is about two times higher than the corresponding *in-situ* measured reflectance. MERIS measurements in particular show a very poor correlation coefficient due to many cloud-contaminated measurements. MODIS and SeaWiFS data show better agreements and are much more reliable according to rather good correlation coefficients, which results from the exclusion of all cloud flagged data.

An evidence for this is given in the “all without cloud flagged” scatterplot where MODIS and SeaWiFS show comparable agreements to the *in-situ* data. MERIS correlation coefficient and agreement are increased drastically respective to the “all data” result due to no cloud flagged data in this category. Nevertheless, the MERIS correlation is still not very conclusive due to many outliers in the scatterplot.

- “No bad” and not flagged data
The outliers in the MERIS comparison for the “all without cloud flagged” category are recognizably reduced in the “no bad” classification where only collocations out of the classifications “no flags”, “medium glint”, “low mixed” and “medium mixed” were considered. Thus, outliers are generated by “high glint” and “pcd_1_13” flagged and “high mixed” categorized pixels. MERIS contributes to the “no bad” classification, just as SeaWiFS with only two medium glint flagged collocations, whereas MODIS contributes with four (see Table 5.1). As it was depicted above, the validation of medium glint flagged data was quite good for MERIS in contrast to poorer agreements to the *in-situ* data for SeaWiFS and MODIS. The fraction of medium glint flagged to not flagged collocations in the “no bad” category is 1/2 for MERIS and 2/3 for MODIS and no not flagged but two medium glint collocations are available for SeaWiFS and the MERIS medium glint data is corrected by the Level-2 algorithm. In conclusion, MERIS shows the best, MODIS and SeaWiFS poorer agreements. There is one collocation from MERIS with unusually high values that was discussed in the “medium glint” flagged classification before and that reduces the quality of the comparison. The MERIS correlation to *in-situ* data would be much better if this collocation was neglected. But as there is no objective way to discard this collocation it was kept in the analysis. As SeaWiFS does not contribute collocations to the “not flagged” category, the “no bad” classification reveals the best agreements to *in-situ* data for this instrument. Therefore, the following comparisons to other studies’ results refer to the “no bad” data for SeaWiFS.

Table 5.5 summarizes statistical values from this current work (for “not flagged”

Table 5.5.: Resulting statistical values slope m , intercept n , correlation coefficient r^2 and number of collocations N from wavelength separated reflectance comparisons from current study (“not flagged” category for MODIS and MERIS and “no bad” category for SeaWiFS), Antoine et al. (2008), Bailey and Werdell (2006) and Park et al. (2006)

	wavelength	current study				Antoine et al. (2008)				Bailey and Werdell (2006)			
		m	n	r^2	N	m	n	r^2	N	m	n	r^2	N
SeaWiFS	412	-1.02	0.06	-0.72		0.74	<0.01	0.44	63	1.07	-	0.9	154
	443	-1.49	0.07	-0.45		0.68	<0.01	0.42	166	1.06	-	0.85	242
	490	-1.94	0.05	-0.45	6	0.57	<0.01	0.32	168	0.97	-	0.74	242
	510	-1.16	0.02	-0.37		0.32	<0.01	0.09	168	1.24	-	0.47	127
	555	-0.6	0.01	-0.23		0.43	<0.01	0.09	107	0.79	-	0.67	242
	all bands	1.61	<0.01	0.98		0.94	<0.01	0.89	888				
MODIS	412.5	2.79	-0.02	0.88		0.84	<0.01	0.59	66				
	443	1.35	<0.01	0.78		0.75	<0.01	0.55	147				
	488	0.95	0.01	0.79		0.64	<0.01	0.48	152				
	531	1.1	<0.01	0.91	31	-	-	-	-				
	551	0.116	<0.01	0.92		0.71	<0.01	0.39	150				
	all bands	1.56	<0.01	0.95		0.91	<0.01	0.91	666				
MERIS										Park et al. (2006)			
	412	0.61	0.01	0.87		0.93	<0.01	0.43	20	2.71	-0.01	0.04	
	443	0.54	<0.01	0.83		0.7	<0.01	0.38	61	0.89	<0.01	0.51	
	490	0.37	0.01	0.67	20	0.69	<0.01	0.44	64	0.81	<0.01	0.88	13
	510	0.25	<0.01	0.41		0.52	<0.01	0.24	64	0.86	<0.01	0.91	
	560	0.06	<0.01	0.03		0.64	<0.01	0.34	63	0.92	<0.01	0.95	
all bands	0.95	<0.01	0.92		1.16	<0.01	0.88	400					

or “no bad” classification) and three other studies (Antoine et al. (2008), Bailey and Werdell (2006) and Park et al. (2006)) for remote sensing reflectance comparisons. Note, that Bailey and Werdell (2006) validated SeaWiFS data only and Park et al. (2006) took *in-situ* data in Belgian case 2 waters to validate MERIS data.

The category “not flagged” contains only four collocations from MERIS and six from MODIS. Hence, the significance of the correlation with the *in-situ* data is small. Nevertheless, the validation of MERIS is clearly positive for all wavelength bands pooled and shows the best result of the entire validation ($m = 0.95$ and $r^2 = 0.92$). This is an expected result as no disturbances influence the satellite data. Antoine et al. (2008) revealed weaker agreements between MERIS and *in-situ* data ($m = 1.16$ and $r^2 = 0.88$). Reasons for this slightly deviating result may be found in differences of the measurement sites. In the present study measurements were accomplished at a large number of different sites, whereas the *in-situ* data in Antoine et al. (2008) were performed with a buoy at one distinguished location in the Mediterranean Sea. Furthermore, the instrumentation used to measure *in-situ* data was different in both studies, as was the determination of the remote sensing reflectance from *in-situ* radiances and irradiances. In our study, for example, a rather new algorithm was used to determine the air-sea-interaction coefficient ρ_{as} (see Chapter 4.1.3 and Doerffer (2008)). Such differences in the analysis and possible slight disparities in measurement conditions may account for the differing results between both studies.

MODIS shows slightly higher values compared to *in-situ* data ($m = 1.56$). Antoine et al. (2008) obtained better agreements to *in-situ* data ($m = 0.93$) and a comparable result for SeaWiFS ($m = 0.94$). Possible causes for this slight difference between both studies are mentioned above. Nevertheless, it is satisfactory that both studies revealed rather comparable agreements between satellite and *in-situ* reflectances.

Wavelength separated analysis from SeaWiFS validation shows poor correlation coefficients. This is understandable considering the small number of collocations. All reflectances are in the same range (see Figure 5.8), indicating that measurement conditions were quite constant (such as optical properties of the water). The regression line of few data points distributed in a small range is not very convincing. Considering all wavelength bands together, the data range gets much larger and thus, the regression line gets more meaningful. Additionally, the statistical values as depicted in Tables 5.6 and 5.5 are from the “no bad” classification, with no “not flagged” data contributing. Comparable poor correlation coefficients for the single wavelength bands for SeaWiFS are shown in Antoine et al. (2008). Bailey and Werdell (2006) revealed more satisfying statistical values, because of wider data ranges due to potentially very different measurement conditions as they collected data globally in case 1 waters.

MODIS wavelength separated analysis provides better correlation coefficients than for Antoine et al. (2008) due to a larger data range in this study. Nevertheless the agreements of satellite data with *in-situ* data vary strongly with the particular wavelength bands. The large disagreement in the 412.5 nm band is a certain indicator for failures in the atmospheric correction (Antoine et al. (2008), Bailey and Werdell (2006) and Park et al. (2006)). The atmospheric correction strongly relies on the correct assessment of absorbing aerosols in the atmosphere. An incorrect estimation of the aerosol amount and distribution will affect the retrieval of water leaving radiance. This effect is more severe for shorter than for larger wavelengths. Thus, the large differences found in the first wavelength bands, specifically 412 nm could be explained with errors in the atmospheric correction, which requires improvement in order to use the first wavelength band. As future satellite mission instruments may be equipped with bands at even shorter wavelength, such as 380 nm, the improvement of atmospheric correction is extremely important.

The large deviation in the lowest wavelength band effects the overall agreement.

Correlation coefficients for MERIS validation varies strongly with wavelength bands. This was also detected by Park et al. (2006). In this study, the slope of the regression line deviates from $m = 1$ stronger with increasing wavelength. This might be due to the correlation between wavelength and reflectance. The larger the wavelength the weaker the reflection. Thus, the large wavelength bands measure the

lowest signals. As explained above, smaller data ranges or values reveal sensitive and less meaningful regression lines.

In summary the present study shows in most cases the impracticality of flagged data for validation purposes. One exception was the “medium glint” flagged category for MERIS data where good agreements to *in-situ* reflectances due to a satisfying correction algorithm were revealed. Similarly, Park et al. (2006) proposed, that under certain conditions some high-glint flagged MERIS pixels can be used for validation in Belgian waters. As *in-situ* data are difficult to procure and immaculate collocations with satellite measurements are scarce, such flagged, but still useful data should be considered for validation purposes.

5.2.2. Chl-*a* product validation

The classifications “all data” and “no bad data” were applied to the validation of band ratios used for satellite chl-*a* retrieval and chl-*a* Level-2 products with RAMSES ρ_w ratios and *in-situ* chl-*a* measurements. The statistical values are summarized in Tables 5.7 and 5.8, respectively. Results from chl-*a* and reflectance comparisons are shown in Table 5.6 for the different studies.

Table 5.6.: Resulting statistical values slope m , intercept n , correlation coefficient r^2 and number of collocations N from reflectance and chl-*a* comparisons from current study (“no bad” and “not flagged” category), Antoine et al. (2008), Bailey and Werdell (2006) and Park et al. (2006)

study		reflectance comparison				chl- <i>a</i> comparison			
		m	n	r^2	N	m	n	r^2	N
SeaWiFS	current “not bad”	1.61	<0.01	0.98	6	6.34	0.35	1	2
	Antoine et al. (2008)	0.94	<0.01	0.89	888	0.45	-0.66	0.51	44
	Bailey and Werdell (2006)	only wavelength separated analysis				0.9	-	0.83	271
MODIS	current “not bad”	1.88	<0.01	0.92	86	0.61	0.03	0.88	5
	current “not flagged”	1.56	<0.01	0.95	31				
	Antoine et al. (2008)	0.93	<0.01	0.91	666	0.77	-0.24	0.82	31
MERIS	current “not bad”	0.9	<0.01	0.82	70	0.68	0.04	0.8	4
	current “not flagged”	0.95	<0.01	0.92	20				
	Antoine et al. (2008)	1.16	<0.01	0.88	400	0.58	-0.48	0.87	15
	Park et al. (2006)	only wavelength separated analysis				0.98	0.1	0.81	14

The MODIS “all data” comparisons reveal reasonably good agreements. The largest correlation coefficient was determined for MODIS “all data” chl-*a* comparison ($r^2 = 0.96$) and both, the ratio and chl-*a* comparison show good agreements with *in-situ* values. Reasons for this good agreements may be a good chl-*a* retrieval algorithm that considers and corrects flagged pixels well and the fact that errors in the satellite derived reflectances may cancel out by taking the ratio of two reflectances.

Table 5.7.: Resulting statistical values slope m , intercept n , correlation coefficient r^2 and number of collocations N from the satellite band ratio to the corresponding *in-situ* RAMSES comparison

Classification	Satellite instrument	m	n	r^2	N
all data	SeaWiFS	0.89	0.6	0.64	15
	MODIS	1.37	-0.91	0.93	12
	MERIS	0.61	0.38	0.26	28
no bad data	SeaWiFS	4.03	-15.47	1	2
	MODIS	1.31	0.82	0.94	11
	MERIS	0.72	0.85	0.86	6

Table 5.8.: Resulting statistical values slope m , intercept n , correlation coefficient r^2 and number of collocations N from the Level-2 product to *in-situ* chl-*a* comparison

Classification	Satellite instrument	m	n	r^2	N
all data	SeaWiFS	0.82	0.06	0.9	8
	MODIS	1.41	-0.01	0.96	6
	MERIS	-4.8	1.91	-0.19	10
no bad data	SeaWiFS	6.34	0.35	1	2
	MODIS	0.61	0.03	0.88	5
	MERIS	0.68	0.04	0.8	4

MODIS shows a slight improvement in the “no bad data” class in comparison to the “all data” category. The agreement of MODIS Level-2 chl-*a* concentrations with *in-situ* measured chl-*a* concentrations is good ($m = 0.61$). Antoine et al. (2008) presented a slightly better agreement with a slope of $m = 0.77$, but the correlation coefficient is a bit smaller. This difference is not surprising considering that the MODIS reflectance comparison was slightly better in the BOUSSOLE project (Antoine et al. (2008)) than in this present study. In addition, the number of data points in the present study is low ($N = 5$) compared to Antoine et al. (2008) ($N = 31$). A proof for this is the fact, that the regression between MODIS Level-2 chl-*a* concentrations and *in-situ* measured chl-*a* varies from $m = 1.41$ to $m = 0.61$ just by deleting one collocation ($N = 6$ and $N = 5$).

The results for SeaWiFS ratio and chl-*a* comparison in the “all data” category are satisfactory. Possible reasons are described above for MODIS and are applicable for SeaWiFS as well.

SeaWiFS statistical values for the “no bad” classification are not meaningful as there are only two data points. However, these two points do not exceed the expected range (defined by the range of the other satellites’ values) and allow the conclusion that the SeaWiFS ratios are in agreement with the *in-situ* ratio. More correlated data has to be collected for validation.

MERIS “all data” ratio comparison shows fairly good agreements ($m = 0.61$) between satellite and RAMSES ratio, although the correlation coefficient is very small ($r^2 = 0.26$). A distinct improvement is shown in the “no bad” category ($m = 0.72$ and $r^2 = 0.86$). Surprisingly, the agreement between MERIS Level-2 chl-*a* and *in-situ* measured chl-*a* concentration is very bad for the “all data” category, although the ratio comparison was fairly good. As MERIS has one chl-*a* product that is out of range, this could be the cause for this bad statistical agreement. In the “no bad data” analysis MERIS shows a much better agreement ($m = 0.68$) and correlation ($r^2 = 0.8$). The results of statistics for MERIS chl-*a* comparison in Antoine et al. (2008) are not as good considering regression and correlation coefficient (see Table 5.6). Reasons for this are the same as for MODIS and SeaWiFS. As the agreement of MERIS reflectances is slightly better in the present study compared to Antoine et al. (2008) the better agreement of chl-*a* concentrations is reasonable. Park et al. (2006) revealed very satisfying regressions for MERIS chl-*a* comparison with a slope of $m = 0.98$ but, as indicated above, this good result is understandable considering the large range of chl-*a* concentrations in the Belgian case 2 waters. Thus, results are not entirely comparable with the case 1 chl-*a* concentrations in this study.

Nevertheless, the present study yields equivalent results of the chl-*a* comparison to results from other studies and projects like Antoine et al. (2008) and Bailey and Werdell (2006).

6. Conclusions and Outlook

In this work remote sensing reflectances were obtained from ship-bourne *in-situ* hyper-spectral radiance and irradiance measurements in order to validate collocated MERIS, MODIS and SeaWiFS reflectances. Additionally, chl-*a* concentrations were measured from *in-situ* water samples and compared to all three satellite instruments' Level-2 chl-*a* products.

The results presented in this thesis reveal that *in-situ* reflectance and chl-*a* measurements can be used for satellite validation purposes. Not flagged MERIS remote sensing reflectances can be used for delivering ocean color information. Results from comparisons of *in-situ* data with MODIS data indicate issues with the atmospheric correction algorithm applied to MODIS data.

The flag-separated analysis confirms the expected effects from flagged satellite pixels. The impact of dominating cloud and high glint flagged pixels in a ROI is an overestimation of the water leaving remote sensing reflectance. Although the cloud flagged pixels are neglected for MODIS and SeaWiFS, the remaining pixel of the ROI are apparently affected by other flags or cloud shadow and thus cannot be used for delivering information on ocean color. The high glint classified collocations are not useful for validation, either. Medium glint data are not suitable as well, except for MERIS. As MERIS Level-2 algorithm corrects measurements for medium glint and the agreement to *in-situ* data was good except for one outlier it has to be examined whether the threshold might be too low or the medium glint correction algorithm fails partially.

Collocations with dominating low or negative or pcd_1_13 flagged pixels could not be confirmed by *in-situ* measurements and are not applicable in terms of validation.

The best agreements for MODIS and MERIS were obtained in the "not flagged" classification. SeaWiFS does not contribute any collocations to this classification. There is a good correlation between the MERIS-derived and the *in-situ* measured water leaving remote sensing reflectances ρ_w , while MODIS shows a greater variability. Discrepancies are obtained, especially in the low wavelength bands. As all satellite sensors measure the TOA radiance and retrieve estimates of the water leaving radiance by applying an atmospheric correction model, the actual satellite products like chl-*a* on the basis of the water leaving radiance, are relying on the quality of the atmospheric correction. Unfortunately, it is rarely possible to consider all environmental conditions in the atmospheric correction, such as absorbing aerosols in the atmosphere. Although such conditions are estimated to be quite constant over case 1 waters, they can vary. Bailey and Werdell (2006) showed that, despite the fact that 40% of their measurements were in deep waters (with depths

> 1000 m), only 5% are from oligotrophic waters and the majority are from mesotrophic and eutrophic waters. This is an example of how environmental conditions in case 1 waters can vary. As an incorrect assessment of aerosol results in a failure of the atmospheric correction with an increasing impact on the retrieved radiance with decreasing wavelength (Bailey and Werdell (2006)) discrepancies between satellite and *in-situ* data in the smaller wavelength bands indicate problems with the atmospheric correction. Results from this present study strengthen the recommendations of former studies, such as Bailey and Werdell (2006) and Antoine et al. (2008), to further improve atmospheric correction algorithms for case 1 waters.

The comparison of satellite ratios for chl-*a* determination and the corresponding *in-situ* ratios yield satisfactory results. A correlation between satellite Level-2 products and *in-situ* measured chl-*a* is perceivable and results are conform with similar studies, such as Antoine et al. (2008), Bailey and Werdell (2006) or Park et al. (2006). Based on the mostly small numbers of collocated measurements the validity of the results should be enhanced by collecting more data.

On that account the next ship cruises are already scheduled. Additionally, RAMSES below surface reflectance measurements will be evaluated to validate the above surface measurements used in this work to determine the *in-situ* water leaving remote sensing reflectance (compare Hooker and Morel (2003)). This will increase the number of available collocations so that a comprehensive data set for further validation will be obtained.

Bibliography

- Antoine, D., F. d'Ortenzio, S. Hooker, G. Bécu, B. Gentili, D. Tailliez, and A. Scott, 2008: Assessment of uncertainty in the ocean reflectance determined by three satellite ocean color sensors (MERIS, SeaWiFS and MODIS-A) at an offshore site in the Mediterranean Sea (BOUSSOLE project). *J. Geophys. Res.*, **113**, C07013, doi:10.1029/2007JC004472.
- Bailey, S. and P. Werdell, 2006: A multi-sensor approach for the on-orbit validation of ocean color satellite data products. *Remote Sensing of the Environment*.
- Bourg, L. and S. Delwart, 2006: Meris Instrument Calibration. *Proceedings of the Second Working Meeting on MERIS and AATSR Calibration and Geophysical Validation (MAVT-2006), 20-24 March 2006, ESRIN*.
- Bracher, A., 2008: Detaillierter Blick aus dem All - Meeresalgen global beobachtet. *Zeitschrift für Geodäsie, Geoinformation und Landmanagement*, **4/2008**, **133.Jg**, 254–261.
- Bracher, A., M. Vountas, T. Dinter, J. Burrows, R. Röttgers, and I. Peeken, 2009: Quantitative observation of cyanobacteria and diatoms from space using PhytoDOAS on SCIAMACHY data. *BGS*, **6**, 751–764. www.biogeosciences.net/6/751/2009.
- Brockmann, C., 2006: Limitations of the Application of the Meris Atmospheric Correction. *Proceedings of the Second Working Meeting on MERIS and AATSR Calibration and Geophysical Validation (MAVT-2006), 20-24 March 2006, ESRIN*.
- Carr, M.-J., M. Friedrichs, M. Schmeltz, M. Aita, D. Antoine, K. Arrigo, I. Asanuma, O. Aumont, R. Barber, M. Behrenfeld, R. Bidigare, E. Buitenhuis, J. Campbell, A. Ciotti, H. Dierssen, M. Dowell, J. Dunne, W. Esaias, B. Gentili, W. Gregg, S. Groom, N. Hoepffner, J. Ishizaka, T. Kameda, C. L. Quéré, S. Lohrenz, J. Marra, F. Mélin, K. Moorex, A. Morel, T. Reddy, J. Ryan, M. Scardi, T. Smyth, K. Turpie, G. Tilstone, K. Waters, and Y. Yamanaka, 2006: A comparison of global estimates of marine primary production from ocean color. *Deep-Sea Research II*.
- Cracknell, A. P. and L. Hayes, 2007: *Introduction to Remote Sensing*. CRC Press, Boca Raton, Florida, USA.
- Dinter, T., W. V. Hoyningen-Huene, J. P. Burrows, A. Kokhanovsky, E. Bierwirth, M. Wendisch, D. Müller, R. Kahn, and M. Diouri, 2009: Retrieval of aerosol optical thickness for desert conditions using MERIS observations during the SAMUM campaign. *Tellus B*, **61**(1), 229–238. Doi:10.1111/j.1600-0889.2008.00391.x.

- Doerffer, R., 2008: The effect of a varying refractive index of seawater on the retrieval of the water leaving radiance reflectance. GKSS.
- Doerffer, R., H. Schiller, H. Krasemann, K. Heyman, W. Cordes, W. Schönfeld, R. Röttgers, I. Behner, and P. Kipp, 2002: Meris Case 2 water Validation - Early Results North Sea/Helgoland/German Bight. *Proceedings of the ENVISAT Validation Workshop (ESA SP-531)*.
- Elachi, C., 1987: *Introduction to the Physics and Techniques of Remote Sensing*. John Wiley Sons, USA.
- Hooker, S. and A. Morel, 2003: Platform and Environmental Effects on Above-Water Determinations of Water-Leaving Radiances. *Journal of Atmospheric and Oceanic Technology*, **20**, 187–205.
- Kirk, J., 1983: *Light and photosynthesis in aquatic ecosystems*. Cambridge University Press, Cambridge.
- Lauscher, F., 1952: Sonnen- und Himmelsstrahlung im Meer und in Gewässern. *Theoretical and Applied Climatology*, **4**(2), 168–192. Springer Verlag.
- Lee, Z. and K. Carder, 2004: Absorption spectrum of phytoplankton pigments derived from hyperspectral remote-sensing reflectance. *Remote Sensing of Environment*, **89**(3), 361 – 368. Doi:10.1016/j.rse.2003.10.013.
- McClain, C. R., 2009: A decade of Satellite Ocean Color Observations. *American Meteorological Society*, **1**, 19–42.
- Morel, A. and L. Prieur, 1977: Analysis of variations in ocean color. *LO*, **22**(4), 709–722.
- Morel, H. C., A., D. Antione, and B. Gentili, 2007: Natural variability of bio-optical properties in Case 1 waters: attenuation and reflectance within the visible and near-UV spectral domains, as observed in South Pacific and Mediterranean waters. *Biogeosciences*, **4**, 913–925.
- Park, Y., B. V. Mol, and K. Ruddick, 2006: Validation of Meris Water Products for Belgian coastal Waters 2002-2005. *Proceedings of the Second Working Meeting on MERIS and AATSR Calibration and Geophysical Validation (MAVT-2006), 20-24 March 2006, ESRIN*.
- Peters, S., 2006: Meris Reflectance and Algal-2 validation at the North Sea. *Proceedings of the Second Working Meeting on MERIS and AATSR Calibration and Geophysical Validation (MAVT-2006), 20-24 March 2006, ESRIN*.
- Ruddick, K., V. D. Cauwer, and Y. Park, 2006: Seaborne measurements of near infrared water-leaving reflectance: The similarity spectrum for turbid waters. *Limnol. Oceanogr.*, **51**(2), 1167–1179.

- Schroeder, T., 2004: *Fernerkundung von Wasserinhaltsstoffen in Küstengewässern mit MERIS unter Anwendung expliziter und impliziter Atmosphärenkorrekturverfahren*. Ph.D. thesis, Freien Universität Berlin.
- Seelye, M., 2004: *An Introduction to Ocean Remote Sensing*. Cambridge University Press, Cambridge.
- Sorensen, K., J. Hokedal, E. Aas, R. Doerffer, and E. Dahl, 2002: Early Results for Validation of MERIS Water Products in the Skagerrak. *Proceedings of the ENVISAT Validation Workshop (ESA SP-531)*, p. 97.1.
- Stramski, D., R. Reynolds, M. Babin, S. Kaszmarek, M. Lewis, R. Röttgers, A. Sciandria, M. Stramska, M. Twardowski, B. Franz, and H. Claustre, 2008: Relationships between the surface concentration of particulate organic carbon and optical properties in the eastern South Pacific and eastern Atlantic Oceans. *Biogeosciences*, **5**, 171–201.
- Voss, K., A. Morel, and D. Antione, 2007: Detailed validation of the bidirectional effect in various Case 1 waters for application to ocean color imagery. *Biogeosciences*, **4**, 781–789.
- Wang, M., 2006: Effects of ocean surface reflectance variation with solar elevation on normalized water-leaving radiance. *Applied Optics*, **45**(17).
- Wernand, M., 2002: Guidelines for (ship-borne) auto-monitoring of coastal and ocean colour. *Steven G. Ackleson-ONR, Charles Trees-NASA, Editors. Oceanographic Society. Ocean Optics XVI, Nov. 18-22, proceedings, Santa Fe, New Mexico, US.*
- Zibordi, G., F. Mélin, S. Hooker, D. D'Alimonte, and B. Holben, 2004: An Autonomous Above-Water System for the Validation of Ocean Color Radiance Data. *IEEE Transactions on Geoscience Remote Sensing*, **42**(2).

A. Appendix

Table A.1.: Collocation assignment to the different classifications

Flag	Instrument	Date	Collocation
low or neg	MODIS	111108	1
pcd1_13	MERIS	020508	3
		030508	1
		111108	1, 2
		131107	1
		131108	1, 2, 3
		141108	1, 2, 3
		151108	1
		171108	1, 2
		201108	3
		221107	2
cloud_high	SeaWiFS	110508	1, 2
		130508	1
		131107	2
		161107	2
	MERIS	010508	1, 2, 3
		021107	1, 2
		181108	1, 2, 3
		231108	1, 2
		241108	1, 2
		041107	1, 2, 3
	MODIS	150508	2
		161107	2
		201108	3
		221108	1
261108	1		
clouds_med	SeaWiFS	021107	1, 2
		121108	1
		141108	2
		171108	1
		261108	1
	MERIS	021107	3, 4
	MODIS	020508	1, 3
		291108	2
	clouds_low	SeaWiFS	020508
030508			1
041107			1
100508			1, 2
110508			1, 2
111108			2
131107			1
150508			1, 2
221107			2
291108			2

continued on next page

Table A.1 – continued from previous page

Flag	Instrument	Date	Collocation
	MODIS	010508	1
		131107	1, 3
		221107	2
high_glint	MERIS	020508	1, 2
		100508	1, 2
		110508	1, 2
		130508	1
		151108	4, 5, 6
		221107	1
	221108	1	
	MODIS	110508	3
med_glint	SeaWiFS	010508	1
		100508	4
	MERIS	041107	1, 2
	MODIS	030508	1
		141108	1
		221107	1
		261108	2
mixed_high	SeaWiFS	201107	1
		221107	1
		221108	1
		291108	1
	MERIS	201108	1, 2
		291108	1
mixed_med	SeaWiFS	100508	3
	MERIS	030508	2
		150508	2
		201107	1
	MODIS	010508	2
		020508	2
		100508	2
		221107	3
mixed_low	MODIS	021107	1
not flagged	MERIS	041107	3
		121108	1, 2
		130508	2
	MODIS	030508	2
		100508	1, 3
		131108	3
		150508	3
		281108	3

Table A.2: List of collocations considered “no bad” classifications containing the collocations that were classified in “no flags”, “med glint”, “low mixed” and “med mixed”)

Instrument	Date	Collocation
SeaWiFS	010508	1
	100508	3,4
MODIS	010508	2
	020508	2
	021107	1
	030508	1, 2
	100508	1, 2, 3
	131108	3
	141108	1
	150508	3
	221107	1, 3
	261108	2
	281108	3
MERIS	030508	2
	041107	1, 2, 3
	121108	1, 2
	130508	2
	150508	2
	201107	1

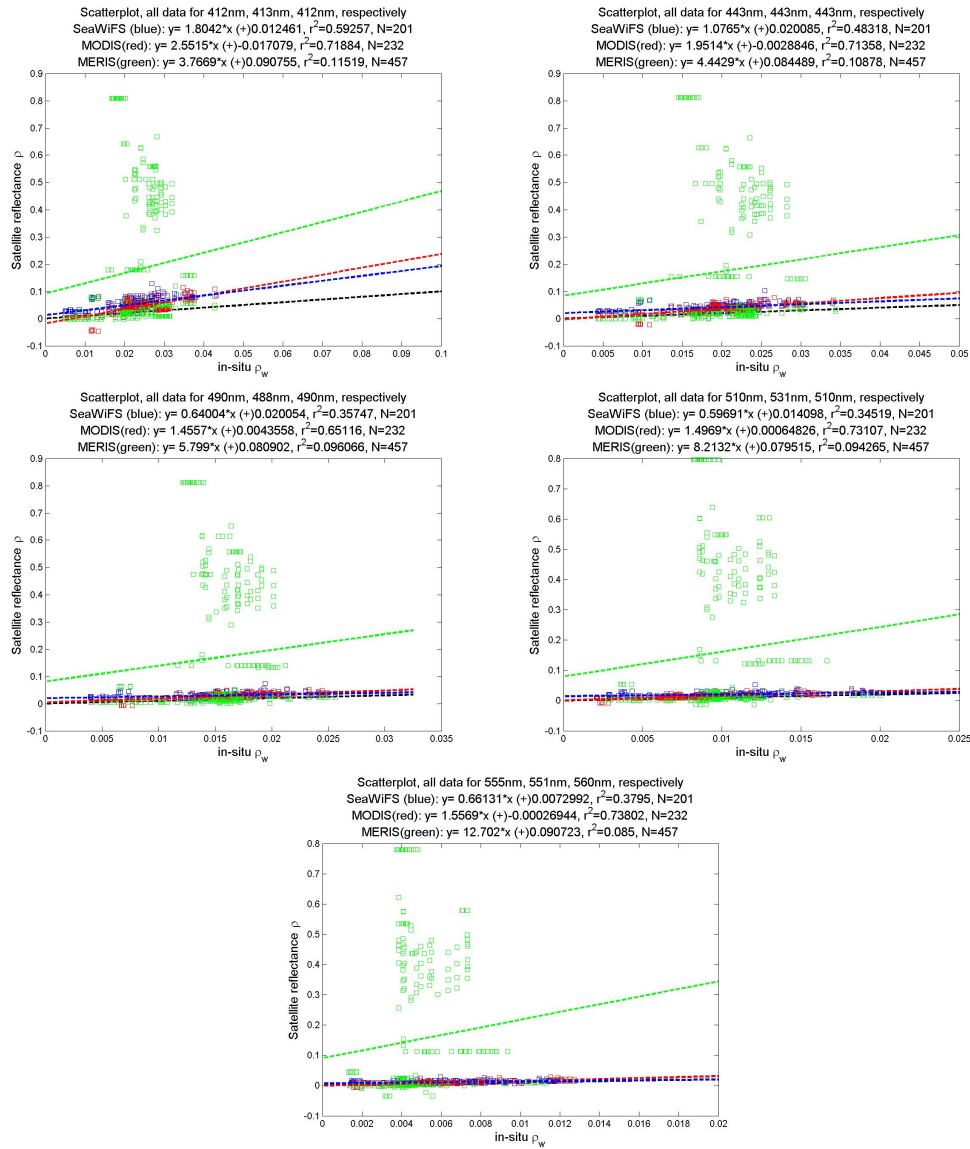


Figure A.1: Comparisons of reflectance ρ of satellite instruments MERIS, MODIS and SeaWiFS for all data to collocated in-situ remote sensing reflectance measurements, ρ_w for different wavelength bands. The dashed black line is the angular bisector (1:1-line).

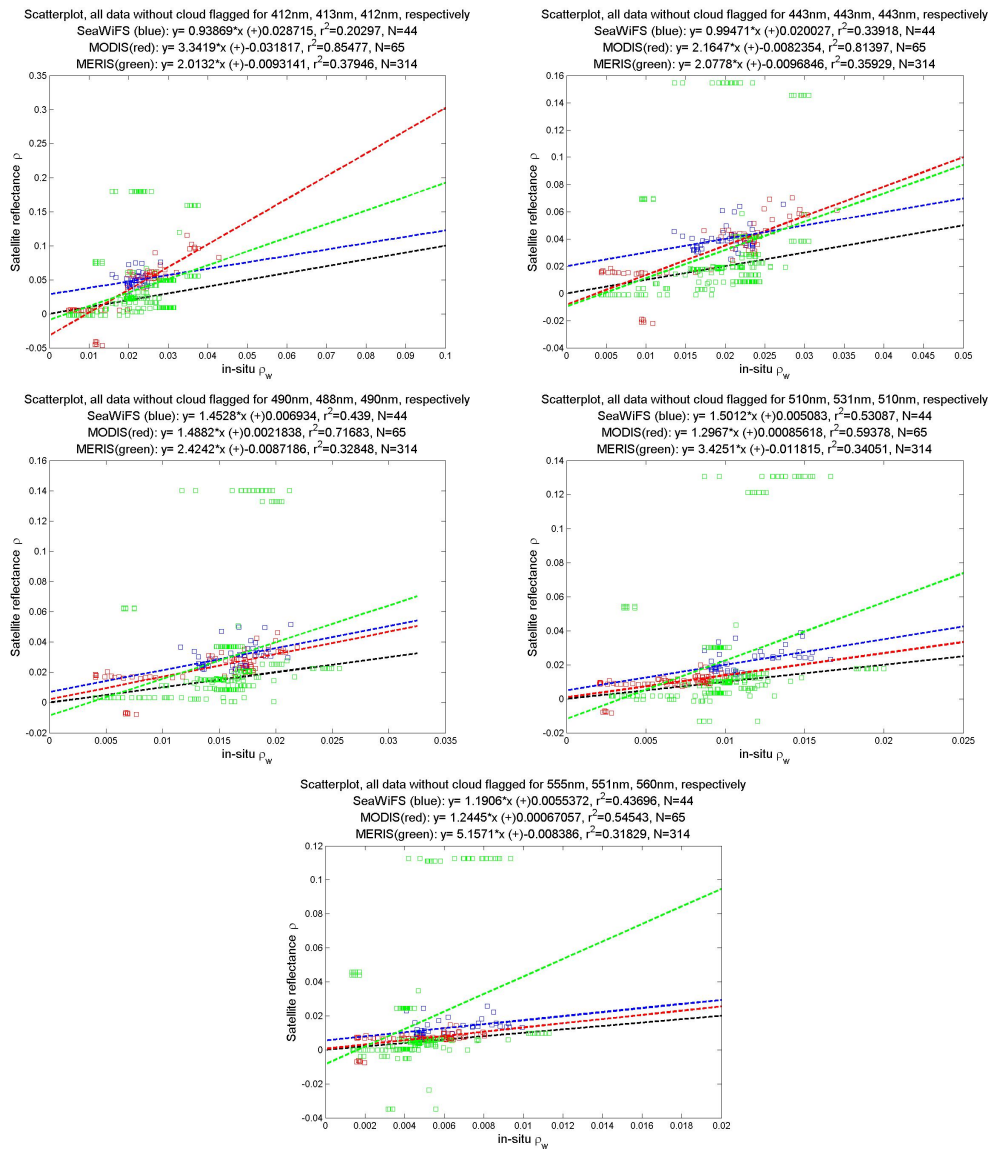


Figure A.2.: Comparisons of reflectance ρ of satellite instruments MERIS, MODIS and SeaWiFS for all data without cloud flagged data to collocated *in-situ* remote sensing reflectance measurements, ρ_w for different wavelength bands. The dashed black line is the angular bisector (1:1-line).

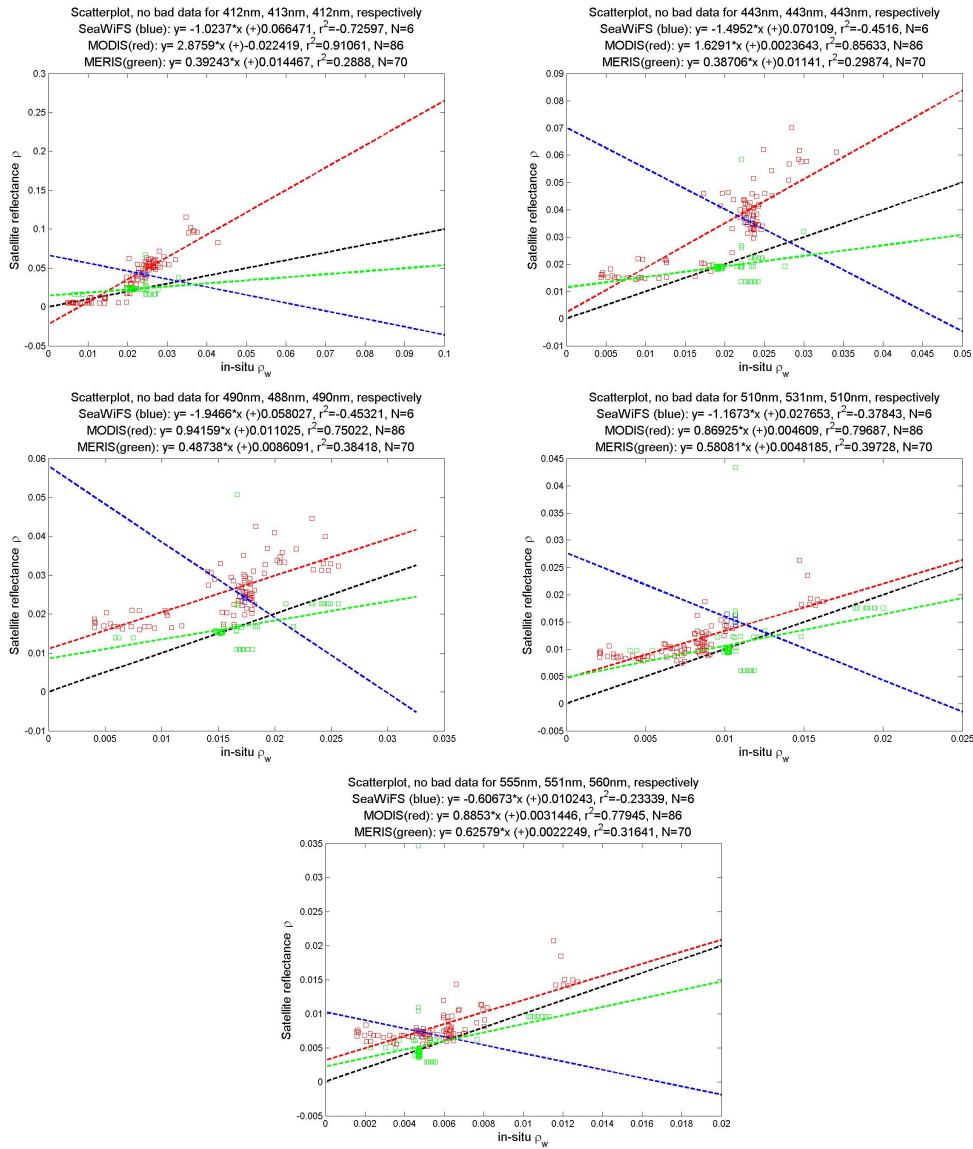


Figure A.3.: Comparisons of reflectance ρ of satellite instruments MERIS, MODIS and SeaWiFS for “no bad” superclassification to collocated *in-situ* remote sensing reflectance measurements, ρ_w for different wavelength bands. The dashed black line is the angular bisector (1:1-line).

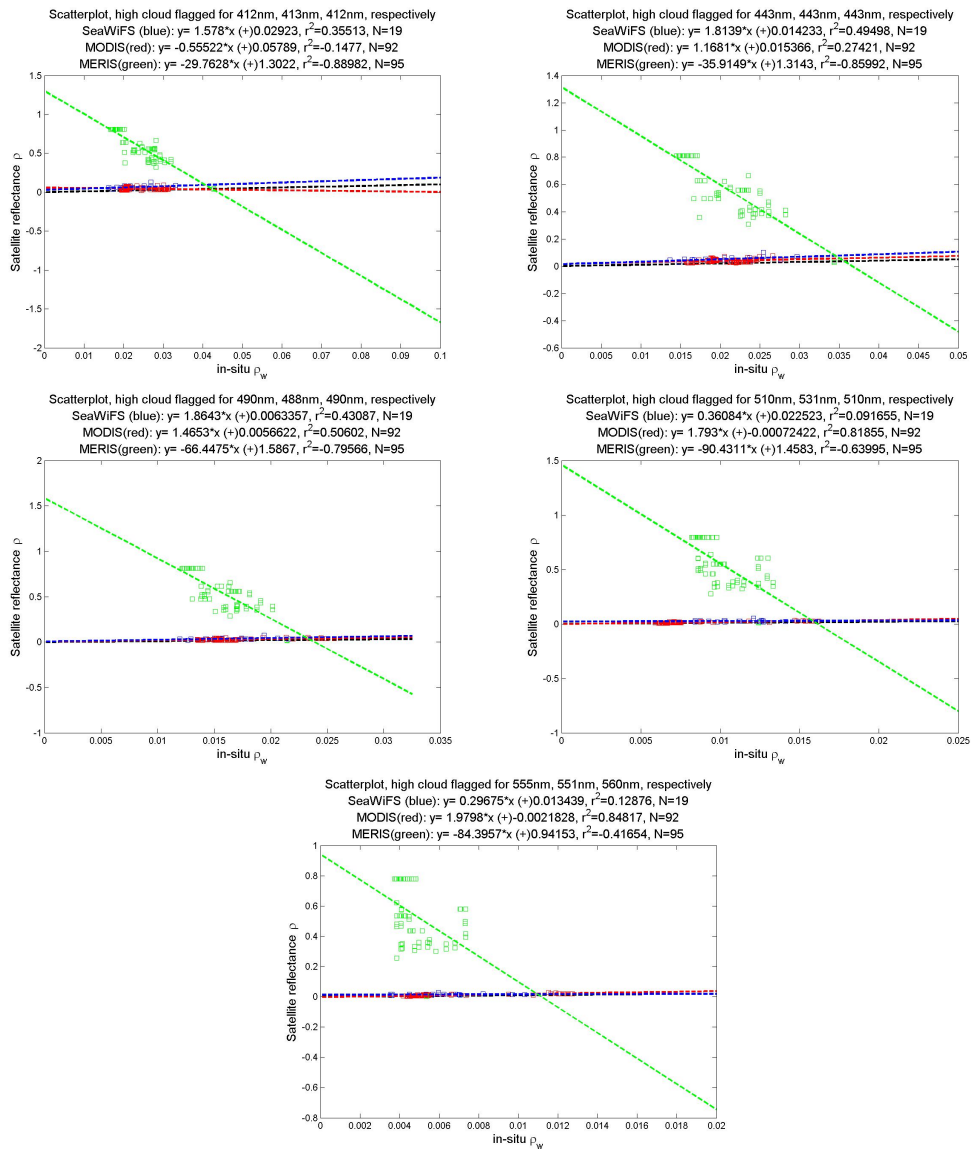


Figure A.4: Comparisons of reflectance ρ of satellite instruments MERIS, MODIS and SeaWiFS for “high cloud flagged” classification to collocated *in-situ* remote sensing reflectance measurements, ρ_w for different wavelength bands. The dashed black line is the angular bisector (1:1-line).

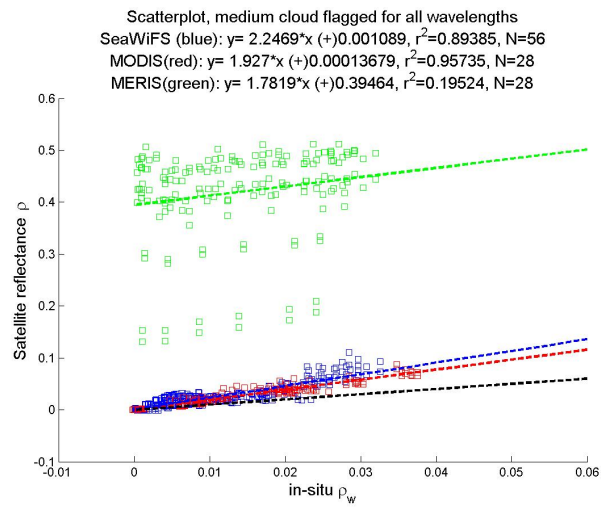


Figure A.5.: Comparison of reflectance ρ of satellite instruments MERIS, MODIS and SeaWiFS for “medium cloud” classification and all wavelength bands to collocated in-situ remote sensing reflectance measurements, ρ_w . The dashed black line is the angular bisector (1:1-line).

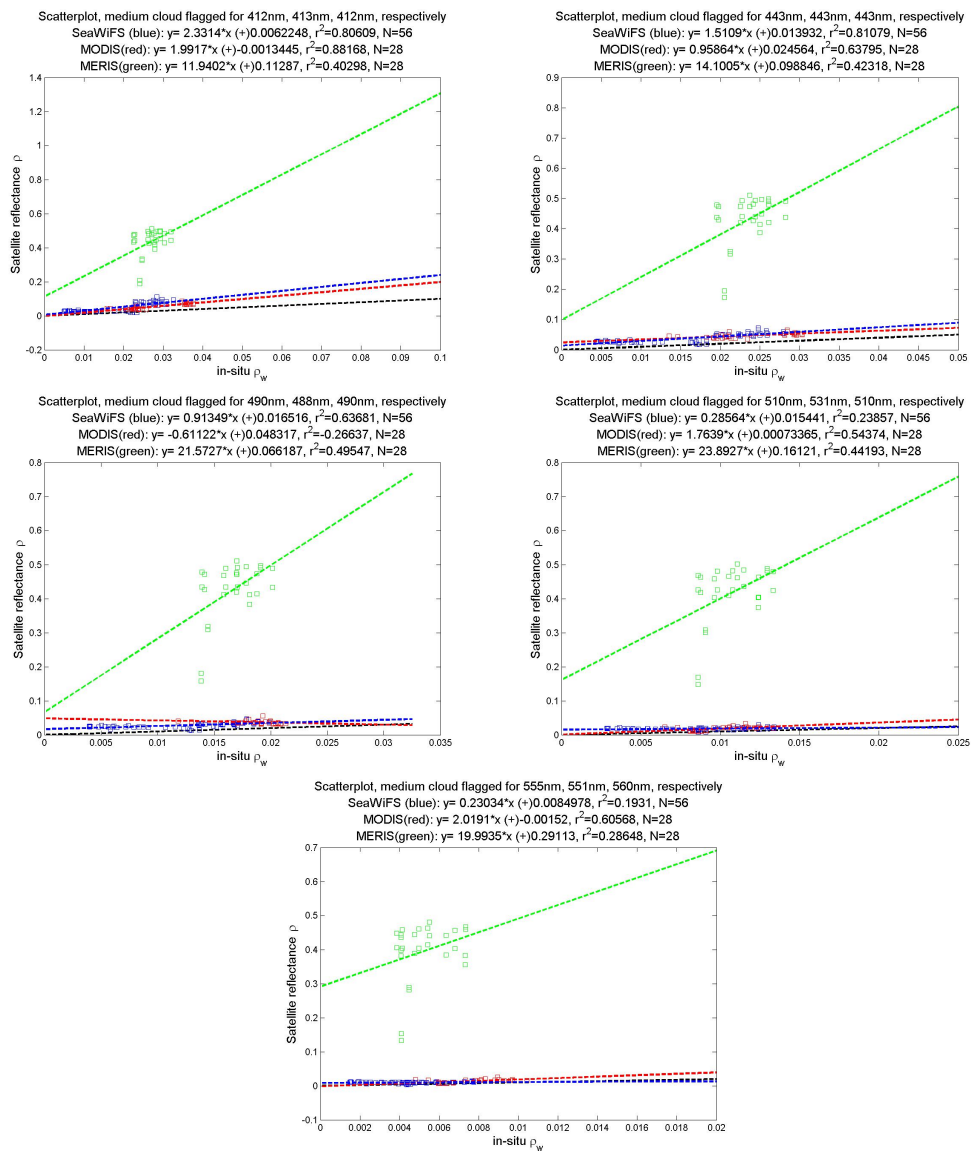


Figure A.6: Comparisons of reflectance ρ of satellite instruments MERIS, MODIS and SeaWiFS for “medium cloud flagged” classification to collocated *in-situ* remote sensing reflectance measurements, ρ_w for different wavelength bands. The dashed black line is the angular bisector (1:1-line).

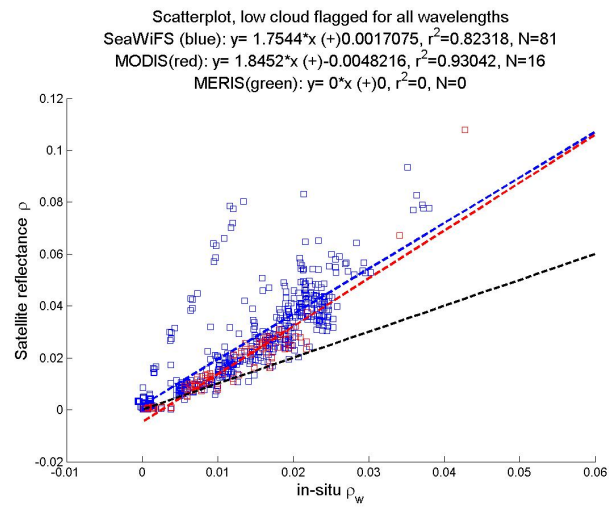


Figure A.7.: Comparison of reflectance ρ of satellite instruments MODIS and SeaWiFS (no data for MERIS) for “low cloud” classification and all wavelength bands to collocated in-situ remote sensing reflectance measurements, ρ_w . The dashed black line is the angular bisector (1:1-line).

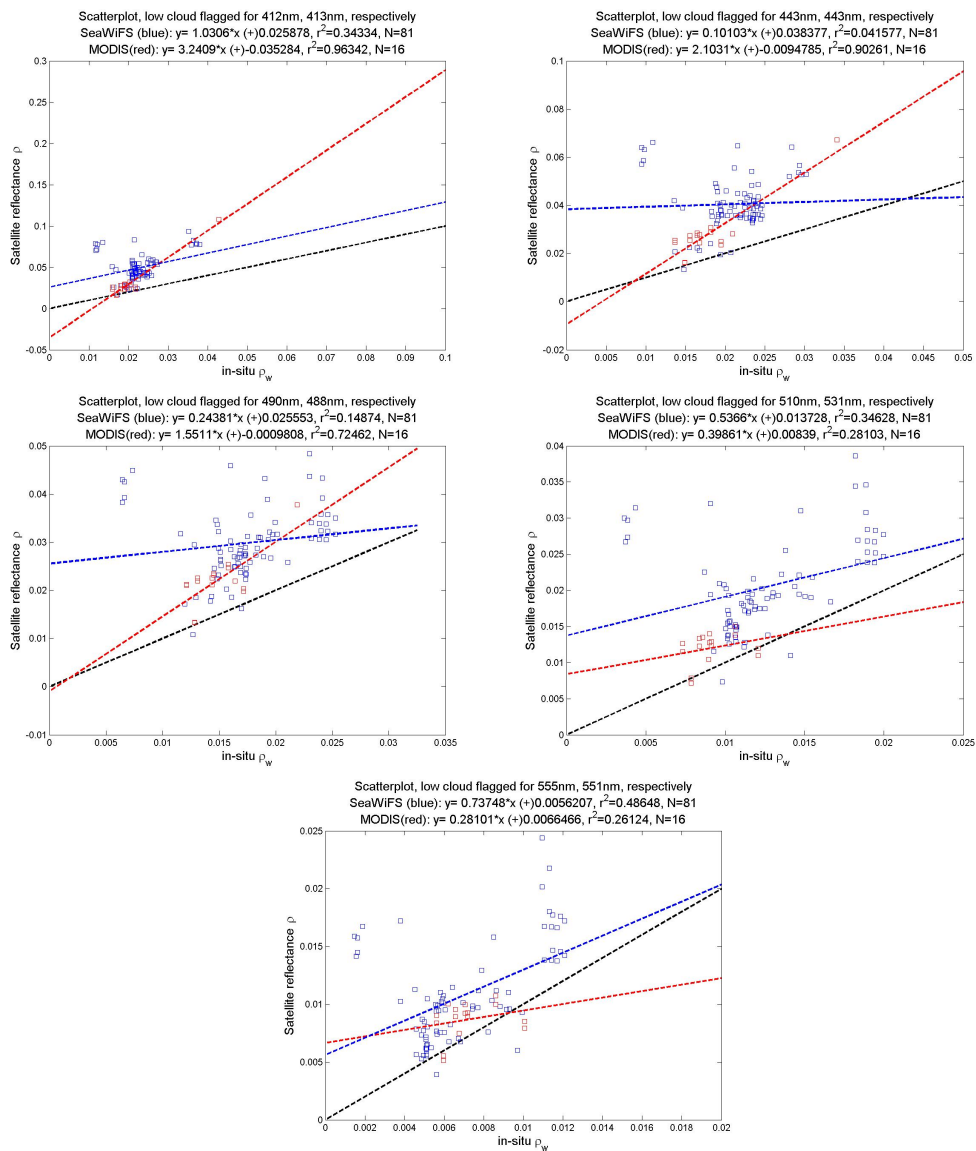


Figure A.8: Comparisons of reflectance ρ of satellite instruments MODIS and SeaWiFS for “low cloud flagged” classification to collocated *in-situ* remote sensing reflectance measurements, ρ_w for different wavelength bands. The dashed black line is the angular bisector (1:1-line).

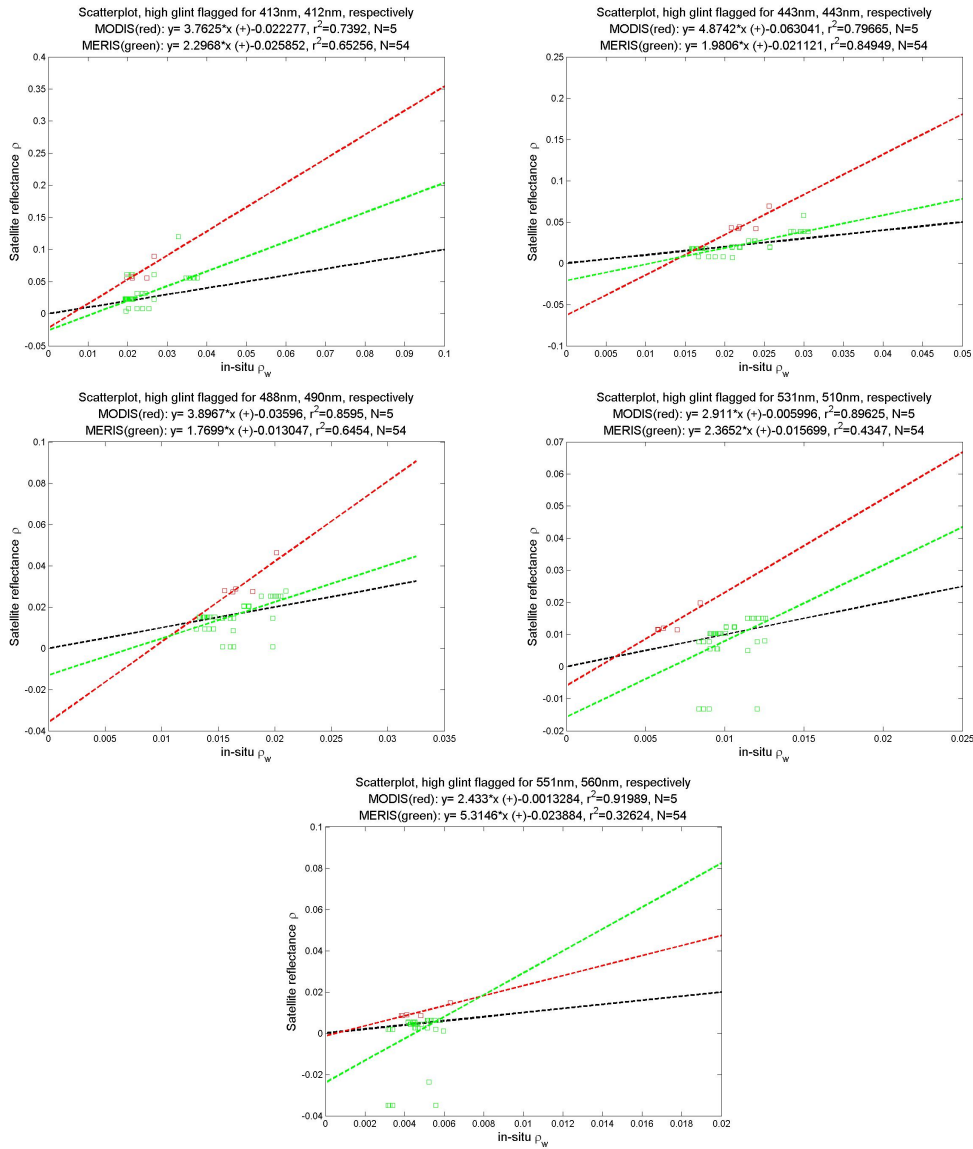


Figure A.9.: Comparisons of reflectance ρ of satellite instruments MERIS and MODIS (no data for SeaWiFS) for “high glint flagged” classification to collocated *in-situ* remote sensing reflectance measurements, ρ_w for different wavelength bands. The dashed black line is the angular bisector (1:1-line).

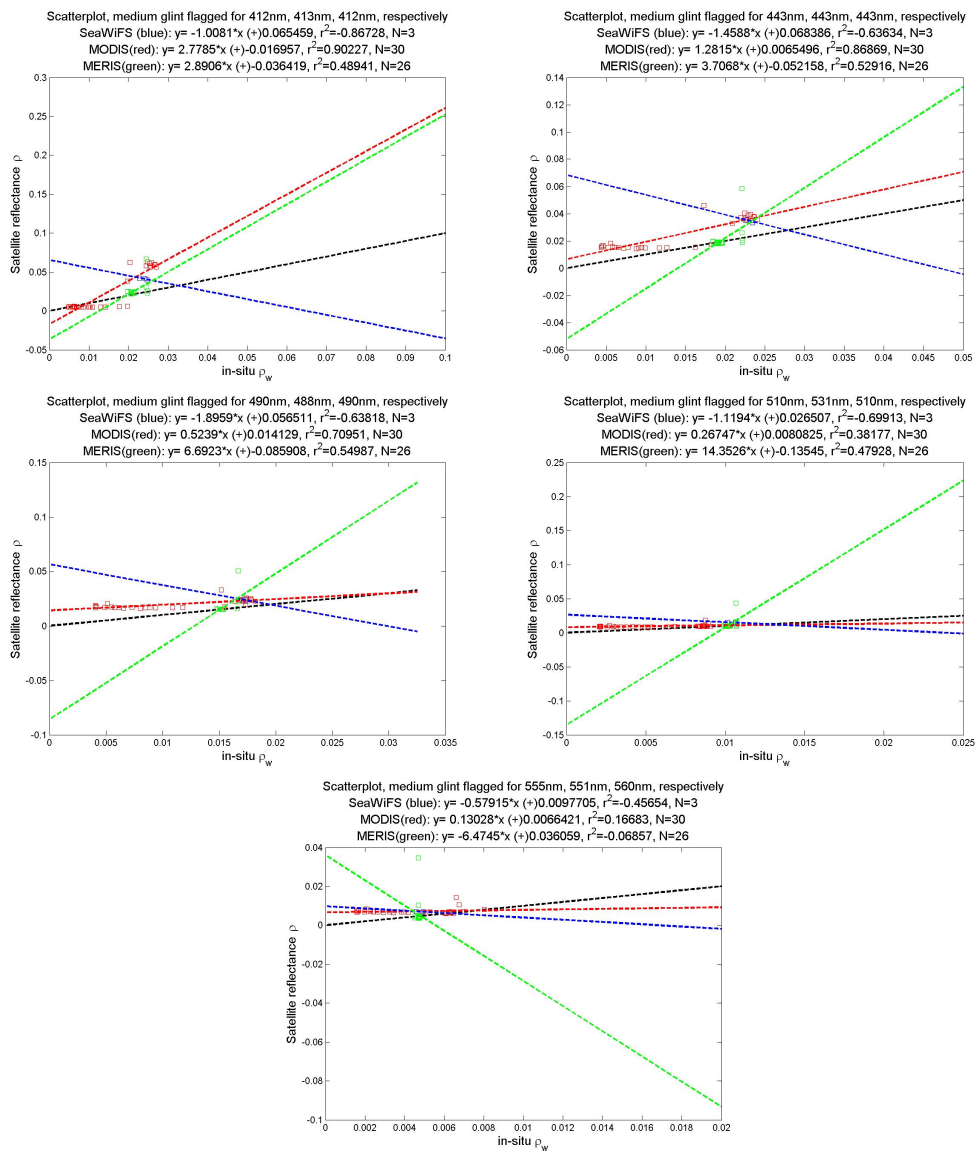


Figure A.10.: Comparisons of reflectance ρ of satellite instruments MERIS, MODIS and SeaWiFS for “medium glint flagged” classification to collocated *in-situ* remote sensing reflectance measurements, ρ_w for different wavelength bands. The dashed black line is the angular bisector (1:1-line).

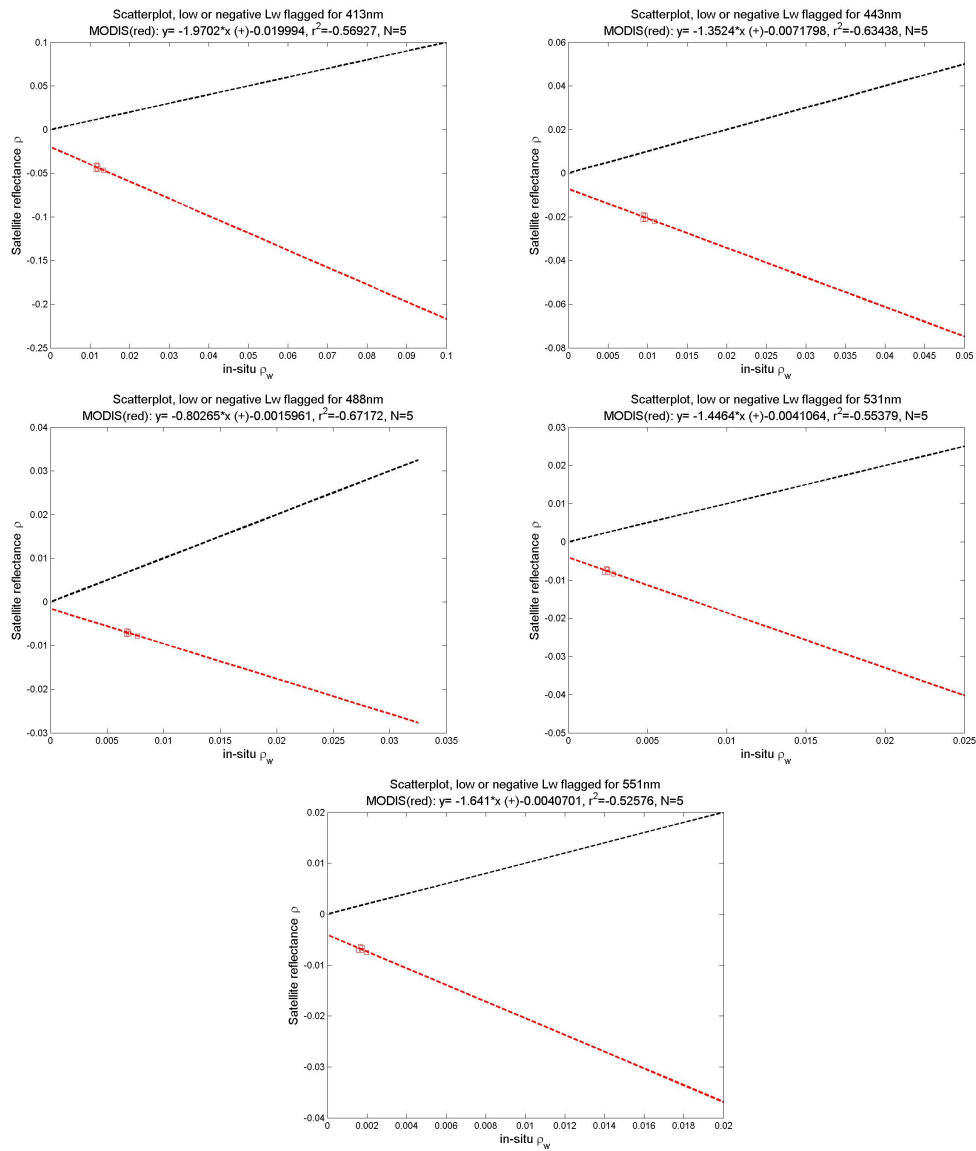


Figure A.11.: Comparisons of reflectance ρ of satellite instrument MODIS for “low or negative L_w ” classification to collocated in-situ remote sensing reflectance measurements, ρ_w for different wavelength bands. The dashed black line is the angular bisector (1:1-line).

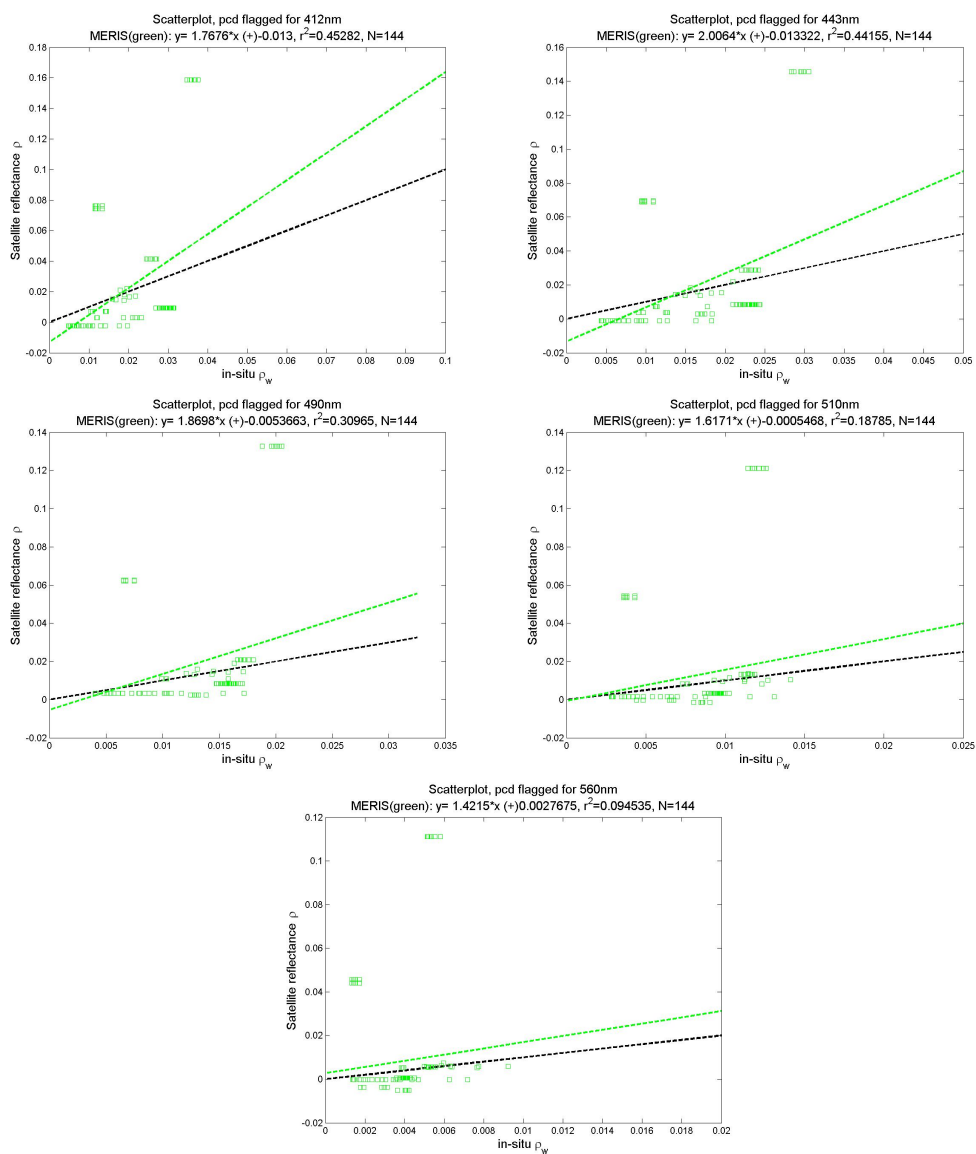


Figure A.12.: Comparisons of reflectance ρ of satellite instrument MERIS for “pcd flagged” classification to collocated *in-situ* remote sensing reflectance measurements, ρ_w for different wavelength bands. The dashed black line is the angular bisector (1:1-line).

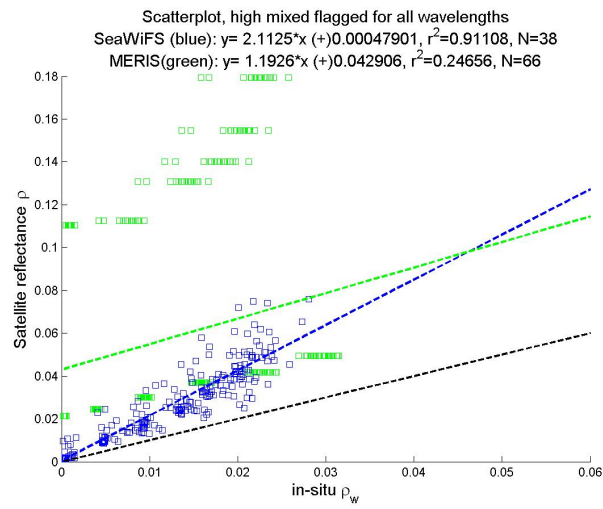


Figure A.13.: Comparison of reflectance ρ of satellite instruments MERIS and SeaWiFS (no data for MODIS) for 'high mixed' classification and all wavelength bands to collocated in-situ remote sensing reflectance measurements, ρ_w . The dashed black line is the angular bisector (1:1-line).

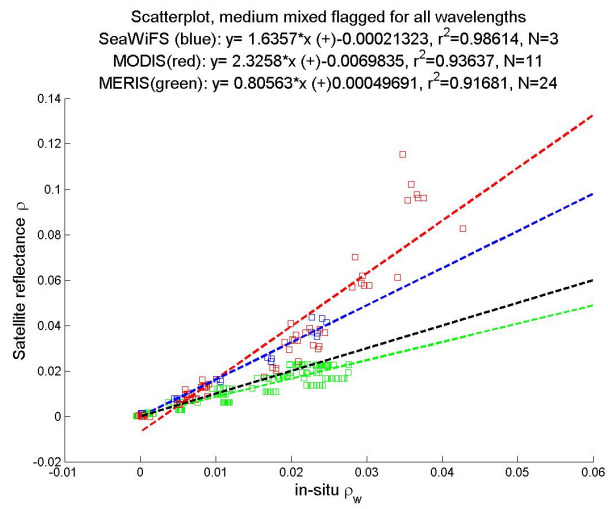


Figure A.14.: Comparison of reflectance ρ of satellite instruments MERIS, MODIS and SeaWiFS for “medium mixed” classification and all wavelength bands to collocated in-situ remote sensing reflectance measurements, ρ_w . The dashed black line is the angular bisector (1:1-line).

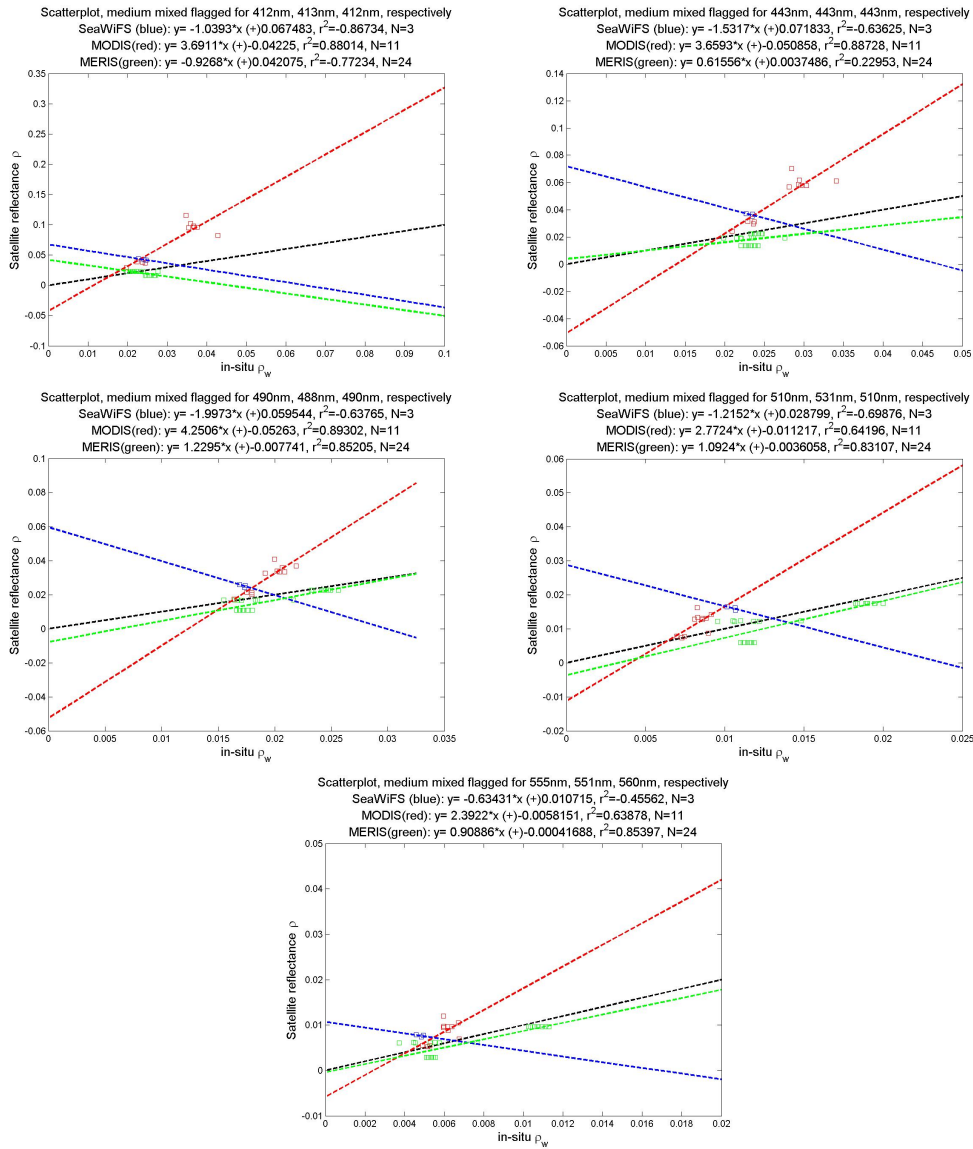


Figure A.15.: Comparisons of reflectance ρ of satellite instruments MERIS, MODIS and SeaWiFS for “medium mixed” classification to collocated *in-situ* remote sensing reflectance measurements, ρ_w for different wavelength bands. The dashed black line is the angular bisector (1:1-line).

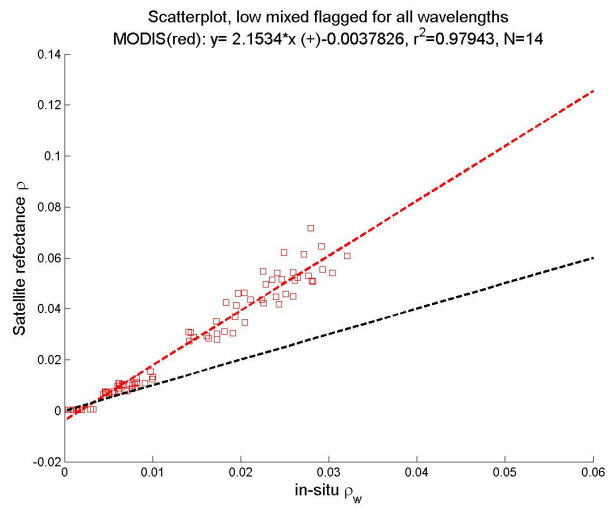


Figure A.16.: Comparison of reflectance ρ of satellite instrument MODIS (no data for MERIS and SeaWiFS) for 'low mixed' classification and all wavelength bands to collocated in-situ remote sensing reflectance measurements, ρ_w . The dashed black line is the angular bisector (1:1-line).

Acknowledgements

I want to thank Dr. Astrid Bracher for her supervision, support and comfortable working atmosphere and Prof. Dr. Peter Lemke for his co-supervision. Dr. Bettina Schmitt, Erika Allhusen, Dr. Tilman Dinter and the remaining members of the PHYTOOPTICS group I thank for the organization and execution of the ship cruises, pleasant collaboration, many helpful tips and progressively assistance.

Further thanks go to:

Jill N. Schwarz for many hints, script submittals, linguistic and technical support,

Roland Doerffer for support and the script for determining ρ_{asr}

Hajo Krasemann, Wolfgang Schönfeld, Rüdiger Roettgers and Oliver Zielinski for suggestions, support and lending devices,

ESA and NASA for deployment of satellite data and necessary software and

the crew of RV Polarstern for helpfulness and support during the cruises.

Finally, big hugs and warm thanks pertain my family and friends who not only endured me, but also encouraged and supported me: Thanks!

Erklärung

Hiermit bestätige ich, dass ich die vorliegende Diplomarbeit selbständig verfasst und keine anderen als die angegebenen Quellen und Hilfsmittel verwendet habe.

Ich versichere, dass diese Arbeit noch nicht zur Erlangung eines Diplomgrades an anderer Stelle vorgelegen hat.

Bremen, November 2009

(Anja Theis)